



Durham E-Theses

High quality electron densities as a tool in Kohn-Sham theory

Allen, Mark J.

How to cite:

Allen, Mark J. (2004) *High quality electron densities as a tool in Kohn-Sham theory*, Durham theses, Durham University. Available at Durham E-Theses Online: <http://etheses.dur.ac.uk/3159/>

Use policy

The full-text may be used and/or reproduced, and given to third parties in any format or medium, without prior permission or charge, for personal research or study, educational, or not-for-profit purposes provided that:

- a full bibliographic reference is made to the original source
- a [link](#) is made to the metadata record in Durham E-Theses
- the full-text is not changed in any way

The full-text must not be sold in any format or medium without the formal permission of the copyright holders.

Please consult the [full Durham E-Theses policy](#) for further details.

High quality electron densities as a tool in
Kohn-Sham theory

Mark J Allen
Graduate Society
Department of Chemistry
University of Durham

2004

**A copyright of this thesis rests
with the author. No quotation
from it should be published
without his prior written consent
and information derived from it
should be acknowledged.**

A thesis submitted in partial fulfilment of the
requirements for the degree of

Doctor of Philosophy



20 APR 2005

Abstract

In this thesis high quality electron densities are used to provide insight into density functional theory (DFT) and to improve the quality of DFT calculations.

Chapter 1 provides an introduction to *ab initio* molecular wavefunction calculations with particular emphasis on the Hartree-Fock method. Chapter 2 outlines important concepts in density functional theory (DFT). This includes a discussion of the Zhao, Morrison and Parr (ZMP) method, which is the key to calculating DFT quantities from high quality densities. In Chapter 3, high quality densities are used to gain an understanding of dispersion interactions in the helium dimer. The investigation seeks to understand the correlation potentials associated with a density distortion that gives rise to the correct dispersion forces. Chapter 4 presents a study of response properties using orbitals and eigenvalues determined from high quality densities. Both magnetic and electric properties are considered and comparisons are made with conventional DFT functionals and wavefunction methods. Chapter 5 makes a comparison between Kohn-Sham eigenvalues and related properties, generated both by conventional functionals and from densities. The influence on NMR shielding constants is considered and two approaches to correcting LUMO eigenvalues are presented. In chapter 6, a DFT exchange-correlation functional determined from a fit to high quality densities is applied to study the *gauche* effect in 2-fluoroethylamine, 2-fluoroethanol and their protonated analogues. Conclusions are presented in Chapter 7.

Acknowledgements

Thanks are due to my colleagues Dr Giuseppina Menconi, Dr Philip Rush-ton, Dr Philip Wilson and Mr Tom Keal for their help, encouragement and stimulating conversation.

Finally, I owe the greatest debt to my supervisor, Dr David Tozer, for his encouragement, assistance and example. He showed me what it is to see what everyone else has seen and think what no one else has thought.

Mark Allen
September 2004

Declaration

The material contained within this thesis has not been previously submitted for a degree at the University of Durham or any other university. The research reported within this thesis has been conducted by the author unless indicated otherwise.

The copyright of this thesis rests with the author. No quotation from it should be published without his prior consent and information derived from it should be acknowledged.

Every attempt to employ mathematical methods in the study of chemical questions must be considered profoundly irrational and contrary to the spirit of chemistry. If mathematical analysis should ever hold a prominent place in chemistry—an aberration which is happily almost impossible—it would occasion a rapid and widespread degeneration of that science.

A. Comte
Philosophie Positive, 1830.

Contents

1	Molecular electronic structure calculations	1
1.1	The Schrödinger equation	2
1.2	The Born-Oppenheimer approximation	4
1.3	Hartree-Fock theory	5
1.3.1	Restricted and unrestricted Hartree-Fock	8
1.3.2	Expansion of the spinorbitals into a basis set	9
1.3.3	Koopmans' Theorem	11
1.4	Electron correlation	12
1.4.1	Configuration interaction	13
1.4.2	Coupled cluster theory	15
1.4.3	Brueckner theory	16
1.4.4	Møller-Plesset perturbation theory	17
2	Density functional theory	19
2.1	The electron density	20
2.2	The models of Thomas, Fermi and Dirac	20
2.3	The Hohenberg-Kohn theorems	22
2.3.1	Unique determination of the Hamiltonian by the density	22
2.3.2	Variational principle	24
2.4	Kohn-Sham density functional theory	24
2.5	Hartree-Fock-Kohn-Sham theory	29
2.6	Exchange-correlation functionals	30
2.7	Local density approximation	30

2.8	Generalised gradient approximation	31
2.8.1	B86	32
2.8.2	B88	32
2.8.3	LYP	33
2.8.4	HCTH	33
2.8.5	1/4	33
2.8.6	PBE	34
2.8.7	KT2	34
2.9	Hybrid functionals	34
2.9.1	B3LYP	36
2.9.2	B97	37
2.9.3	B97-1	38
2.9.4	B97-2	38
2.9.5	PBE0	39
2.10	The Zhao, Morrison and Parr (ZMP) method for the calculation of exchange-correlation potentials	39
2.11	This thesis	41
3	Dispersion forces and correlation potentials in He₂	43
3.1	Intermolecular interactions	44
3.1.1	Supermolecular calculations and basis set superposition error	46
3.2	Performance of DFT for intermolecular interactions	47
3.3	Calculation of intermolecular forces	51
3.3.1	Computational details	53
3.4	Dispersion forces and the atomic density distortion	56
3.5	DFT forces and correlation potentials	63
3.6	Partitioning the correlation potential	67
3.7	The hydrogen molecule	72
3.8	Summary	77

4	Magnetic and electric response properties	78
4.1	Kohn-Sham magnetic response theory	79
4.1.1	MKS magnetic response properties	83
4.2	Chemical shifts	84
4.3	Kohn-Sham electric response theory	93
4.3.1	MKS electric response properties	96
4.4	MKS polarisabilities	97
4.4.1	Analytical versus numerical calculations	97
4.4.2	Error analysis and vibrational corrections	98
4.4.3	Isotropic and anisotropic polarisabilities	99
4.4.4	Variation of isotropic polarisabilities with F_{xc}	104
4.4.5	The HCTH[LDAX] method	109
4.5	MKS excitation energies	109
4.6	Summary	111
5	Eigenvalues, integer discontinuities and NMR shieldings	115
5.1	HOMO-LUMO eigenvalue differences	116
5.1.1	NMR shielding constants	117
5.1.2	The integer discontinuity	119
5.2	HOMO eigenvalues	122
5.2.1	NMR shielding constants	124
5.2.2	Excitation energies	126
5.3	Summary	128
6	The <i>gauche</i> effect	130
6.1	The <i>gauche</i> effect	131
6.2	Conformational preference of substituted ethanes	131
6.3	Theoretical studies	134
6.4	Solid state studies	139
6.5	Summary	142
7	Concluding remarks	149

A Atomic Units	152
B Differentiation of SAPT energy	153
C Geometries and experimental data used in calculations	156
D Publications and conferences	162
D.1 Publications	162
D.2 Conferences and seminars attended	163

List of Figures

3.1	Typical intermolecular potential energy function.	45
3.2	Energy plots for the He dimer from (a) wavefunction methods, (b) LDA and GGA DFT functionals and (c) a hybrid DFT functional. In each case, a BD energy plot is included for reference. Note different scale for (b).	50
3.3	SAPT interaction energy E_{SAPT} and force F_{SAPT} , together with long-range dispersion contributions E_{disp} and force F_{disp} for He ₂	58
3.4	Density differences $\Delta\rho(\mathbf{r})$ determined from BD(T) densities, plotted along the He-He bond axis for the three R values. The nuclei are symmetrically placed either side of $z = 0$	64
3.5	Density difference $\Delta\rho(\mathbf{r})$ determined from HF-SCF densities, plotted along the He-He bond axis for $R = 5.6$ au. The nuclei are symmetrically placed either side of $z = 0$	65
3.6	Density differences $\Delta\rho(\mathbf{r})$ determined from BD(T) densities (solid line), plotted along the He-He bond axis for $R = 9.0$ au, compared with $\Delta\rho(\mathbf{r})$ from HFKS calculations (dashed lines) using (a) LYP and (b) ZMP potentials.	66
3.7	Correlation potentials $v_{\text{C,ZMP}}^{\text{Dimer}}(\mathbf{r})$ plotted along the He-He bond axis for the three R values.	68
3.8	Correlation potentials $v_{\text{C,ZMP}}^{\text{Dimer}}(\mathbf{r})$ (solid curve) and $v_{\text{C,LYP}}^{\text{Dimer}}(\mathbf{r})$ (dashed curve), plotted along the He-He bond axis for $R = 9.0$ au.	69
3.9	Interaction correlation potentials $v_{\text{C,ZMP}}^{\text{Int}}(\mathbf{r})$ plotted along the He-He bond axis for the three R values.	71

3.10	Potential energy curves of H ₂	73
3.11	H ₂ correlation potentials v_c^{BD} (solid curves) and v_c^{UHF} (dashed curves), (a) $R = 3.78$ bohr and (b) $R = 9.45$ bohr.	75
3.12	H ₂ interaction potentials, (a) $R = 3.78$ bohr and (b) $R = 9.45$ bohr. Note different scales.	76
6.1	Ethane staggered and eclipsed conformations	132
6.2	Propane staggered and eclipsed conformations	132
6.3	Butane <i>anti</i> and <i>gauche</i> conformations	133
6.4	1,2-difluoroethane <i>anti</i> and <i>gauche</i> conformations	133
6.5	Minimum conformations of 2-fluoroethylamine. The stars denote lone pairs	135
6.6	Minimum conformations of 2-fluoroethylammonium	137
6.7	Minimum conformations of 2-fluoroethanol	138
6.8	Minimum conformations of protonated 2-fluoroethanol	140
6.9	Systems for which solid-state X-ray crystal structures have been determined.	141
6.10	Molecular solid-state structure of 2-fluoroethylammonium chloride	142
6.11	X-ray crystal structure of 2-fluoroethylammonium chloride	143
6.12	Molecular solid-state structure of N,N-dibenzyl-2-fluoroethylammonium hydrochloride	143
6.13	X-ray crystal structure of N,N-dibenzyl-2-fluoroethylammonium hydrochloride	144
6.14	Molecular solid-state structure of 4-(2-Fluoroethyl) morpholin-4-ium chloride	144
6.15	X-ray crystal structure of 4-(2-Fluoroethyl) morpholin-4-ium chloride	145
6.16	Molecular solid-state structure of N-2-Fluoroethylamine hydrochloride	146
6.17	X-ray crystal structure of N-2-Fluoroethylamine hydrochloride	146

6.18 Molecular solid-state structure of di(2-fluoroethyl)amine hydrochloride	147
6.19 X-ray crystal structure of di(2-fluoroethyl)amine hydrochloride	148

List of Tables

3.1	Binding energies D_e and equilibrium separations R_e of He_2 . . .	51
3.2	Parameters for the fit of the SAPT potential	57
3.3	The force on nucleus A in He_2 , in units of $\times 10^{-6} E_h$, for internuclear separations $R = 8.0, 8.5,$ and 9.0 au. All forces act along the He-He bond axis. A positive force represents an attraction between the nuclei.	59
4.1	LDA isotropic shielding constants in ppm. Calculations are performed at TZP BP86 geometries.	85
4.2	LDA reference shieldings σ_{ref} and mean absolute errors in isotropic chemical shifts for the 36 molecules in Table 4.3. Values for Poater <i>et al.</i> [132] and Patchkovskii <i>et al.</i> [131] have been re-calculated from the data in the original references. All quantities are in ppm.	87
4.3	Isotropic chemical shifts in ppm. SAOP values have been re-calculated from the data in Ref. [132]. Unless otherwise stated, calculations are performed at TZP BP86 geometries.	88
4.4	Reference shieldings σ_{ref} and mean absolute errors in isotropic chemical shifts for the 36 molecules in Table 4.3. SAOP values have been re-calculated from the data in Ref. [132]. Unless otherwise stated, calculations are performed at TZP BP86 geometries. All quantities are in ppm.	91

4.5	Static isotropic polarisabilities (in atomic units), determined using the Sadlej basis set. MKS calculations use the LDAX F_{XC}	100
4.6	Static anisotropic polarisabilities (in atomic units), determined using the Sadlej basis set. MKS calculations use the LDAX F_{XC}	103
4.7	Dipole moments (in atomic units) determined using the Sadlej basis set	104
4.8	MKS static isotropic polarisabilities (in atomic units) determined using the Sadlej basis and the LDAX+VWN F_{XC}	105
4.9	MKS static isotropic polarisabilities (in atomic units) determined using the Sadlej basis set and the BLYP F_{XC}	106
4.10	MKS static isotropic polarisabilities (in atomic units) determined using the Sadlej basis set and the HCTH F_{XC}	107
4.11	MKS static isotropic polarisabilities (in atomic units) determined using the Sadlej basis set and the 1/4 F_{XC}	108
4.12	Summary of variation of mean errors with F_{XC} cf. BD(T) . . .	109
4.13	HCTH[LDAX] static isotropic polarisabilities (in atomic units) determined using the Sadlej basis set	110
4.14	Vertical excitation energies of CO (in eV), computed using the augmented Sadlej basis set.	112
4.15	Vertical excitation energies of N ₂ (in eV), computed using the augmented Sadlej basis set.	112
4.16	Vertical excitation energies of H ₂ CO (in eV), computed using the Sadlej basis set.	113
4.17	Vertical excitation energies of C ₂ H ₄ (in eV), for states formed by single excitations from the $b_{3u} = \pi$ orbital (molecule lies in yz plane), computed using the augmented Sadlej basis set. . .	114
5.1	HOMO-LUMO eigenvalue differences $\Delta\epsilon = \epsilon_{LUMO} - \epsilon_{HOMO}$ determined from the ZMP approach, compared to those from the HCTH, PBE, and 1/4 functionals. Experimental values of $I - A$ and calculated $\Delta_{XC} = I - A - \Delta\epsilon^{ZMP}$ are also presented. All values are in au.	117

5.2	Isotropic NMR shieldings (in ppm) at near-experimental geometries, determined using the Huzinaga IGLO IV basis set.	120
5.3	Anisotropic NMR shieldings (in ppm) at near-experimental geometries, determined using the Huzinaga IGLO IV basis set.	121
5.4	HOMO eigenvalues from ZMP, HCTH, PBE, and 1/4, compared to $-I$ and the average HOMO $\epsilon_{\text{HOMO}}^{\text{average}}$ defined in Eqn. (5.13). All values are in au.	123
5.5	Vertical excitation energies of CO (in eV), computed using the augmented Sadlej basis set.	127
5.6	Vertical excitation energies of N ₂ (in eV), computed using the augmented Sadlej basis set.	127
5.7	Vertical excitation energies of H ₂ CO (in eV), computed using the Sadlej basis set.	128
5.8	Vertical excitation energies of C ₂ H ₄ (in eV), for states formed by single excitations from the $b_{3u} = \pi$ orbital (molecule lies in yz plane), computed using the augmented Sadlej basis set.	129
6.1	F-C-C-N dihedral angles, absolute energies and <i>gauche anti</i> energy differences of 2-fluoroethylamine and 2-fluoroethylammonium	136
6.2	F-C-C-O dihedral angles, absolute energies and <i>gauche anti</i> energy differences of 2-fluoroethanol and protonated 2-fluoroethanol	139
A.1	Atomic units	152
C.1	Optimised BP86/TZP molecular geometries, Cartesian co-ordinates, Angstroms	157
C.2	Geometries of systems and additional basis functions used for excitation energy calculations	159
C.3	Geometries of systems for shielding and polarisability calculations	160
C.4	Experimental vertical ionisation potentials and electron affinities	161

Chapter 1

Molecular electronic structure calculations

In this chapter, quantum chemical methods which seek to obtain an approximate solution to the Schrödinger equation are examined. Beginning with the Hartree-Fock method (the least computationally expensive *ab initio* method in general use), the theory is described in detail and the concepts of exchange, correlation, restricted and unrestricted calculations and expansion into a basis set are introduced. These concepts will be relevant for later discussion of density functional theory.

The limitations imposed by the approximations employed in the Hartree-Fock method are discussed. More sophisticated techniques which seek to circumvent these limitations (at a cost of increased complexity) are then introduced. These methods will be used later in this thesis to generate high quality electron densities for use in density functional theory calculations.



1.1 The Schrödinger equation

Mathematical expressions exist that describe all phenomena of interest to chemists to an accuracy that is in negligible disagreement with experimental values. Unfortunately, except for a few trivially simple systems the equations are too complicated to solve when applied to atomic or molecular systems. Thus computational chemistry is the search for approximate mathematical models which will provide qualitative insight into chemical processes and allow quantitative predictions to be made. At present, a compromise must generally be made between accuracy of results and scope of the applicability of a given method.

Schrödinger's wave mechanics [1] was inspired by de Broglie's hypothesis that particles of matter have associated wavelengths [2]. Schrödinger developed a mathematical expression to describe these matter waves, and it is this wave equation that is known as the Schrödinger equation. The most general form of the Schrödinger equation is the time-dependent case

$$\hat{H}\Psi = i\hbar \frac{\partial\Psi}{\partial t} \quad (1.1)$$

which describes how the wavefunction, Ψ , (which describes the dynamical properties of the system in question) evolves in time. The symbol \hbar is Planck's constant divided by 2π , t is time and \hat{H} is the operator corresponding to the total energy of the system¹. In the realm of atomic theory, Schrödinger interpreted the wavefunction as a description of the spatial distribution of electronic charge that he considered to constitute an electron [1]. However, this view has been largely replaced by that put forward by Born [3], that $\Psi^*\Psi$ is the probability density. Hence Ψ is a probability amplitude and has no obvious physical interpretation.

There is no way to derive the Schrödinger equation, just as there is no way to derive Newton's Laws of motion. Arguments can be made for the plausibility of the relations described by the equation, but in general the

¹known as the Hamiltonian operator. In classical physics, the Hamiltonian is the sum of the kinetic energy and potential energy $H = T + V$

Schrödinger equation is treated as a postulate of quantum mechanics and its adoption rationalised by its quantitative agreement with experimental results.

Many properties of isolated systems are independent of time. Therefore, when calculating such properties it is both valid and convenient to separate the Schrödinger equation into expressions for the time and space variation of the wavefunction. From this separation may be developed the time-independent Schrödinger equation

$$\hat{H}\Psi = E\Psi \quad (1.2)$$

which makes it possible to construct expressions describing systems of interest in quantum chemistry. For the case of a particle of mass m and total energy E , moving in one dimension x , experiencing a potential V , the Schrödinger wave equation for that particle is

$$\left(-\frac{\hbar^2}{2m}\frac{\partial^2}{\partial x^2} + V\right)\Psi = E\Psi \quad (1.3)$$

and so the Hamiltonian is

$$\hat{H} = -\frac{\hbar^2}{2m}\frac{\partial^2}{\partial x^2} + V \quad (1.4)$$

For a molecular system of M nuclei and N electrons, neglecting energy due to translational motion, the non-relativistic Hamiltonian \hat{H} is a differential operator representing the total internal energy of the system. In the absence of external magnetic or electric fields, and working in atomic units ($e = \hbar = m_e = 4\pi\epsilon_0 = 1$)

$$\hat{H} = -\sum_A \frac{\nabla_A^2}{2M_A} - \sum_i \frac{\nabla_i^2}{2} - \sum_{iA} \frac{Z_A}{r_{iA}} + \sum_{i>j} \frac{1}{r_{ij}} + \sum_{A>B} \frac{Z_A Z_B}{r_{AB}} \quad (1.5)$$

The first and second terms are the kinetic energy operators for the nuclei and electrons, respectively. The third term is the coulomb attraction between the electrons and the nuclei and the fourth and fifth terms are the electron-electron and nuclear-nuclear repulsion, respectively. M_A is the ratio of the

mass of nucleus A to the mass of an electron and Z_A is the atomic number of nucleus A . The Laplacian operators ∇_A^2 and ∇_i^2 involve differentiation with respect to the coordinates of the A th nucleus and the i th electron, respectively

$$\nabla \equiv \frac{\partial}{\partial x} \mathbf{i} + \frac{\partial}{\partial y} \mathbf{j} + \frac{\partial}{\partial z} \mathbf{k} \quad (1.6)$$

and

$$\nabla^2 = \nabla \cdot \nabla \equiv \frac{\partial^2}{\partial x^2} + \frac{\partial^2}{\partial y^2} + \frac{\partial^2}{\partial z^2} \quad (1.7)$$

1.2 The Born-Oppenheimer approximation

The time-independent Schrödinger equation (1.2) is a second order differential equation in $3(N + M)$ variables. In order to simplify this expression, the great difference between the mass of the nuclei and the mass of the electrons² is exploited. This difference in mass suggests that any change in the position of the nuclei can be accommodated almost instantaneously by the electronic motion. In consequence, electronic and nuclear motion may be considered separately, to a good approximation. This is the Born-Oppenheimer [4, 5] or clamped-nuclei approximation. The nuclei are considered to be fixed in position and the electronic Schrödinger equation

$$\hat{H}_{\text{elec}} \Psi_{\text{elec}} = E_{\text{elec}} \Psi_{\text{elec}} \quad (1.8)$$

is solved for the electrons in the static potential due to the nuclei. The wavefunction, Ψ_{elec} , has a parametric dependence on the nuclear coordinates and the electronic Hamiltonian, \hat{H}_{elec} , is

$$\hat{H}_{\text{elec}} = - \sum_i \frac{\nabla_i^2}{2} - \sum_{iA} \frac{Z_A}{r_{iA}} + \sum_{i>j} \frac{1}{r_{ij}} \quad (1.9)$$

The variation of the energy with the nuclear coordinates defines the potential energy surface (PES); the minimum on this surface defines the equilibrium geometry. The force is minus the derivative of the energy with respect to the

²the smallest nucleus, a single proton, has a mass over 1800 times that of an electron

nuclear coordinates, so when considering forces on nuclei (as will be done in Chapter 3) the PES determines the quality of calculated forces.

When nuclear movements must be taken into account, as in spectroscopic measurements, for example, an effective Hamiltonian is used consisting of the nuclear kinetic energy operator and the potential energy from the fixed-nuclei approximation.

In all work described in this thesis the Born-Oppenheimer approximation is used, so the electronic subscripts will be omitted for clarity.

1.3 Hartree-Fock theory

Even after the nuclear and electronic motion have been decoupled using the Born-Oppenheimer approximation, the electronic Schrödinger equation is still a many-body problem. Although it is possible to describe the motion of individual electrons, the motion of the electrons is coupled, meaning that their equations of motion must be solved simultaneously. When there are two coupled particles (a 2-body problem) the system of equations is exactly solvable, but an n -body problem (where $n \geq 3$) is, in general, unsolvable analytically³. Hence it is not generally possible to solve the electronic Schrödinger equation directly and simplifying assumptions about the form of the many-electron wavefunction must be made.

Within Hartree-Fock theory [6, 7] the electronic wavefunction for an N -electron system is approximated by an anti-symmetrised product (a Slater determinant) of N one-electron wavefunctions, $\chi_i(\mathbf{x})$. These one-electron wavefunctions are termed spinorbitals and they are the product of a spatial orbital function and a spin function

$$\chi_i(\mathbf{x}) = \phi_i^\sigma(\mathbf{r})\sigma(s), \quad \sigma = \alpha, \beta \quad (1.10)$$

³certain particular n -body problems can be solved analytically and all can (in principle) be solved numerically

The Hartree-Fock wavefunction, Ψ_{HF} , is generally written

$$\Psi_{\text{HF}} = \frac{1}{\sqrt{N!}} \begin{vmatrix} \chi_1(\mathbf{x}_1) & \chi_2(\mathbf{x}_1) & \cdots & \chi_N(\mathbf{x}_1) \\ \chi_1(\mathbf{x}_2) & \chi_2(\mathbf{x}_2) & \cdots & \chi_N(\mathbf{x}_2) \\ \vdots & \vdots & & \vdots \\ \chi_1(\mathbf{x}_N) & \chi_2(\mathbf{x}_N) & \cdots & \chi_N(\mathbf{x}_N) \end{vmatrix} \quad (1.11)$$

where $1/\sqrt{N!}$ is a normalisation constant. It is necessary to use the antisymmetrised product of the one-electron wavefunctions, since a simple product (as employed in the Hartree method [8]) would not satisfy the Pauli principle, which requires that the total electronic wavefunction, Ψ , be antisymmetric with respect to the interchange of the space and spin coordinates of two electrons. A short hand notation for eqn. (1.11), which will be employed later in this text, gives just the diagonal elements

$$\Psi_{\text{HF}} = \frac{1}{\sqrt{N!}} \det \{ \chi_1(\mathbf{x}_1) \chi_2(\mathbf{x}_2) \cdots \chi_N(\mathbf{x}_N) \} \quad (1.12)$$

The energy associated with a general Slater determinant, Φ_{SD} , is just the expectation value

$$E[\Phi_{\text{SD}}] = \langle \Phi_{\text{SD}} | \hat{H} | \Phi_{\text{SD}} \rangle \quad (1.13)$$

Expanding this expression gives

$$\begin{aligned} E[\Phi_{\text{SD}}] = & -\frac{1}{2} \sum_i \langle \chi_i | \nabla^2 | \chi_i \rangle + \int \rho(\mathbf{r}) v_{\text{ext}}(\mathbf{r}) d\mathbf{r} \\ & + \frac{1}{2} \int \int \frac{\rho(\mathbf{r})\rho(\mathbf{r}')}{|\mathbf{r} - \mathbf{r}'|} d\mathbf{r}d\mathbf{r}' - \int \int \frac{\rho_1(\mathbf{r}, \mathbf{r}')^2}{|\mathbf{r} - \mathbf{r}'|} d\mathbf{r}d\mathbf{r}' \end{aligned} \quad (1.14)$$

where $v_{\text{ext}}(\mathbf{r})$ is the external potential

$$v_{\text{ext}}(\mathbf{r}) = - \sum_A \frac{Z_A}{|\mathbf{r}_A - \mathbf{r}|} \quad (1.15)$$

$\rho(\mathbf{r})$ is the electron density, which may be expressed in terms of the spinorbitals

$$\rho(\mathbf{r}) = \sum_i |\chi_i(\mathbf{r})|^2 \quad (1.16)$$

and $\rho_1(\mathbf{r}, \mathbf{r}')$ is the reduced 1-particle density matrix

$$\rho_1(\mathbf{r}, \mathbf{r}') = \sum_i \chi_i(\mathbf{r}) \chi_i^*(\mathbf{r}') \quad (1.17)$$

The first term in eqn. (1.14) is the kinetic energy, the second is the nuclear-electron attraction energy, the third is the classical electron-electron repulsion (the coulomb or Hartree term) and the fourth term is the exchange energy. The exchange energy does not have a simple classical interpretation, but is defined by its effects. The Pauli exclusion principle means that two electrons cannot occupy the same state, and hence two electrons with the same spin cannot be located at the same point in space. This tendency of electrons of like spin to avoid one another means that the true average repulsion energy will be lower than that computed from the coulomb term. The exchange energy is the correction made to take into account the reduced probability of finding two electrons of the same spin near one another.

Using the variational principle⁴ it can be shown that any energy computed from a trial wavefunction will be an upper bound to the true energy: Hence, the spinorbitals are varied

$$\chi_i \rightarrow \chi_i + \delta\chi_i \quad (1.18)$$

to find the Slater determinant that gives the lowest energy

$$E_{\text{HF}} = \min_{\Phi_{\text{SD}} \rightarrow N} E[\Phi_{\text{SD}}] \quad (1.19)$$

subject to the constraint that the orbitals remain orthonormal. Following an appropriate unitary transformation (a rotation of the orbitals that maintains orthonormality), this gives the Hartree-Fock equations

$$\left[-\frac{1}{2} \nabla^2 + v_{\text{ext}}(\mathbf{r}) + v_{\text{J}}(\mathbf{r}) \right] \chi_i(\mathbf{r}) - \int \frac{\rho_1(\mathbf{r}, \mathbf{r}')}{|\mathbf{r} - \mathbf{r}'|} \chi_i(\mathbf{r}') d\mathbf{r}' = \epsilon_i \chi_i(\mathbf{r}) \quad (1.20)$$

where $v_{\text{J}}(\mathbf{r})$ is the coulomb potential

$$v_{\text{J}}(\mathbf{r}) = \int \frac{\rho(\mathbf{r}')}{|\mathbf{r} - \mathbf{r}'|} d\mathbf{r}' \quad (1.21)$$

⁴The theorem states that $\langle \Psi_{\text{trial}} | \hat{H} | \Psi_{\text{trial}} \rangle = E_{\text{trial}} \geq E_0 = \langle \Psi_0 | \hat{H} | \Psi_0 \rangle$ for any trial wavefunction

The value of this potential at \mathbf{r} depends on the value of ρ at all points \mathbf{r}' , so it is termed non-local. It is also termed multiplicative, since the effect of the operator on the spinorbital at \mathbf{r} depends only on the value of that spinorbital at \mathbf{r} ; there is a well-defined potential at all points in space. It is important to note that the exchange operator

$$\int \frac{\rho_1(\mathbf{r}, \mathbf{r}')}{|\mathbf{r} - \mathbf{r}'|} \chi_i(\mathbf{r}') d\mathbf{r}' \quad (1.22)$$

is also non-local in the same sense as the Coulomb potential is non-local. However, the effect of the operator on the spin orbital depends on the value of the orbital at all points in space, and so the operator is termed non-multiplicative; there is not a well-defined potential at each point in space.

The notation may be further simplified through the introduction of the Fock operator, \hat{F} such that

$$\int \hat{F}(\mathbf{r}, \mathbf{r}') \chi_i(\mathbf{r}') d\mathbf{r}' = \epsilon_i \chi_i(\mathbf{r}) \quad (1.23)$$

Since the spinorbitals are obtained by solving an equation involving the Fock operator, and the Fock operator in turn depends on all the other spinorbitals, the solution must be known in order to set up the equations. The way around this is to solve the equations in a self-consistent, iterative manner. A guess is made for an initial set of spinorbitals and these are used to formulate the Fock operator. The Hartree-Fock equations are then solved to obtain a new set of spinorbitals and this process is repeated until convergence (in the energy or some other term) is achieved. In this thesis the method is denoted Hartree-Fock Self Consistent Field (HF-SCF).

1.3.1 Restricted and unrestricted Hartree-Fock

When dealing with closed-shell atoms or molecules it is usual to make the assumption that each pair of electrons shares the spatial form of their spinorbitals

$$\Psi_{\text{HF}} = \frac{1}{\sqrt{N!}} \det \{ \chi_1(1) \chi_1(2) \cdots \chi_{N/2}(N) \} \quad (1.24)$$

This is the restricted Hartree-Fock (RHF) method. Note that a system having an even number of electrons is not equivalent to it being a closed-shell system. Consider the case of the neutral carbon atom, which has six electrons. If the electrons that occupy the p orbitals are constrained to share the spatial form for their spinorbitals a state will exist that is lower in energy. According to Hund's rule of maximum multiplicity, the state with the highest multiplicity is synonymous with that with the lowest energy. Thus the energy could be lowered by relaxing the paired-electron constraint and allowing the p orbital electrons to occupy different orbitals.

For open-shell systems there are two commonly used procedures. In the restricted open-shell formalism all electrons, except those explicitly required to occupy open-shell orbitals, occupy closed-shell orbitals. This has the advantage that the wavefunction is an eigenfunction of \hat{S}^2 . However, the spatial equations are more complicated than those of unrestricted Hartree-Fock (UHF), and the constraint of occupying orbitals in pairs raises the variational energy. Alternatively, in the unrestricted open-shell formalism [9] there is no constraint that electrons occupy orbitals in pairs. The relaxing of this constraint lowers the variational energy, but at a price: the wavefunction is no longer an eigenfunction of \hat{S}^2 .

1.3.2 Expansion of the spinorbitals into a basis set

The HF-SCF procedure can be implemented for atoms, since their spherical symmetry allows numerical solution of the HF-SCF equations for the spinorbitals. This is not the case for molecular systems, and it becomes necessary to modify the method. Roothaan and Hall's procedure for expanding the spatial part of the spinorbitals into a known basis set [10, 11] transforms the HF-SCF coupled equations into an algebraic problem that can be solved using standard matrix techniques. Nearly all modern implementations of the HF-SCF method use these matrix techniques for both atomic and molecular applications, although numerical solutions are possible for atomic systems. All calculations in this thesis involve expansion into a basis set.

Consider the restricted Hartree-Fock method. The introduction of a set of known basis functions allows us to expand the orbital functions $\phi_p(\mathbf{r})$ as linear combinations of the basis functions $\eta_\beta(\mathbf{r})$

$$\phi_p(\mathbf{r}) = \sum_{\beta} C_{\beta p} \eta_{\beta}(\mathbf{r}) \quad (1.25)$$

This expansion is only exact if the set of basis functions is complete (the basis set limit). Since this would require an infinite basis set, it is not achievable in practice. Because of this, the selection of basis functions is an important optimising step, as limiting the number of basis functions used reduces computational costs, but the basis set must provide an appropriate expansion for the orbitals.

Taking the Hartree-Fock equations expressed in terms of the Fock operator, eqn. (1.23), and integrating out spin gives

$$\int \hat{F}(\mathbf{r}, \mathbf{r}') \phi_i(\mathbf{r}') d\mathbf{r}' = \epsilon_i \phi_i(\mathbf{r}) \quad (1.26)$$

Substituting the basis functions into this HF-SCF expression for the spatial wavefunctions gives

$$\int \hat{F}(\mathbf{r}, \mathbf{r}') \sum_{\beta} C_{\beta i} \eta_{\beta}(\mathbf{r}') d\mathbf{r}' = \epsilon_i \sum_{\beta} C_{\beta i} \eta_{\beta}(\mathbf{r}) \quad (1.27)$$

To transform this into a matrix equation each side is multiplied by $\eta_{\alpha}^*(\mathbf{r})$ and integrated over $d\mathbf{r}$

$$\sum_{\beta} C_{\beta i} \int \int \eta_{\alpha}^*(\mathbf{r}) \hat{F}(\mathbf{r}, \mathbf{r}') \eta_{\beta}(\mathbf{r}') d\mathbf{r} d\mathbf{r}' = \epsilon_i \sum_{\beta} C_{\beta i} \int \eta_{\alpha}^*(\mathbf{r}) \eta_{\beta}(\mathbf{r}) d\mathbf{r} \quad (1.28)$$

which is one of a set of M simultaneous equations (one for each value of i). The introduction of two matrices simplifies the notation. First, the overlap matrix \mathbf{S} with elements

$$S_{\alpha\beta} = \int \eta_{\alpha}^*(\mathbf{r}) \eta_{\beta}(\mathbf{r}) d\mathbf{r} \quad (1.29)$$

and the Fock matrix \mathbf{F}

$$F_{\alpha\beta} = \int \int \eta_{\alpha}^*(\mathbf{r}') \hat{F}(\mathbf{r}, \mathbf{r}') \eta_{\beta}(\mathbf{r}) d\mathbf{r} d\mathbf{r}' \quad (1.30)$$

Thus eqn. (1.28) can be re-written in compact matrix notation

$$\mathbf{FC} = \mathbf{SC}\epsilon \quad (1.31)$$

\mathbf{C} and ϵ are both $M \times M$ matrices; \mathbf{C} is composed of the coefficients $C_{\beta i}$ and ϵ is a diagonal matrix of the orbital energies ϵ_i . Eqn. (1.31) has non-trivial solutions only if

$$\det |\mathbf{F} - \epsilon_i \mathbf{S}| = 0 \quad (1.32)$$

Again, a self-consistent, iterative approach is needed to solve this matrix problem.

1.3.3 Koopmans' Theorem

There is considerable theoretical interest and some confusion over the physical significance and the interpretation of the orbitals in Kohn-Sham density functional theory. Before considering this issue in detail (see Chapter 5) it is useful to describe the original Koopmans' theorem [12], which provides a physical interpretation of the Hartree-Fock orbital energies.

Koopmans' theorem states that the orbital energy, ϵ_i obtained from Hartree-Fock theory is an approximation to minus the ionisation energy (I) associated with the removal of an electron from that particular orbital, i.e.

$$\epsilon_i \approx E_N - E_{N-1}^i = -I(i) \quad (1.33)$$

Thus for the HOMO eigenvalue

$$\epsilon_{\text{HOMO}} \approx -I \quad (1.34)$$

The theorem is approximate because it ignores reorganisation (the tendency of a system to relax into a lower energy configuration when an electron is removed) and electron correlation (see Section 1.4). Fortunately, these errors tend to cancel one another. In general, the HF-SCF HOMO eigenvalue is a reasonable approximation to minus the experimental ionisation potential. However, the virtual orbitals from HF-SCF theory are often not bound.

1.4 Electron correlation

Even if the calculation is carried out in the basis set limit, the ground state Hartree-Fock energy does not correspond to the exact non-relativistic ground state energy (within the Born-Oppenheimer approximation) of the system being modelled. This discrepancy is due to the neglect of what are termed correlation effects within the Hartree-Fock method. The computational efficiency of the Hartree-Fock method is achieved through the use of a single determinant to represent the wavefunction. However, this leads to the neglect of the instantaneous coupling of the motion of the electrons. Instead, each electron moves in a potential that arises from the average effects of the other electrons.

A precise, universal definition of correlation (effects or energy) is problematic because it is defined as those phenomena or components of an energy expression that are neglected by a particular approximate scheme. The conventional definition of the correlation energy is that due to Löwdin [13]

“The correlation energy for a certain state with respect to a specified Hamiltonian is the difference between the exact eigenvalue of the Hamiltonian and its expectation value in the Hartree-Fock approximation for the state under consideration.”

For the purpose of this work the difference between the exact, non-relativistic ground state energy within the Born-Oppenheimer approximation and the Hartree-Fock ground state energy is taken to be the *correlation energy*

$$E_C^{\text{HF}} = E_0 - E_{\text{HF}} \quad (1.35)$$

This is a negative quantity since $E_{\text{HF}} \geq E_0$ (see Section 1.3).

It is common to identify separate contributions to the electron correlation. Dynamical correlation arises because the instantaneous repulsion of the electrons is not covered by the effective HF-SCF potential. Therefore, the electrons get too close to one another in the HF-SCF scheme. This means that the electron-electron repulsion term is too large, so $E_{\text{HF}} > E_0$. This is

referred to as dynamical correlation because it relates to the movement of individual electrons and is a short-range effect.

Non-dynamical or left-right correlation arises under circumstances where a single determinant fails to adequately describe the true ground state. It is referred to as left-right correlation because it is most often discussed in the context of diatomic molecules. The canonical example is the dissociation of H_2 . As the internuclear separation $R \rightarrow \infty$ there can be no dynamical correlation, as there are no electron-electron interactions (there are two independent hydrogen atoms with one electron on each, and they are infinitely far apart, so $1/r \rightarrow 0$). However, although the restricted Hartree-Fock scheme describes the H_2 system reasonably well at equilibrium distances, the error increases as the internuclear separation increases.

The next consideration is how to introduce a description of the electron correlation into the approximate solution of the Schrödinger equation. The modelling of correlation in density functional theory will be a major component of Chapter 3. Remaining within wavefunction theory, the introduction of electron correlation depends on increasing the number of determinants used to approximate the N -electron wavefunction. Several such procedures are examined below.

These correlated methods will be used in subsequent chapters to calculate electronic densities that will be employed to generate density functional theory quantities.

1.4.1 Configuration interaction

Conceptually, configuration interaction (CI) is the simplest procedure for taking into account correlation effects. The exact ground-state and excited-state wavefunctions can be expressed as a linear combination of all possible N -electron Slater determinants arising from a complete set of spinorbitals [13]. Thus the exact ground-state or excited state electronic wavefunction Ψ of a system can be written as a linear combination of the ground state and

excited configuration state functions (CSF)⁵

$$\Psi = C_0\Phi_0 + \sum_{i,a} C_i^a \Phi_i^a + \sum_{\substack{i<j \\ a<b}} C_{ij}^{ab} \Phi_{ij}^{ab} + \sum_{\substack{i<j<k \\ a<b<c}} C_{ijk}^{abc} \Phi_{ijk}^{abc} + \dots \quad (1.36)$$

where C denotes an expansion coefficient. The limits in the summations ensure that a given excited determinant appears only once in the summation. The energy associated with eqn. (1.36) is the exact non-relativistic ground state energy (within the Born-Oppenheimer approximation). The difference between this energy and the Hartree-Fock limit is the correlation energy.

As always, computational considerations limit the practical calculations that are feasible. Firstly, as in the HF-SCF method, it is only feasible to employ finite basis set, meaning that all CSFs are constructed from a finite set of one-electron spin orbitals. Full CI refers to a CI calculation using all the CSFs of the appropriate symmetry for a given finite basis set. The difference between the HF-SCF ground state energy and a full CI calculation using the same basis set is called the basis set correlation energy. In the limit of a complete basis full CI gives the exact wavefunction, and the basis set correlation energy is equal to the correlation energy.

In addition to the limits of the basis set, it is also computationally very demanding to handle large numbers of determinants. Even with a small number of electrons and a small basis the number of determinants quickly becomes very large indeed. Thus it is almost always necessary to truncate eqn. (1.36), e.g. truncation at double excitations gives CI singles-doubles (CISD).

This truncation causes an additional problem besides reducing the accuracy of the method. Full CI is size-consistent, but truncated CI is not. A method is size-consistent if the sum of the energy of two isolated fragments is

⁵a configuration state function is an N -electron Slater determinant constructed from a set of spinorbitals, or a linear combination of a small number of Slater determinants. Thus the Slater determinant that is used to approximate the N -electron wavefunction in Hartree-Fock theory is a CSF, but many more CSFs can be constructed from the same spinorbitals, with one or more electrons promoted from occupied to virtual orbitals.

equal to the energy of those two fragments in a dimer when the internuclear distance is infinite.

1.4.2 Coupled cluster theory

Introduced to quantum chemistry in the late 1960s by Čížek and Paldus [14, 15, 16], the coupled cluster (CC) method, like CI, expresses the wavefunction as a linear combination of Slater determinants. Unlike CI, truncated CC methods are size-consistent. The exact, non-relativistic ground-state molecular electronic wavefunction is given as

$$\Psi = e^{\hat{T}}\Phi_0 \quad (1.37)$$

where Φ_0 is a normalised, ground-state wavefunction⁶ and $e^{\hat{T}}$ is an operator defined as a Taylor-series expansion

$$e^{\hat{T}} \equiv 1 + \hat{T} + \frac{\hat{T}^2}{2!} + \frac{\hat{T}^3}{3!} + \dots = \sum_{k=0}^{\infty} \frac{\hat{T}^k}{k!} \quad (1.38)$$

where the *cluster operator* \hat{T} is

$$\hat{T} \equiv \hat{T}_1 + \hat{T}_2 + \dots + \hat{T}_n \quad (1.39)$$

where n is the number of electrons in the molecule. \hat{T}_1 is the one-particle excitation operator defined as

$$\hat{T}_1\Phi_0 \equiv \sum_{b=n+1}^{\infty} \sum_{i=1}^n t_i^a \Phi_i^a \quad (1.40)$$

where Φ_i^a is a singly excited Slater determinant with the occupied spinorbital ϕ_i replaced by the virtual spinorbital ϕ_a , while t_i^a is a numerical coefficient the value of which is dependent on i and a and is determined by considering (1.37) to be a necessary condition. Similarly \hat{T}_2 is the two-particle excitation operator

$$\hat{T}_2\Phi_0 \equiv \sum_{b=a+1}^{\infty} \sum_{a=n+1}^{\infty} \sum_{j=1+1}^n \sum_{i=1}^{n-1} t_{ij}^{ab} \Phi_{ij}^{ab} \quad (1.41)$$

⁶often, but not necessarily, the Hartree-Fock wavefunction.

Thus the effect of the $e^{\hat{T}}$ operator is to express the wavefunction as a linear combination of Slater determinants that include Φ_0 and all possible excitations of electrons from occupied to virtual spinorbitals. Two approximations are used to make calculations feasible

1. a finite basis set is used to express the spinorbitals
2. not all of the operators $\hat{T}_1 + \hat{T}_2 + \dots + \hat{T}_n$ are used, instead \hat{T} is approximated by using only some of these operators

Two commonly used truncations are the coupled cluster singles and doubles (CCSD)

$$\hat{T} = \hat{T}_1 + \hat{T}_2 \quad (1.42)$$

and CC singles, double and triples (CCSDT)

$$\hat{T} = \hat{T}_1 + \hat{T}_2 + \hat{T}_3 \quad (1.43)$$

1.4.3 Brueckner theory

Brueckner's theory for infinite nuclear matter [17] was first proposed for use with systems of atoms and molecules by Nesbet [18]. For our purposes, Brueckner theory can be considered to be a variant on coupled cluster theory. It is possible to carry out a CCSD calculation in which the effects of the single excitations are absorbed into the orbitals. This was first proposed by Chiles and Dykstra [19] and Handy and co-workers [20, 21, 22] similarly implemented the procedure—which is generally referred to as Brueckner Doubles (BD)—along with a perturbational triplet correction (BD(T)) and analytical energy gradients. The ground state determinant used in the expansion is chosen to have the maximum overlap with the exact wavefunction possible for a single determinant

$$\max\langle\psi|\Phi\rangle \quad (1.44)$$

and the resulting orbitals are called Brueckner orbitals.

1.4.4 Møller-Plesset perturbation theory

Configuration interaction calculations are variational but they have the disadvantage that they are not size-consistent (except for full CI). An alternative method for approaching the correlation energy in a systematic manner arises from perturbation theory. The exact Hamiltonian is expressed in terms of the known Hamiltonian of a simpler system and a correction

$$\hat{H} = \hat{H}^{(0)} + \hat{H}^{(1)} \quad (1.45)$$

The resulting scheme is size-consistent, though energies calculated in this way are not variational.

Perturbation theory applied to molecular systems (or, more generally, systems composed of many interacting particles) is usually referred to as *many-body perturbation theory* (MBPT). When the zeroth-order Hamiltonian is composed of a sum of the Hartree-Fock SCF Fock operators (see eqn. (1.26)) then the procedure is called *Møller-Plesset perturbation theory* (MPPT). The zeroth-order Hamiltonian in MP theory is defined as

$$\hat{H}^{(0)} = \sum_{i=1}^n \hat{F}_i \quad (1.46)$$

The perturbation is expressed in terms of the zeroth-order Hamiltonian

$$\hat{H}^{(1)} = \hat{H} - \sum_{i=1}^n \hat{F}_i \quad (1.47)$$

where \hat{H} is the electronic Hamiltonian, see eqn. (1.9). The Hartree-Fock energy is given by the expectation value

$$E_{\text{HF}} = \langle \Phi_{\text{SD}} | \hat{H} | \Phi_{\text{SD}} \rangle \quad (1.48)$$

or equivalently

$$E_{\text{HF}} = \langle \Phi_{\text{SD}} | \hat{H}^{(0)} + \hat{H}^{(1)} | \Phi_{\text{SD}} \rangle \quad (1.49)$$

Since the zeroth and first order corrections to the energy can be expressed as

$$E^{(0)} = \langle \Phi_{\text{SD}} | \hat{H}^{(0)} | \Phi_{\text{SD}} \rangle \quad (1.50)$$

and

$$E^{(1)} = \langle \Phi_{\text{SD}} | \hat{H}^{(1)} | \Phi_{\text{SD}} \rangle \quad (1.51)$$

it is clear that the Hartree-Fock energy is equal to the sum of the zeroth and first order energy corrections

$$E_{\text{HF}} = E^{(0)} + E^{(1)} \quad (1.52)$$

This implies that second order perturbation theory is required to obtain the first order correction to the ground-state energy

$$E^{(2)} = \sum_{J \neq 0} \frac{\langle \Phi_J | \hat{H}^{(1)} | \Phi_0 \rangle \langle \Phi_0 | \hat{H}^{(1)} | \Phi_J \rangle}{E^{(0)} - E_J} \quad (1.53)$$

This yields the following expression for the second order correction to the energy (the inclusion of which is referred to as MP2)

$$E^{(2)} = -\frac{1}{4} \sum_{ijab} \frac{[(ai|bj) - (aj|bi)]^2}{\epsilon_a + \epsilon_b - \epsilon_i - \epsilon_j} \quad (1.54)$$

which includes contributions from double excitations only, since only doubly excited determinants contribute to the second order energy correction.

Chapter 2

Density functional theory

Density functional theory (DFT) is an alternative approach to the electronic structure problem. This chapter covers early formulations of density functional theory, general proofs of the validity of using the electron density as the fundamental variable in electronic structure calculations and a discussion of Kohn-Sham density functional theory, which is the formalism underpinning the majority of calculations carried out in this work.

Also introduced is the method of Zhao, Morrison and Parr (ZMP) which enables the construction of DFT orbitals, eigenvalues and potentials from electron densities. This is the formalism by which high quality densities will be introduced into DFT calculations, the major component of this thesis.

2.1 The electron density

Expressing the electronic energy in terms of the electron density (as opposed to using the wavefunction of the system) has a number of advantages. While the wavefunction is a (possibly complex) function of $4N$ variables, the electron density is a simple function of three variables (x , y and z , the electronic Cartesian coordinates). Also, the wavefunction is not an observable, while the density is and may be probed through the use of (for example) X-ray diffraction.

The density may be expressed in terms of the wavefunction

$$\rho(\mathbf{r}_1) = N \int \cdots \int |\Psi(\mathbf{x}_1, \mathbf{x}_2, \dots, \mathbf{x}_N)|^2 ds_1 d\mathbf{x}_2 \cdots d\mathbf{x}_N \quad (2.1)$$

such that $\rho(\mathbf{r})d\mathbf{r}_1$ is the probability of finding any of the N electrons in a volume element $d\mathbf{r}_1$ with arbitrary spin, while the $N - 1$ other electrons have arbitrary positions and spin. For finite molecular systems this function is positive everywhere, vanishes at infinity and integrates to the number of electrons

$$\int \rho(\mathbf{r})d\mathbf{r} = N \quad (2.2)$$

2.2 The models of Thomas, Fermi and Dirac

Independently derived by Thomas [23] and Fermi [24] the Thomas-Fermi method sought to determine the effective electric field inside atoms. By making certain assumptions, namely that

1. Relativistic considerations may be neglected;
2. In an atom there exists an effective field that depends only on the distance from the nucleus;
3. Electrons are uniformly distributed at the rate of two for each h^3 of volume (h^3 is a convenient unit of volume in a six-dimensional phase space with three dimensions of space and three of momentum);

4. The potential is determined by the nuclear charge and the electron distribution;

it was possible to derive an expression for the energy of an atom in terms of the electron density.

The Thomas-Fermi kinetic energy expression uses a quantum statistical model of the electrons (based on the uniform electron gas)

$$T_{\text{TF}}[\rho(\mathbf{r})] = \frac{3}{10}(3\pi^2)^{2/3} \int \rho^{5/3}(\mathbf{r}) d\mathbf{r} \quad (2.3)$$

while classical expressions are used for the nuclear-electron and electron-electron interactions

$$V_{\text{ne}} = Z \int \frac{\rho(\mathbf{r})}{r} d\mathbf{r} \quad (2.4)$$

$$V_{\text{ee}} = \frac{1}{2} \int \int \frac{\rho(\mathbf{r})\rho(\mathbf{r}')}{|\mathbf{r} - \mathbf{r}'|} d\mathbf{r} d\mathbf{r}' \quad (2.5)$$

so the Thomas-Fermi expression for the energy of an atom

$$E_{\text{TF}}[\rho(\mathbf{r})] = \frac{3}{10}(3\pi^2)^{2/3} \int \rho^{5/3}(\mathbf{r}) d\mathbf{r} - Z \int \frac{\rho(\mathbf{r})}{r} d\mathbf{r} + \frac{1}{2} \int \int \frac{\rho(\mathbf{r})\rho(\mathbf{r}')}{|\mathbf{r} - \mathbf{r}'|} d\mathbf{r} d\mathbf{r}' \quad (2.6)$$

includes an approximation to the kinetic energy and the classical parts of the nuclear-electron and electron-electron interactions, all in terms of the electron density only. To find the correct electron density, $\rho(\mathbf{r})$, the variational principle is used. The density is varied to minimise $E_{\text{TF}}[\rho(\mathbf{r})]$ subject to the constraint in eqn. (2.2).

The description of the energy of atoms by the Thomas-Fermi model is poor, and it fails to predict molecular binding. This is not surprising, since T_{TF} is a very crude approximation to the kinetic energy and both exchange and correlation are completely neglected. The neglect of the exchange was addressed by Dirac [25] through the inclusion of a term

$$K_{\text{D}}[\rho(\mathbf{r})] = -\frac{3}{4} \left(\frac{3}{\pi} \right)^{1/3} \int \rho^{4/3}(\mathbf{r}) d\mathbf{r} \quad (2.7)$$

but the resulting Thomas-Fermi-Dirac model fails to improve substantially upon the Thomas-Fermi model. However, the importance of these methods is that all parts of the energy are expressed in terms of the electron density.

It should be noted that, at the time these methods were proposed, the validity of expressing the energy in terms of the density and the use of the variational principle were assumptions.

2.3 The Hohenberg-Kohn theorems

Although the models of Thomas, Fermi and Dirac had shown that an expression for the electronic energy in terms of the electron density was feasible and could provide qualitatively correct results for atomic systems, the poor description of atomic energies and the failure to describe molecular binding meant that these first density functional theories were extremely limited. Also, there was no formal proof that the mapping of electron density to electronic energy was valid, nor that use of the variational principle was appropriate.

In 1964 Hohenberg and Kohn published a paper [26] containing two theorems. These showed that the ground state energy is a unique functional of the density and that the representation of the energy in terms of the electron density is a variational method. No new method was proposed in the paper, but it demonstrated that an exact density functional theory existed in principle, and the methods of Thomas, Fermi and Dirac could be considered approximations to this exact theory. The theorems of Hohenberg and Kohn provide the theoretical underpinning of nearly all subsequent development of density functional theory.

2.3.1 Unique determination of the Hamiltonian by the density

The first theorem states that the external potential $v_{\text{ext}}(\mathbf{r})$ is a unique functional of the density $\rho(\mathbf{r})$ (to within a constant). Since the density fixes the number of electrons N and, in turn, N and $v_{\text{ext}}(\mathbf{r})$ fix the Hamiltonian \hat{H} , \hat{H} is a unique functional of $\rho(\mathbf{r})$. To prove this statement, it is sufficient

to consider the contradiction that arises when two external potentials are postulated, $v_{\text{ext}}(\mathbf{r})$ and $v'_{\text{ext}}(\mathbf{r})$, which differ by more than a constant and give rise to the same electron density $\rho(\mathbf{r})$. The corresponding Hamiltonians are

$$\begin{aligned}\hat{H} &= \hat{T} + \hat{V}_{\text{ee}} + \sum_i \hat{v}_{\text{ext}}(\mathbf{r}_i) \\ \hat{H}' &= \hat{T} + \hat{V}_{\text{ee}} + \sum_i \hat{v}'_{\text{ext}}(\mathbf{r}_i)\end{aligned}\quad (2.8)$$

the kinetic energy and Coulomb terms being identical. We can express the relationship of the two potentials to the single, unique density as

$$v_{\text{ext}}(\mathbf{r}) \Rightarrow \hat{H} \Rightarrow \Psi \Rightarrow \rho(\mathbf{r}) \Leftarrow \Psi' \Leftarrow \hat{H}' \Leftarrow v'_{\text{ext}}(\mathbf{r}) \quad (2.9)$$

Since the two wavefunctions Ψ and Ψ' are different, Ψ' can be used as a trial wavefunction for \hat{H} and vice versa. From the variational principle the expectation value from the trial wavefunction must be above the exact energy

$$E_0 < \langle \Psi' | \hat{H} | \Psi' \rangle = \langle \Psi' | \hat{H}' | \Psi' \rangle + \langle \Psi' | \hat{H} - \hat{H}' | \Psi' \rangle \quad (2.10)$$

and since the Hamiltonian operators differ only in their external potential

$$E_0 < E'_0 + \left\langle \Psi' \left| \sum_i v_{\text{ext}}(\mathbf{r}_i) - \sum_i v'_{\text{ext}}(\mathbf{r}_i) \right| \Psi' \right\rangle \quad (2.11)$$

Repeating the above steps for the case where Ψ is used as a trial wavefunction for \hat{H}' yields the equivalent equation

$$E'_0 < E_0 - \left\langle \Psi \left| \sum_i v_{\text{ext}}(\mathbf{r}_i) - \sum_i v'_{\text{ext}}(\mathbf{r}_i) \right| \Psi \right\rangle \quad (2.12)$$

The contradiction becomes clear when equations (2.11) and (2.12) are added together

$$E_0 + E'_0 < E'_0 + E_0 \quad (2.13)$$

This establishes that it is impossible to have two different external potentials that yield the same ground state electron density.

2.3.2 Variational principle

Having established that the ground state density uniquely determines the Hamiltonian, and therefore can (in principle) be used to obtain any properties of interest, it is important to know whether or not a certain density is the ground state density. The second theorem presented by Hohenberg and Kohn states that the energy associated with a certain density is a minimum if and only if the density is the true ground state density $\rho_0(\mathbf{r})$. In other words, the Hohenberg-Kohn formalism is variational.

The ground state energy of a many-electron system may be written

$$E[\rho] = T[\rho] + \int \rho(\mathbf{r})v_{\text{ext}}(\mathbf{r})d\mathbf{r} + V_{\text{ee}}[\rho] \quad (2.14)$$

where the three terms are the kinetic energy, nuclear-electron and electron-electron interactions respectively. Minimising the energy with respect to the density, subject to the constraint

$$\int \rho(\mathbf{r})d\mathbf{r} = N \quad (2.15)$$

gives the Euler-Lagrange equation

$$\mu = \frac{\delta T[\rho]}{\delta \rho(\mathbf{r})} + v_{\text{ext}}(\mathbf{r}) + \frac{\delta V_{\text{ee}}[\rho]}{\delta \rho(\mathbf{r})} \quad (2.16)$$

It should be noted that the variational principle for the Hohenberg-Kohn formalism is valid only for the exact functional which returns the ground state energy of a system for an input density. We do not know the form of the exact functional and are forced to use approximations to it. Therefore, it is not possible to use the principle that the lower the energy returned the better the agreement between the trial density and the exact density.

2.4 Kohn-Sham density functional theory

Although the theorems of Hohenberg and Kohn (Section 2.3) provided the theoretical underpinnings upon which nearly all modern density functional

theory is based, they were simply proofs of existence. They established that the ground state electron density uniquely determines the ground state energy, but they offered no clues as to how a practical functional that returns the energy associated with a density might be constructed.

The Thomas-Fermi (TF) and Thomas-Fermi-Dirac (TFD) methods (Section 2.2) provide expressions for the energy explicitly in terms of the electron density by making drastic assumptions, but the price paid is low accuracy. The TF and TFD models give very poor results, and a major reason for this is their treatment of the kinetic energy. From the virial theorem

$$T \sim -E \quad (2.17)$$

and this implies that an accurate description of the kinetic energy is vital. Kohn and Sham [27] proposed the introduction of orbitals, rather than constructing an energy explicitly in terms of the density, and this led to a simple expression that accounts for a large proportion of the kinetic energy, leaving a small remainder to be handled separately. The exact expression for the ground state kinetic energy, in terms of orbitals, is

$$T = -\frac{1}{2} \sum_i n_i \langle \chi_i | \nabla^2 | \chi_i \rangle \quad (2.18)$$

where χ_i are the natural orbitals and n_i are their occupation numbers. From the Pauli principle the occupation numbers must be in the range $0 \leq n_i \leq 1$. T is a functional of the density since

$$\rho(\mathbf{r}) = \sum_i n_i |\chi_i(\mathbf{r})|^2 \quad (2.19)$$

For any interacting system eqn. (2.18) will involve an infinite number of terms. The problem must be approached differently if progress is to be made.

Within HF-SCF the wavefunction is approximated by a single Slater determinant composed of N spin-orbitals. However, this determinant could also be considered to be the exact wavefunction of a fictitious system of

N non-interacting electrons. The expression for the kinetic energy of this non-interacting system is

$$T_S = -\frac{1}{2} \sum_i^N \langle \chi_i | \nabla^2 | \chi_i \rangle \quad (2.20)$$

and the density becomes

$$\rho(\mathbf{r}) = \sum_i^N |\chi_i(\mathbf{r})|^2 \quad (2.21)$$

Equations (2.20) and (2.21) are the special case of (2.18) and (2.19) where $n_i = 1$ for N orbitals and $n_i = 0$ for the rest. Thus Kohn and Sham invoked a non-interacting reference system with the Hamiltonian

$$\hat{H}_S = -\frac{1}{2} \sum_i^N \nabla_i^2 + \sum_i^N v_S(\mathbf{r}_i) \quad (2.22)$$

which introduces the effective potential $v_S(\mathbf{r})$. Since for a non-interacting system $T[\rho] = T_S[\rho]$ and $V_{ee}[\rho] = 0$ the Euler-Lagrange equation (eqn. (2.16)) in the effective potential $v_S(\mathbf{r})$ becomes

$$\mu = \frac{\delta T_S[\rho]}{\delta \rho(\mathbf{r})} + v_S(\mathbf{r}) \quad (2.23)$$

The ground state wavefunction of the non-interacting system is exactly given by a single Slater determinant (in analogy with eqn. (1.11) but switching to Θ and φ to avoid confusion with the Hartree-Fock equations)

$$\Theta_S = \frac{1}{\sqrt{N!}} \begin{vmatrix} \varphi_1(1) & \varphi_2(1) & \cdots & \varphi_N(1) \\ \varphi_1(2) & \varphi_2(2) & \cdots & \varphi_N(2) \\ \vdots & \vdots & & \vdots \\ \varphi_1(N) & \varphi_2(N) & \cdots & \varphi_N(N) \end{vmatrix} \quad (2.24)$$

The one-particle equations for this non-interacting system are

$$\left[-\frac{1}{2} \nabla^2 + v_S(\mathbf{r}) \right] \varphi_i = \epsilon_i \varphi_i \quad (2.25)$$

The connection of this fictitious system to the real system of interest is achieved through the selection of the effective potential $v_S(\mathbf{r})$. To see how this is possible an alternative expression for the energy is now introduced.

The exact energy may be written as the sum of the kinetic energy, the nuclear-electron interaction and the electron-electron interaction

$$E[\rho] = T[\rho] + \int \rho(\mathbf{r})v_{\text{ext}}(\mathbf{r})d(\mathbf{r}) + V_{\text{ee}}[\rho] \quad (2.26)$$

Kohn and Sham defined a term called the exchange-correlation energy

$$E_{\text{xc}}[\rho] = (T[\rho] - T_S[\rho]) + (V_{\text{ee}}[\rho] - J[\rho]) \quad (2.27)$$

where $J[\rho]$ is the coulomb term (first encountered in the context of Hartree-Fock theory, in eqn. (1.14))

$$J[\rho] = \frac{1}{2} \int \int \frac{\rho(\mathbf{r})\rho(\mathbf{r}')}{|\mathbf{r} - \mathbf{r}'|} d\mathbf{r}d\mathbf{r}' \quad (2.28)$$

and hence the exchange-correlation energy contains the difference between the exact kinetic energy and the kinetic energy of the non-interacting system and all the non-classical parts of the electron-electron interactions. The energy expression can now be rewritten

$$E[\rho] = T_S[\rho] + \int \rho(\mathbf{r})v_{\text{ext}}(\mathbf{r})d(\mathbf{r}) + J[\rho] + E_{\text{xc}}[\rho] \quad (2.29)$$

Minimising the energy expression with respect to the density (under the constraint that the orbitals remain orthonormal, eqn. (2.2)) gives the Euler-Lagrange equation

$$\mu = \frac{\delta T_S[\rho]}{\delta \rho(\mathbf{r})} + v_{\text{eff}}(\mathbf{r}) \quad (2.30)$$

where the Kohn-Sham effective potential

$$\begin{aligned} v_{\text{eff}}(\mathbf{r}) &= v_{\text{ext}}(\mathbf{r}) + \frac{\delta J[\rho]}{\delta \rho(\mathbf{r})} + \frac{\delta E_{\text{xc}}[\rho]}{\delta \rho(\mathbf{r})} \\ &= v_{\text{ext}}(\mathbf{r}) + \int \frac{\rho(\mathbf{r}')}{|\mathbf{r} - \mathbf{r}'|} d\mathbf{r}' + v_{\text{xc}}(\mathbf{r}) \end{aligned} \quad (2.31)$$

which in turn defines the exchange-correlation potential

$$v_{\text{xc}}(\mathbf{r}) = \frac{\delta E_{\text{xc}}[\rho]}{\delta \rho(\mathbf{r})} \quad (2.32)$$

Comparing eqn. (2.30) and eqn. (2.23) it is clear that if

$$v_S = v_{\text{eff}} \quad (2.33)$$

then the Euler equations are identical. In this way, it is possible to obtain an exact expression for the energy in independent particle form, with the only unknown being the form of $E_{\text{xc}}[\rho]$. The Kohn-Sham orbitals are obtained from N one-electron equations

$$\left[-\frac{1}{2}\nabla^2 + v_{\text{ext}}(\mathbf{r}) + \int \frac{\rho(\mathbf{r}')}{|\mathbf{r} - \mathbf{r}'|} d\mathbf{r}' + v_{\text{xc}}(\mathbf{r}) \right] \varphi_i(\mathbf{r}) = \epsilon_i \varphi_i(\mathbf{r}) \quad (2.34)$$

$v_{\text{eff}}(\mathbf{r})$ depends on $\rho(\mathbf{r})$ so the equations (2.34) must be solved self-consistently. A guess is made for $\rho(\mathbf{r})$, $v_{\text{eff}}(\mathbf{r})$ is constructed and a new $\rho(\mathbf{r})$ generated via

$$\rho(\mathbf{r}) = \sum_i^N |\varphi_i(\mathbf{r})|^2 \quad (2.35)$$

This process is repeated until convergence is reached. Once a density has been constructed the energy may be determined using

$$\begin{aligned} E[\rho] = & -\frac{1}{2} \sum_i^N \langle \varphi_i | \nabla^2 | \varphi_i \rangle + \int \rho(\mathbf{r}) v_{\text{ext}}(\mathbf{r}) d\mathbf{r} \\ & + \frac{1}{2} \int \int \frac{\rho(\mathbf{r})\rho(\mathbf{r}')}{|\mathbf{r} - \mathbf{r}'|} d\mathbf{r} d\mathbf{r}' + E_{\text{xc}}[\rho] \end{aligned} \quad (2.36)$$

where the first term is the kinetic energy of the non-interacting system; the second is the nuclear-electron attraction; the third term is the classical coulomb interaction of the electrons and the fourth term is the exchange-correlation energy.

Several parallels may be drawn between the Kohn-Sham (2.34) and the Hartree-Fock equations (1.20). The first three terms in both equations are the kinetic energy, the external potential due to the nuclei and the Coulomb potential due to the electron-electron interaction. Since the Coulomb term depends on the orbitals the Kohn-Sham one-electron equations, like the Hartree-Fock equations, must be solved in a self-consistent, iterative manner. The only difference between the equations is that the non-multiplicative

exchange operator is replaced by the multiplicative exchange-correlation potential.

In this work the procedure of obtaining the electronic energy via (2.36) using the Kohn-Sham orbitals defined in (2.34) is denoted Kohn-Sham density functional theory (KS-DFT).

2.5 Hartree-Fock-Kohn-Sham theory

In most approximations to the exchange correlation energy a separation is made into exchange and correlation components

$$E_{xc}[\rho] = E_x[\rho] + E_c[\rho] \quad (2.37)$$

Since the exchange energy can be written explicitly in terms of orbitals (and hence, indirectly, in terms of the density)

$$E_x[\rho] = - \int \int \frac{\rho_1(\mathbf{r}, \mathbf{r}')^2}{|\mathbf{r} - \mathbf{r}'|} d\mathbf{r} d\mathbf{r}' \quad (2.38)$$

it is possible to include exchange exactly in the Kohn-Sham scheme, leaving the unknown functional the task of approximating the correlation energy (a small fraction of $E_{xc}[\rho]$) and the difference between the exact kinetic energy and the kinetic energy of the non-interacting system. The inclusion of exchange in this way was first suggested by Kohn and Sham [27] and in this thesis it is referred to as Hartree-Fock-Kohn-Sham (HFKS) theory.

The one-particle equations become

$$\left[-\frac{1}{2}\nabla^2 + v_{\text{ext}}(\mathbf{r}) + v_J(\mathbf{r}) + v_C(\mathbf{r}) \right] \varphi_i(\mathbf{r}) - \int \frac{\rho_1(\mathbf{r}, \mathbf{r}')}{|\mathbf{r} - \mathbf{r}'|} \varphi_i(\mathbf{r}') d\mathbf{r}' = \epsilon_i \varphi_i(\mathbf{r}) \quad (2.39)$$

Here $v_C(\mathbf{r})$ is the correlation potential

$$v_C(\mathbf{r}) = \frac{\delta E_c[\rho]}{\delta \rho(\mathbf{r})} \quad (2.40)$$

just as $v_{xc}(\mathbf{r})$ is the exchange-correlation potential (eqn. (2.32)). The energy is now expressed

$$\begin{aligned}
E_{\text{HFKS}}[\rho] &= E_{\text{HF}}[\{\varphi_i\}] + E_{\text{C}}[\rho] \\
&= -\frac{1}{2} \sum_i \langle \varphi_i | \nabla^2 | \varphi_i \rangle + \int \rho(\mathbf{r}) v_{\text{ext}}(\mathbf{r}) d\mathbf{r} \\
&\quad + \frac{1}{2} \int \int \frac{\rho(\mathbf{r})\rho(\mathbf{r}')}{|\mathbf{r} - \mathbf{r}'|} d\mathbf{r}d\mathbf{r}' - \int \int \frac{\rho(\mathbf{r}, \mathbf{r}')^2}{|\mathbf{r} - \mathbf{r}'|} d\mathbf{r}d\mathbf{r}' + E_{\text{C}}[\rho] \quad (2.41)
\end{aligned}$$

The Hartree-Fock-Kohn-Sham method will be used extensively in Chapter 3.

2.6 Exchange-correlation functionals

If the exact form of the exchange-correlation functional were known then KS-DFT would return the exact, ground-state, non-relativistic energy within the Born-Oppenheimer approximation, including the effects of electron correlation. However, the exact form of the functional is not known and therefore approximate forms must be employed. Many of these will be used later in this thesis.

2.7 Local density approximation

In the case of an inhomogeneous system with a density $\rho(\mathbf{r})$, the local density approximation (LDA) approximates the exchange correlation energy as:

$$E_{\text{xc}}[\rho] = \int \rho(\mathbf{r}) \varepsilon_{\text{xc}}(\rho) d\mathbf{r} \quad (2.42)$$

where ε_{xc} is the exchange-correlation energy per electron in a homogeneous electron gas of constant density. This may be divided into exchange and correlation parts

$$\varepsilon_{\text{xc}}(\rho) = \varepsilon_{\text{x}}(\rho) + \varepsilon_{\text{c}}(\rho) \quad (2.43)$$

The exchange term is given by [28]

$$\varepsilon_{\text{x}}^{\text{LDA}}(\rho) = -\frac{3}{4} \left(\frac{3}{\pi} \right)^{1/3} \rho^{1/3}(\mathbf{r}) \quad (2.44)$$

which gives the Dirac expression (eqn. (2.7)) for the exchange energy

$$E_x^{\text{LDA}}[\rho] = -\frac{3}{4} \left(\frac{3}{\pi}\right)^{1/3} \int \rho^{4/3}(\mathbf{r}) d\mathbf{r} \quad (2.45)$$

There is no corresponding explicit expression for the correlation energy per electron, $\varepsilon_c(\rho)$. Instead, accurate values for $\varepsilon_c(\rho)$ have been determined using quantum Monte-Carlo calculations [29] and Vosko, Wilk and Nusair (VWN) [30] interpolated these values to obtain an analytical form for $\varepsilon_c(\rho)$.

The local density approximation has proved remarkably accurate considering its simplicity. It generally gives good results for bond lengths, bond angles and vibrational frequencies [31, 32, 33]. However, the LDA has a strong overbinding tendency [34], often of the order of >20 kcal mol⁻¹ per bond. It has been shown [35] that many such discrepancies result from errors in the LDA approximation to the exchange energy.

2.8 Generalised gradient approximation

The local density approximation is obviously incorrect as the electron density in an atom or molecule is not uniformly distributed. In the generalised gradient approximation (GGA) a correction based on the gradient of the density is added to eqn. (2.42) to account for this. In other words, the exchange-correlation energy density $\epsilon_{\text{xc}}[\rho]$ is a function of $\rho(\mathbf{r})$ and its gradient.

The lowest order gradient correction (LGC) for exchange is

$$E_x^{\text{LGC}} = E_x^{\text{LDA}} - \beta \sum_{\sigma} \int \frac{(\nabla \rho_{\sigma}(\mathbf{r}))^2}{\rho_{\sigma}^{4/3}(\mathbf{r})} d\mathbf{r} \quad (2.46)$$

where β is a constant. This is uniquely determined by dimensional analysis [36, 37]. However, this functional has severe problems. In particular, the corresponding exchange potential diverges asymptotically and thus requires adjustment for any practical application.

2.8.1 B86

In an attempt to correct this problem, Becke [38] introduced a modified gradient-corrected exchange-energy functional, referred to as B86

$$E_x = E_x^{\text{LDA}} - \beta \sum_{\sigma} \int \rho_{\sigma}^{4/3} \frac{x_{\sigma}^2}{(1 + \gamma x_{\sigma}^2)} d\mathbf{r} \quad (2.47)$$

where x_{σ} is the dimensionless ratio

$$x_{\sigma} = \frac{|\nabla \rho_{\sigma}|}{\rho_{\sigma}^{4/3}} \quad (2.48)$$

and β and γ are parameters chosen by a least-squares fit to atomic data, meaning that the functional is semi-empirical. Unlike eqn. (2.46) the exchange potential is well-behaved in the asymptotic exponential tail of charge distribution. However, the asymptotic behaviour of (2.47) is incorrect.

2.8.2 B88

This led Becke [39] to propose a new functional that reproduces the exact asymptotic behaviour of the exchange-energy density of a finite many-electron system

$$\lim_{r \rightarrow \infty} U_x^{\sigma} = -\frac{1}{r} \quad (2.49)$$

(where U_x^{σ} is the Coulomb potential of the exchange charge density) and the asymptotic behaviour of the spin density [40], given by

$$\lim_{r \rightarrow \infty} \rho_{\sigma} = e^{-a_{\sigma} r} \quad (2.50)$$

where a_{σ} is a constant related to the ionisation potential of the system. This functional, referred to as B88, has the form

$$E_x = E_x^{\text{LDA}} - \beta \sum_{\sigma} \int \rho_{\sigma}^{4/3} \frac{x_{\sigma}^2}{(1 + 6\beta x_{\sigma} \sinh^{-1} x_{\sigma})} d\mathbf{r} \quad (2.51)$$

where β is a constant. This parameter was determined by a least-squares fit to exact atomic Hartree-Fock data, and a best-fit value of $\beta = 0.0042$ au is quoted. It should be noted that, although the exchange-energy *density* has the correct r^{-1} asymptotic behaviour, the *potential* has a form of r^{-2} , not the correct r^{-1} .

2.8.3 LYP

The Lee-Yang-Parr (LYP) correlation functional [41] is based on an approximate correlation energy formula for helium by Colle and Salvetti [42] and involves the gradient and the laplacian. Integration by parts eliminates the laplacian [43] and for closed shell systems

$$E_C = - a \int \frac{\rho}{1 + d\rho^{-1/3}} d\mathbf{r} - ab \int \omega \rho^2 \left[C_F \rho^{8/3} + |\nabla \rho|^2 \left(\frac{5}{12} - \delta \frac{7}{72} \right) \right] - \frac{11}{24} \rho^2 |\nabla \rho|^2 d\mathbf{r} \quad (2.52)$$

where

$$\omega = \frac{\exp(-c\rho^{-1/3})}{1 + d\rho^{-1/3}} \rho^{-11/3} \quad (2.53)$$

$$\delta = c\rho^{-1/3} + \frac{d\rho^{-1/3}}{1 + d\rho^{-1/3}}. \quad (2.54)$$

Here a , b , c and d are the Colle-Salvetti parameters and $a = 0.04918$, $b = 0.132$, $c = 0.2533$ and $d = 0.349$.

2.8.4 HCTH

HCTH [44] is an empirical GGA functional that employs the same functional form as B97 [45], but does not include orbital exchange. The fifteen parameters of the functional were determined by fitting to thermochemical data and ZMP exchange-correlation potentials for a set of 93 atoms and molecules. For more details on the development of functionals that have flexible functional forms with many parameters determined through a least-squares fit, see refs. [46, 47, 48].

2.8.5 1/4

The 1/4 functional [49] is a GGA having the same functional form as HCTH, but fitted solely to ZMP potentials for the 93 systems used in the HCTH fit. No thermochemical data was explicitly included in the fitting procedure. Geometries determined using 1/4 are generally an improvement over HCTH.

2.8.6 PBE

PBE is a non-empirical functional developed by Perdew, Burke and Ernzerhof [50]. It is designed to satisfy exact conditions, but only in energetically important regions, simplifying it in comparison with many previous GGA functionals. It uses only fundamental constants as parameters.

2.8.7 KT2

KT2 is the second of a series of functionals developed by Keal and Tozer [51] with the aim of improving the description of shielding constants using GGA functionals. The first in the series, KT1, uses a mathematical form (the LDA functional augmented with a second-order exchange-gradient expansion-based term) chosen such that its potential exhibits structure close to that of high-quality potentials. The parameters defining the gradient correction were optimised against experimental shielding constant results. KT2 utilises the same form as KT1, except that the LDA exchange and correlation terms are scaled by fitting to atomisation energies and ionisation potentials, which has the effect of relaxing the uniform gas condition.

2.9 Hybrid functionals

The combining of density functional theory and the Hartree-Fock method has an obvious attraction when their—seemingly complementary—respective strengths are considered. Hartree-Fock provides a treatment of exchange that is both exact and scales well with molecular size, while ignoring electron correlation. Extensions to HF that take into account electron correlation are complicated and in general do not scale well with molecular size. Density functional theory, on the other hand, includes correlation and is simple and cheap to implement.

However, a simplistic addition of electron gas correlation to Hartree-Fock energies has proven extremely weak in thermochemical tests [52]. If exchange

is treated exactly and an approximate form used for the correlation only then, for the LDA form of the correlation energy

$$E_{\text{xc}} = E_{\text{x}} + E_{\text{c}}^{\text{LDA}} \quad (2.55)$$

where E_{x} is the exchange energy of the Slater determinant of the Kohn-Sham orbitals and $E_{\text{c}}^{\text{LDA}}$ is the local density approximation correlation energy. Note that E_{x} is not the conventional Hartree-Fock exchange energy, as Kohn-Sham and Hartree-Fock orbitals are not the same. However, this approximation is often made.

The above formulation has proved useful in atomic applications [53, 54], but cannot describe molecular bonding. The difficulty relates to the separation of the correlation energy into dynamic and non-dynamic components (see Section 1.4). Hartree-Fock exchange, plus dynamic correlation plus non-dynamic correlation gives the exact exchange-correlation energy. However, because of the nature of the local approximations to the exchange-correlation energy, the breakdown of the components of the energy is not straightforward. In general, the GGA exchange energy picks up not only the exchange energy but also the non-dynamic correlation energy. This does not cause a problem when used in conjunction with a GGA approximation to the correlation energy, as these only model the dynamic correlation. Thus when GGA correlation energy is added to exact (Hartree-Fock) exchange, the non-dynamic correlation energy is not accounted for. This will be considered in more detail in Chapter 3.

An alternative partitioning, proposed by Becke [55], was designed to ameliorate this problem. If we define an interelectronic coupling-strength parameter, λ , and U_{xc}^{λ} is the potential energy of exchange-correlation at coupling strength λ then

$$E_{\text{xc}} = \int_0^1 U_{\text{xc}}^{\lambda} d\lambda. \quad (2.56)$$

λ effectively “switches on” the $\frac{1}{r}$ Coulomb repulsion between electrons. This is a rigorous *ab initio* definition of the Kohn-Sham exchange-correlation energy and is known as the “adiabatic connection”. *Ab initio* calculation of

exchange-correlation energies from eqn. (2.56) is, of course, impractical, but it provides the starting point for the development of approximate functionals.

A first approximation to the integral eqn. (2.56) is a linear interpolation

$$E_{\text{xc}} \simeq \frac{1}{2}U_{\text{xc}}^0 + \frac{1}{2}U_{\text{xc}}^1 \quad (2.57)$$

U_{xc}^0 is the exchange-correlation energy of the non-interacting reference system, which is the pure exchange energy of the Kohn-Sham Slater determinant and can, therefore, be evaluated exactly. U_{xc}^1 is the exchange-correlation energy of the fully interacting system.

The above method explains the basic principle of Becke's hybridisation of Kohn-Sham DFT and Hartree-Fock methods. However, despite performing well for energy differences, total energies are poor within this methodology. To address this, and several other shortcomings of the basic "half-and-half" methodology, Becke [56] introduced an extension to the previous work that included gradient corrections and relaxed the linear λ dependence. The exchange-correlation approximation now becomes

$$E_{\text{xc}} = E_{\text{xc}}^{\text{LDA}} + a_0(E_{\text{x}}^{\text{exact}} - E_{\text{x}}^{\text{LDA}}) + a_{\text{x}}\Delta E_{\text{x}}^{\text{B88}} + a_{\text{c}}\Delta E_{\text{c}}^{\text{PW91}} \quad (2.58)$$

where $E_{\text{xc}}^{\text{LDA}}$ is the exchange-correlation functional from the local density approximation, $E_{\text{x}}^{\text{exact}}$ is the exact exchange energy and $E_{\text{x}}^{\text{LDA}}$ is the exchange energy of the local density approximation. $\Delta E_{\text{x}}^{\text{B88}}$ is Becke's 1988 gradient correction to the LDA for exchange [39] and $\Delta E_{\text{c}}^{\text{PW91}}$ is Perdew and Wang's 1991 gradient correction for correlation [57]. a_0 , a_{x} and a_{c} are semiempirical coefficients determined by fitting to experimental data. Optimised parameters are $a_0 = 0.20$, $a_{\text{x}} = 0.72$ and $a_{\text{c}} = 0.81$ and this formulation is designated B3P86.

2.9.1 B3LYP

The B3LYP functional [58] has the same form as B3P86 and uses the same parameters but uses the Lee-Yang-Parr correlation functional in place of Perdew and Wang's. Since LYP has no easily separable local component the

VWN local correlation expression is used to provide the different coefficients of local and gradient corrected correlation functionals

$$E_{XC}^{B3LYP} = E_{XC}^{LDA} + a_0(E_X^{\text{exact}} - E_X^{LDA}) + a_X \Delta E_X^{B88} + a_C \Delta E_C^{LYP} + (1 - a_C) E_C^{VWN} \quad (2.59)$$

2.9.2 B97

Becke [45] has introduced a 10 parameter functional, denoted B97, that includes a fraction of exact exchange and is optimised in a non-self consistent manner using only energetic data.

$$E_{XC}^{B97} = E_{GGA}^{B97} + c_X E_X^{\text{HF}} \quad (2.60)$$

The GGA part is separated into exchange and correlation parts, thus

$$E_{GGA}^{B97} = E_X + E_C \quad (2.61)$$

where the exchange part

$$E_X = \sum_{\sigma} \int e_{X\sigma}^{\text{LSDA}}(\rho_{\sigma}) g_{X\sigma}(s_{\sigma}^2) d\mathbf{r} \quad (2.62)$$

$$g_X = \sum_{i=0}^m c_{X\sigma,i} u_{X\sigma}^i \quad (2.63)$$

$$u_{X\sigma} = \gamma_{X\sigma} s_{\sigma}^2 (1 + \gamma_{X\sigma} s_{\sigma}^2)^{-1} \quad (2.64)$$

where $\gamma_{X\sigma} = 0.004$. The correlation part is separated into parallel ($\sigma\sigma$) and antiparallel ($\alpha\beta$) spin correlation functionals

$$E_C = \sum_{\sigma} E_{C\sigma\sigma} + E_{C\alpha\beta} \quad (2.65)$$

where the parallel functional

$$E_{C\sigma\sigma} = \int e_{C\sigma\sigma}^{\text{LSDA}}(\rho_{\sigma}) g_{C\sigma\sigma}(s_{\sigma}^2) d\mathbf{r} \quad (2.66)$$

$$g_{C\sigma\sigma} = \sum_{i=0}^m c_{C\sigma\sigma,i} u_{C\sigma\sigma}^i \quad (2.67)$$

$$u_{C\sigma\sigma} = \gamma_{C\sigma\sigma} s_{\sigma}^s (1 + \gamma_{C\sigma\sigma} s_{\sigma}^2)^{-1} \quad (2.68)$$

where $\gamma_{C\sigma\sigma} = 0.2$. The antiparallel functional

$$E_{C\alpha\beta} = \int e_{C\alpha\beta}^{\text{LSDA}}(\rho_{\alpha}, \rho_{\beta}) g_{C\alpha\beta}(s_{\text{avg}}^2) d\mathbf{r} \quad (2.69)$$

$$g_{C\alpha\beta} = \sum_{i=0}^m c_{C\alpha\beta,i} u_{C\alpha\beta}^i \quad (2.70)$$

$$u_{C\alpha\beta} = \gamma_{C\alpha\beta} s_{\text{avg}}^s (1 + \gamma_{C\alpha\beta} s_{\text{avg}}^2)^{-1} \quad (2.71)$$

$$s_{\sigma}^2 = |\nabla\rho_{\sigma}|^2 \rho_{\sigma}^{-8/3} \quad (2.72)$$

$$s_{\text{avg}}^2 = \frac{1}{2}(s_{\alpha}^2 + s_{\beta}^2) \quad (2.73)$$

where $\gamma_{C\alpha\beta} = 0.006$.

2.9.3 B97-1

B97-1 [44] is a ten parameter hybrid functional using the same functional form as B97, fitted to thermochemical data for the 93 systems used in the fitting procedure for HCTH. Results are comparable to or more accurate than those of B3LYP.

2.9.4 B97-2

B97-2 [59] takes the same form as B97-1 except it was determined by fitting to both thermochemical data and high quality potentials (modified to take in to account the presence of orbital exchange) for the same 93 systems. It improves upon B97-1 for reaction barriers, polarisabilities and NMR shieldings. Other quantities are comparable.

2.9.5 PBE0

PBE0 [60, 61] is a hybrid analogue of the PBE GGA functional. The fraction of exact-exchange included (25%) was chosen from perturbation theory considerations [62].

2.10 The Zhao, Morrison and Parr (ZMP) method for the calculation of exchange-correlation potentials

The Kohn-Sham orbitals, orbital energies, exchange-correlation potentials and kinetic energies associated with a ground state density $\rho_0(\mathbf{r})$ can be obtained from the Zhao, Morrison and Parr (ZMP) method [63, 64, 65]. This method begins with Levy and Perdew's constrained search minimisation procedure [66]. The electron nuclear attraction, Coulomb and exchange-correlation energy are explicit functionals of the density. If only orbitals that yield the exact density are considered, then the Kohn-Sham orbitals are those that minimise the non-interacting kinetic energy

$$T_s[\rho] = \min_{\Theta \rightarrow \rho_0} \langle \Theta | \hat{T} | \Theta \rangle \quad (2.74)$$

where \hat{T} is the kinetic energy operator $-\frac{1}{2} \sum_i \nabla_i^2$ and Θ is the Slater determinant composed of the Kohn-Sham orbitals φ_i . The orbital constraint is written

$$\sum_i^N |\varphi_i|^2 = \rho_0(\mathbf{r}) \quad (2.75)$$

and to enforce this constraint ZMP imposed that the self-repulsion be zero

$$C[\rho, \rho_0] = \frac{1}{2} \int \int \frac{[\rho(\mathbf{r}) - \rho_0(\mathbf{r})][\rho(\mathbf{r}') - \rho_0(\mathbf{r}')]}{|\mathbf{r} - \mathbf{r}'|} d\mathbf{r} d\mathbf{r}' = 0 \quad (2.76)$$

To find extrema of a function $f(x)$ (in this case, the minimum) with the constraint that $g(x) = 0$, another function is introduced

$$F(x, \lambda) = f(x) + \lambda g(x) \quad (2.77)$$

where λ is the Lagrange multiplier. Differentiating F with respect to x and λ gives a system of equations that, equated to zero, must be satisfied at any point where a constrained minimum occurs. Minimisation with respect to the form of the orbitals gives the orbital equations

$$\left[-\frac{1}{2}\nabla^2 + v_c^\lambda(\mathbf{r}) \right] \varphi_i^\lambda(\mathbf{r}) = \epsilon_i^\lambda \varphi_i^\lambda(\mathbf{r}) \quad (2.78)$$

where the superscript λ indicates a dependence on the value of the Lagrange multiplier and

$$v_c^\lambda(\mathbf{r}) = \lambda \int \frac{\rho(\mathbf{r}') - \rho_0(\mathbf{r}')}{|\mathbf{r} - \mathbf{r}'|} d\mathbf{r}' \quad (2.79)$$

To bring (2.78) into the usual Kohn-Sham form two additional terms are added to the minimisation; the electron-nuclear attraction energy and the Coulomb energy so that eqn. (2.78) becomes

$$\left[-\frac{1}{2}\nabla^2 + v_{\text{ext}}(\mathbf{r}) + v_J^\lambda(\mathbf{r}) + v_c^\lambda(\mathbf{r}) \right] \varphi_i = \epsilon_i \varphi_i \quad (2.80)$$

where

$$v_J^\lambda(\mathbf{r}) = \int \frac{\rho^\lambda(\mathbf{r}')}{|\mathbf{r}' - \mathbf{r}|} d\mathbf{r}' \quad (2.81)$$

(Because the electron-nuclear and Coulomb energies are explicit functionals of the density they may be added to the Perdew-Levy minimisation without affecting the final orbitals.) The Coulomb potential is multiplied by the Fermi-Amaldi factor

$$\left(1 - \frac{1}{N} \right) \quad (2.82)$$

such that the final form of the orbital equation is

$$\left[-\frac{1}{2}\nabla^2 + v_{\text{ext}}(\mathbf{r}) + \left(1 - \frac{1}{N} \right) v_J^\lambda + v_c^\lambda(\mathbf{r}) \right] \varphi_i^\lambda(\mathbf{r}) = \epsilon_i^\lambda \varphi_i^\lambda(\mathbf{r}) \quad (2.83)$$

The inclusion of this factor speeds convergence and increases numerical stability, and also ensures the correct long-range behaviour of v_{xc} . In the limit as λ tends to infinity

$$v_{\text{xc}} = \lim_{\lambda \rightarrow \infty} \left[v_c^\lambda - \frac{1}{N} v_J^\lambda \right] \quad (2.84)$$

and the last term ensures the correct $-\frac{1}{r}$ behaviour. Since φ_i are the Kohn-Sham orbitals, equations (2.83) are the Kohn-Sham equations and ϵ_i are the

Kohn-Sham energies. Thus given $\rho_0(\mathbf{r})$ it is possible to solve eqn. (2.83) self-consistently.

In practice the exact density is not known, so theoretical approximations must be used. The use of finite basis sets means that the constraint in (2.76) cannot be satisfied [67]. It is therefore necessary to use a finite value of a Lagrange multiplier λ . Previous investigations [67, 68] suggest that $\lambda = 900$ is appropriate.

2.11 This thesis

The primary aim of the work described in this thesis is the development of novel applications of the ZMP method to

1. provide benchmark values against which DFT calculations of molecular properties might be compared. The better the quality of the density supplied to the ZMP calculation, the better the quality of the resulting Kohn-Sham orbitals, eigenvalues and potentials. A ZMP calculation using a high-quality *ab initio* density will indicate the potential accuracy available within the Kohn-Sham formalism for a given basis set. Comparison with conventional DFT calculations will then indicate how well a particular exchange-correlation functional performs.
2. aid understanding of the performance of DFT calculations. By comparing ZMP orbitals, eigenvalues and potentials with the corresponding Kohn-Sham quantities determined using conventional exchange-correlation functionals, it is often possible to rationalise the performance of such functionals.
3. provide insight into possible new methodologies. Just as ZMP quantities may provide insight into the performance of conventional functionals, they may also suggest new directions for functional development or corrections to existing functionals.

In Chapter 3 the first use of the ZMP method to calculate Kohn-Sham dispersion forces is presented. A relation between the forces and the electron density is exploited to make explicit the relation between the correlation potential and the accuracy of DFT dispersion forces. Previous work [69] has shown that ZMP calculations can determine NMR shielding constants to high accuracy. Chapter 4 extends this to chemical shifts and then goes on to consider electrical as well as magnetic response properties (static polarisabilities and vertical excitation energies). Kohn-Sham orbitals and eigenvalues are known to play an important role in the determination of such response properties, and in Chapter 5 explicit consideration is given to such quantities, using eigenvalues and eigenvalue differences determined from ZMP calculations. Chapter 6 presents an application of the B97-2 semi-empirical exchange-correlation functional, which was fitted to both thermochemical data and multiplicative exchange-correlation potentials determined using the ZMP approach. The *gauche* conformational preference of a class of organic molecules is investigated. All calculations use the CADPAC program [70].

Chapter 3

Dispersion forces and correlation potentials in He₂

In this chapter, high quality electron densities are used to help understand dispersion interactions in DFT. The majority of studies of dispersion interactions determine the variation of the electronic energy when systems interact, but here an alternative approach is taken, considering the forces on the nuclei.

Using the electrostatic theorem of Feynman it can be shown that the interaction forces can be understood in terms of distortion of densities. Within the Hartree-Fock-Kohn-Sham formalism (see Section 2.5) this density distortion (and hence the force) is determined solely by the correlation potential. The density distortion and the correlation potentials that give rise to the density distortions are investigated for the case of the helium dimer. Related potentials are also presented for the H₂ molecule.

3.1 Intermolecular interactions

The phrase 'intermolecular interactions' generally refers to forces between neutral, closed shell atoms or molecules that have no tendency to form chemical bonds. The evidence for the existence of such forces is readily apparent. The fact that condensed phases of matter exist at all, indicates that there must exist attractive forces at long-range. Equally, since these condensed phases have a definite density and are not easily compressed, at short range the forces become repulsive.

This behaviour is visualised in Figure 3.1, which illustrates the variation of the interaction energy of a pair of atomic or molecular systems as a function of their separation R . The lowering of the energy at long-range (relative to the isolated molecules) means that an attractive force exists between the systems in this region. A sharp increase in the interaction energy (becoming positive relative to the isolated molecules) at short range indicates the repulsive forces that resist compression. The minimum (R_e) is the equilibrium separation of the system, where the attractive and repulsive forces are balanced.

The attractive and repulsive forces that constitute intermolecular interactions may be subdivided into separate contributions, each of which may be identified with a specific physical phenomenon. The contributions to the long-range forces are [71]:

1. electrostatic – the classical interaction between the static charge distributions of two molecules. Both molecules must have a permanent electric multipole (at its simplest, an electrical charge, but this could also be a dipole or higher multipole). The electrostatic interaction may be attractive or repulsive, and this will depend on the charge distribution of the molecules and their relative orientation.
2. induction – the interaction between a distorted molecule and its neighbours. For example, a polar molecule near a polarisable molecule (which might itself be polar) can distort the second molecule's charge distribution. The interaction between this *induced* multipole and the

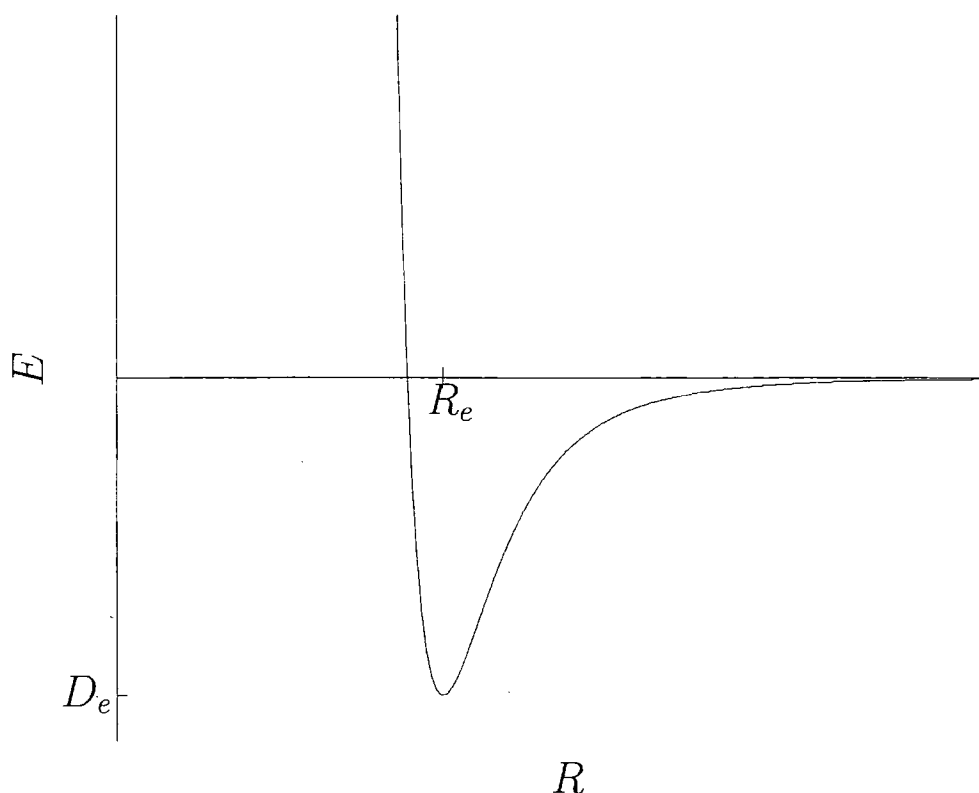


Figure 3.1: Typical intermolecular potential energy function.

original multipole gives rise to an attractive force. This is often referred to as a dipole-induced dipole interaction.

3. dispersion – there is no simple classical picture that explains the dispersion interaction, but it arises because of the coupling between constantly fluctuating electron densities. Dispersive interactions exist between all systems, whether nonpolar, polar or charged. They are always attractive.

For short range forces, the most important contribution is from the exchange (or overlap) repulsion. Other effects arise because of modifications to the electrostatic, induction and dispersion interactions when the disparate systems overlap to a significant degree.

3.1.1 Supermolecular calculations and basis set superposition error

An obvious way to proceed when considering interaction energies is the supermolecule method: the interaction energy is taken to be the difference between the energy of the interacting system and the sum of the energies of the separate molecules. For a pair of molecules, A and B

$$E_{\text{int}} = E_{AB} - E_A - E_B. \quad (3.1)$$

The procedure is attractively straightforward, but this beguiling simplicity conceals unexpected complications that mean that the method must be employed with caution.

When two monomers are brought together and a calculation is performed on the resulting supermolecule, then the basis set of each monomer becomes available to the other. Thus, if the interaction energy is calculated in the obvious way

$$E_{\text{int}}^0 = E_{AB}(AB) - E_A(A) - E_B(B) \quad (3.2)$$

where $E_{AB}(AB)$ denotes the energy of the dimer system using the basis sets of A and B , while $E_A(A)$ is the energy of system A using basis (A) only, then the improved description of the monomers in the supermolecule calculation will lead to an artificial lowering of the energy relative to the isolated monomers. This error is the basis set superposition error (BSSE) and is simply a result of the inability to use infinite basis sets.

The procedure used to correct for this error is the so-called 'counterpoise correction' suggested by Boys and Bernardi [72]. All calculations, those on the isolated monomers as well as the supermolecule, are performed using the supermolecular basis set, so the BSSE corrected interaction energy is

$$E_{\text{int}}^{\text{CP}} = E_{AB}(AB) - E_A(AB) - E_B(AB). \quad (3.3)$$

An alternative (but equivalent) formulation of the BSSE corrected energy is

$$E_{\text{int}}^{\text{CP}} = E_{\text{int}}^0 + (E_A(A) - E_A(AB)) + (E_B(B) - E_B(AB)) \quad (3.4)$$

where E_{int}^0 refers to the uncorrected definition of the interaction energy (eqn. (3.2)). Hence for differentiation with respect to the nuclear co-ordinate (as when evaluating forces)

$$\frac{\partial E_{\text{int}}^{\text{CP}}}{\partial \lambda} = \frac{\partial E_{\text{int}}^0}{\partial \lambda} - \frac{\partial E_A(AB)}{\partial \lambda} - \frac{\partial E_B(AB)}{\partial \lambda} \quad (3.5)$$

$E_A(A)$ and $E_B(B)$ are constants with respect to variation of λ , since all basis functions are centred on (and move with) the nucleus under consideration. However, $E_A(AB)$ and $E_B(AB)$ are not constants with respect to variation of λ because there are basis functions at the other atomic position and hence the energy will vary with interatomic separation.

3.2 Performance of DFT for intermolecular interactions

Given that dispersion is a correlation effect, it is not accounted for by Hartree-Fock calculations. Unfortunately, dispersion forces are especially important in many biological systems that, because of their size, are not amenable to investigation by correlated wavefunction methods. Because of this, the efficient manner in which DFT models correlation effects means that there is a great deal of interest in the use of DFT to model intermolecular interactions.

An exact DFT would include all correlation effects, including dispersion interactions. However, a local approximation for the exchange-correlation energy cannot, even in principle, describe the interaction with another, distant system. The total exchange-correlation energy of two non-overlapping charge distributions is the sum of the individual contributions for any local DFT. Neither the use of functionals which employ the gradient (GGAs) and higher derivatives (meta GGAs) of the density, nor the inclusion of a fraction of exact exchange (hybrid functionals) alters this, despite the fact that hybrid functionals are rigorously non-local.

This limitation would seem to preclude the use of approximate DFT to describe any long-range interactions. However, even systems where inter-

molecular interactions are dominated by dispersion often have minimum energy conformations where there is appreciable overlap between the systems. In such cases, a local approximation to the exchange-correlation energy might be able to describe approximate dispersion interactions.

The literature contains assessments of the performance of conventional exchange-correlation functionals in describing dispersion interactions for a range of systems including rare gas dimers [73, 74, 75, 76, 77, 78, 79, 80, 81, 82], C₆H₆ dimer [75, 79, 81, 83], CH₄ and C₂H₂ dimers [81, 84], He ... CO₂ [85, 86], N₂ dimer [87], C₆H₆ ... X (X = O₂, N₂, CO [88], Ne, Ar [75]) and other nonbonded dimeric complexes [89]. Across these disparate systems, particular functionals are consistent in their behaviour. Use of the local density approximation (LDA) leads to overbinding [73, 74, 76, 77, 88]: well depths are too deep and bond lengths are too short. If one moves to generalised gradient approximation (GGA) or hybrid functionals the results are variable and sensitive to the choice of approximate exchange functional. Functionals based on Becke 1988 exchange [90] often predict a repulsive interaction [73, 74, 75, 77, 78, 79, 80, 81, 83, 84, 85, 87, 88, 89]; those based on PW91 [91] or PBE [50] exchange do tend to bind, although they do not provide quantitative accuracy [76, 77, 78, 79, 80, 81, 86, 87, 88]. This sensitivity to exchange functional has been attributed [77, 88] to the behaviour of the exchange enhancement factor at large reduced density gradient s ; the Becke 1988 enhancement factor diverges, whereas the PW91 and PBE factors are better behaved. For a recent review of van der Waals studies using conventional functionals, see ref. [92].

Preliminary work carried out as part of the present investigation was consistent with the conclusions from the literature. In Figure 3.2 potential energy curves for the helium dimer, generated using various wavefunction and DFT methods, are presented. Figure 3.2(a) presents plots of energy versus interatomic separation for three wavefunction methods; Hartree-Fock (HF-SCF), MP2 and BD. Binding energies (D_e) and equilibrium separations (R_e) for these methods are presented in Table 3.1. The extensive *7s5p4d* basis set

was used and results were corrected for BSSE using the procedure described in Section 3.1.1. DFT calculations were also corrected for integration grid superposition error by including the integration grid of both atoms in all calculations. HF-SCF, which includes no correlation, does not bind the helium dimer. If a description of electron correlation is included via MP2 then the helium dimer is bound and the equilibrium separation is reasonable, though the minimum is too shallow. The BD method, a more expensive correlated method discussed in Section 1.4.3, is in better agreement.

Potential energy curves generated using local density and generalised gradient approximation functionals are presented in Figure 3.2(b). The LDAX functional, which includes no correlation, overbinds the helium dimer. With the LDA exchange-correlation functional this overbinding becomes worse—the binding energy is too large by an order of magnitude. The HCTH functional barely binds, while the 1/4 functional displays a reasonable equilibrium separation, though the binding is too strong. This is consistent with the above discussion of the exchange enhancement factor. The HCTH enhancement factor increases rapidly with increasing s , while the 1/4 enhancement factor is better behaved and increases more gradually [95].

The B3LYP functional does not bind, whereas, as shown in Figure 3.2(c), the more recently developed B97-2 approximation is surprisingly good.

Though no local density functional theory can rigorously describe long-range dispersion interactions (since these interactions are fundamentally non-local), qualitatively correct behaviour can therefore be seen in regions of density overlap,¹ because the interaction energy in these regions is composed of several terms; as well as the dispersion there is the exchange-dispersion, electrostatic, exchange-repulsion, etc. The DFT description breaks down as the separation increases to regions where the overlap is negligible and the interaction is dominated by the long-range dispersion energy.

¹This gives a rationale for the importance of large basis sets and integration grids in DFT dispersion calculations: the separation between systems will be relatively large, and hence the long range description of the density must be accurate to allow useful calculations to be carried out.

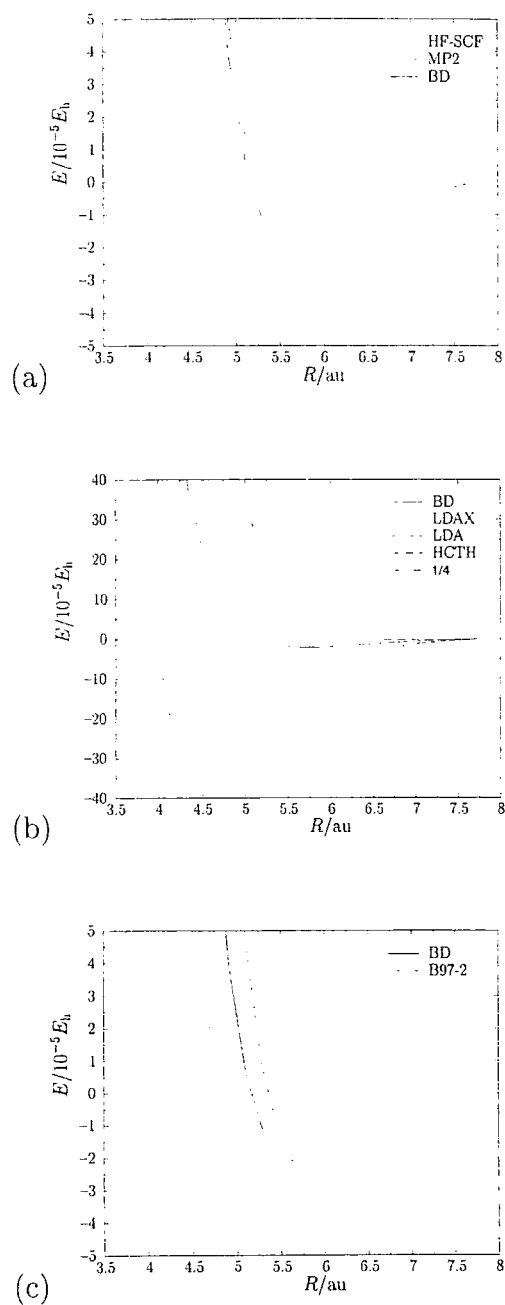


Figure 3.2: Energy plots for the He dimer from (a) wavefunction methods, (b) LDA and GGA DFT functionals and (c) a hybrid DFT functional. In each case, a BD energy plot is included for reference. Note different scale for (b).

Table 3.1: Binding energies D_e and equilibrium separations R_e from wavefunction and DFT methods for He_2 . A dash indicates that no binding is observed

	$D_e/10^{-5}E_h$	R_e/au
HF-SCF	–	–
MP2	1.8	5.9
BD	2.1	5.7
LDA	34.6	4.5
LDAX	19.5	4.7
BLYP	–	–
HCTH	0.3	6.8
1/4	8.3	5.3
B3LYP	–	–
B97-2	2.6	5.9
Expt. ¹	3.3	5.6

¹Refs [93, 94]

It is possible to introduce the dispersion terms in an empirical manner [96], though it is clearly more satisfying to include them in a rigorous manner. This has been done using long-range [97, 98, 99, 100, 101, 102, 103, 104] and seamless [105, 106, 107, 108, 109] approaches, and an assessment of some of these methods is presented in ref. [110]. Another approach to dispersion interactions that makes use of conventional DFT is the employment of Kohn-Sham orbitals within symmetry-adapted perturbation theory [111, 112].

3.3 Calculation of intermolecular forces

In this study, we consider the long-range interaction in DFT from the viewpoint of the force on a nucleus, rather than from the viewpoint of the electronic energy. We consider the helium dimer He_2 , for a number of reasons.

The interaction between two He atoms is known to a high accuracy. The small size of the system allows the use of high-order wavefunction calculations for comparison purposes, and enables large basis sets to be employed, reducing basis set truncation errors. This last point is important, as the interaction of the helium dimer is an extremely challenging computational problem. The well depth D_e is extremely shallow (only $3.3 \times 10^{-5} E_h$) and the zero-point vibrational energy is approximately equal to the well depth. This means that it is necessary to calculate the potential energy curve to a very high degree of accuracy simply to yield a bound state. This difficulty in achieving accurate results for the helium dimer means that it represents an important challenge for DFT methods.

Since dispersion arises because of correlation between electronic charge densities the Hartree-Fock-Kohn-Sham (HFKS) method is employed, treating exchange exactly and approximating the correlation. The details of the HFKS formalism are given in Section 2.5, but the main equations are presented again here in an alternative form, to emphasise both the connection with the HF-SCF method and the importance of the correlation potential. The HFKS electronic energy may be expressed as the sum of the Hartree-Fock energy functional and an approximate correlation energy functional

$$E_{\text{DFT}} = E_{\text{HF}}[\{\varphi_i\}] + E_C[\rho]. \quad (3.6)$$

Expansion of the orbitals $\{\varphi_i\}$ in a basis set $\{\eta_\beta\}$ allows the HFKS equations

$$\int F_{\text{HF}}(\mathbf{r}, \mathbf{r}') \varphi_i(\mathbf{r}') d\mathbf{r}' + v_C(\mathbf{r}) \varphi_i(\mathbf{r}) - \epsilon_i \varphi_i(\mathbf{r}) = 0 \quad (3.7)$$

to be recast as secular equations

$$\sum_{\beta} \int \eta_{\alpha}(\mathbf{r}) \left[\int F_{\text{HF}}(\mathbf{r}, \mathbf{r}') \eta_{\beta}(\mathbf{r}') d\mathbf{r}' + v_C(\mathbf{r}) \eta_{\beta}(\mathbf{r}) - \epsilon_i \eta_{\beta}(\mathbf{r}) \right] d\mathbf{r} C_{\beta i} = 0 \quad (3.8)$$

where $F_{\text{HF}}(\mathbf{r}, \mathbf{r}')$ is the co-ordinate representation of the Hartree-Fock operator, as in eqn. (1.23). The HFKS force on nucleus A is then

$$\mathbf{F}_{\text{DFT}} = -\frac{\partial E_{\text{DFT}}}{\partial \mathbf{R}_A} = -E_{\text{HF}}^{\mathbf{R}_A}[\{\varphi_i\}] - \int \rho^{\mathbf{R}_A}(\mathbf{r}) v_C(\mathbf{r}) d\mathbf{r} + \sum_i \epsilon_i S_{ii}^{\mathbf{R}_A} \quad (3.9)$$

where $E_{\text{HF}}^{\mathbf{R}_A}[\{\varphi_i\}]$, $\rho^{\mathbf{R}_A}(\mathbf{r})$, and $S_{ii}^{\mathbf{R}_A}$ are the basis-function-only derivatives of the Hartree-Fock functional, density, and orbital overlap matrix, respectively, with respect to the nuclear co-ordinate vector \mathbf{R}_A . Other than $v_c(\mathbf{r})$, all the terms in eqn. (3.9) can be constructed from the solutions to eqn. (3.8), and the only approximated term in eqn. (3.8) is $v_c(\mathbf{r})$. *This means that $v_c(\mathbf{r})$ determines the quality of the force calculated for a given basis set.* This is consistent with the approximations in the HFKS method: since $E_c[\rho]$ is the only approximation in the expression for the total energy, the derivative of $E_c[\rho]$ ($v_c(\mathbf{r})$) determines the derivative of the energy (the force).

When the basis set is complete the dependence of the force on $v_c(\mathbf{r})$ is especially clear. In the case of a complete basis eqn. (3.9) reduces to the Hellmann-Feynman force [113] (see below). For a given Born-Oppenheimer configuration the Hellmann-Feynman force depends only upon the density, which is governed entirely by $v_c(\mathbf{r})$ through eqns. (2.21) and (3.7).

The dispersion interaction dominates van der Waals molecules at large internuclear separations, so the force on the nuclei in such a system is almost entirely due to the dispersion. In calculating such dispersion forces using the HFKS formalism, the accuracy will depend upon the quality of the representation of $v_c(\mathbf{r})$ at large separation. $v_c(\mathbf{r})$ is, therefore, a key quantity, determining both the dispersion force and the dispersion energy (which can be recovered from the force by integration along the dissociation path).

The aim of this study is to investigate the relationship between the correlation potential, $v_c(\mathbf{r})$, and dispersion forces in the helium dimer. The correlation potentials considered are generated using BD(T) electron densities. We commence by presenting computational details. In particular, we outline a modification of the ZMP procedure that allows $v_c(\mathbf{r})$ to be determined from high quality densities.

3.3.1 Computational details

All force and density calculations used an extensive $7s5p4d$ basis set on the He atoms. This basis consists of the nuclear centred part of the DC+BS

(Dc147) basis set of ref. [114] with the f functions removed (the ZMP code employed cannot utilise f functions). All forces are calculated analytically. Where possible, numerical stability has been confirmed by comparing the analytic forces with numerical forces determined from energies at perturbed geometries.

Basis set superposition errors (BSSE) affect the shape of the interaction energy curve, so also affect the calculated forces. All forces are corrected for BSSE by differentiating the counterpoise energy correction, see eqn. (3.5). For DFT calculations, the integration grid on the ghost atom was also included, in order to account for integration grid superposition error. Given the extensive basis set, large internuclear separations, and near-saturated integration grids, the BSSE corrections to the total forces are very small. To the number of decimal places quoted they are negligible for all methods except BD(T) (where it contributes 0.1×10^{-6} au (about 2%) to the forces at 8.0 and 8.5 au). BSSE corrections to Hellmann-Feynman forces are slightly larger.

All BD(T) densities are relaxed densities. HFKS correlation potentials, $v_C(\mathbf{r})$, are determined from these densities using the methodology of refs. [59, 115], which is a modification of the ZMP approach (Section 2.10) and is denoted ZMPX. The method is as follows. The HFKS energy expression (eqn. (3.6)) can be rewritten

$$E[\rho] = T_S[\rho] + \int \rho(\mathbf{r})v_{\text{ext}}(\mathbf{r})d(\mathbf{r}) + J[\rho] + E_x^{\text{HF}}[\rho] + E_c[\rho]. \quad (3.10)$$

The only terms in eqn. (3.10) that are not explicit functionals of the density are the non-interacting kinetic energy $T_S[\rho]$ and orbital exchange energies $E_x^{\text{HF}}[\rho]$. By analogy with the constrained search procedure [66]

$$T_S[\rho] + E_x^{\text{HF}}[\rho] = \min_{2 \sum_i |\varphi_i|^2 \rightarrow \rho_0} \left[\sum_i -\langle \varphi_i | \nabla^2 | \varphi_i \rangle - \sum_{i,j} \int \int \frac{\varphi_i(\mathbf{r})\varphi_j(\mathbf{r})\varphi_i(\mathbf{r}')\varphi_j(\mathbf{r}')}{|\mathbf{r} - \mathbf{r}'|} d\mathbf{r}d\mathbf{r}' \right]. \quad (3.11)$$

As in the ZMP procedure, the constrained minimisation is enforced through eqn. (2.76). Also, as in standard ZMP, a Lagrange multiplier is attached.

In order to convert the Lagrangian into the same form as the HFKS equations (3.7) explicit functionals of the density are added and minimisation with respect to orbital variations gives the one-electron equations

$$\left[-\frac{1}{2}\nabla^2 + v_{\text{ext}}(\mathbf{r}) + v_j^\lambda(\mathbf{r}) + v_x^\lambda(\mathbf{r}) + v_c^\lambda(\mathbf{r}) \right] \varphi_i = \epsilon_i \varphi_i \quad (3.12)$$

cf. eqn. (2.80). $v_j^\lambda(\mathbf{r})$ is defined in eqn. (2.81) and $v_c^\lambda(\mathbf{r})$ is defined in eqn. (2.79).

$$v_x^\lambda(\mathbf{r}) = - \sum_i \int \frac{\varphi_i^\lambda(\mathbf{r})\varphi_i^\lambda(\mathbf{r}')}{|\mathbf{r} - \mathbf{r}'|} P_{rr'} d\mathbf{r}' \quad (3.13)$$

Comparison of the equations then allows $v_c(\mathbf{r})$ to be identified in terms of the BD(T) density, the iterating density, and a Lagrange multiplier λ associated with the density constraint.

$$v_c^{\text{HFKS}}(\mathbf{r}) = \lim_{\lambda \rightarrow \infty} v_c^\lambda(\mathbf{r}). \quad (3.14)$$

The inclusion of exact exchange obviates the need to include the Fermi-Amaldi factor (2.82) as is done in the ZMP procedure to compel the correct long range behaviour of the potential. The one-electron equations are solved within a basis set framework and the potential is tabulated numerically on a DFT numerical integration grid.

In the case where the iterating density exactly reproduces the BD(T) density, the Lagrange multiplier is formally infinite. Working within a (finite) basis set it is not possible to reproduce the BD(T) density exactly, so an infinite Lagrange multiplier is inappropriate. Three alternatives to an infinite Lagrange multiplier were evaluated: a finite value of $\lambda = 900$, as used in ref [115]; an extrapolation scheme [116] involving an expansion from λ^{-3} to λ^{+1} , where the latter term represents basis set incompleteness; a second extrapolation scheme (similar to that in ref. [63]) where λ^{+1} is replaced by λ^{-4} . To make an assessment of these various schemes, we employed the fact that the ZMP iterating density should equal the BD(T) density, and so Hellmann-Feynman forces from the two should be identical. Forces relating to the two densities were calculated for each scheme and their agreement compared. The agreement in the case of the first extrapolation scheme was

poor, and so it was abandoned; a similar conclusion was reached in ref. [115]. Both $\lambda = 900$ and the second extrapolation scheme performed well, and since there was little to choose between them, a value of $\lambda = 900$ was selected for simplicity. $\lambda = 900$ is used throughout.

The helium nuclei (labelled A and B) are positioned at z -coordinates z_A and z_B , where $z_B > z_A$. Thus the internuclear separation is $z_B - z_A$ and forces on nuclei act along the z axis. Because He_2 is homonuclear the forces on the nuclei are equal and opposite. (Forces constructed using approximate ZMP potentials do not generally satisfy this translational invariance condition. This is because the potentials are not exact functional derivatives.) Values quoted are for the force on nucleus A. Positive forces equate to attractions; a negative force conversely represents a repulsion.

3.4 Dispersion forces and the atomic density distortion

In order to ensure that the quantities under consideration are (as far as possible) due only to the dispersion interaction, it is necessary to choose internuclear separations where the dispersion interaction dominates. To this end, a high-accuracy interaction energy for He_2 is compared with the long-range dispersion energy. In the region where the two energies become indistinguishable the dispersion is considered to be the dominant factor. Korona et al. [114] have fitted an accurate symmetry-adapted perturbation theory (SAPT) interaction energy to the analytic form

$$E_{\text{SAPT}} = Ae^{-\alpha R + \beta R^2} - \sum_{n=3}^8 f_{2n}(R, b) \frac{C_{2n}}{R^{2n}} \quad (3.15)$$

where A , α , β and b are parameters adjusted during the fitting process, C_n are the dispersion coefficients and f_n is the damping function of Tang and Toennies [117]

$$f_{2n}(R) = 1 - \left(\sum_{k=0}^{2n} \frac{(bR)^k}{k!} \right) \exp(-bR). \quad (3.16)$$

Table 3.2: Parameters for the fit of the SAPT potential

Parameter	Value	Unit
C_6	1.460 977 8	(au)
C_8	14.117 855	(au)
C_{10}	183.691 25	(au)
C_{12}	3265.0	(au)
C_{14}	76 440.0	(au)
C_{16}	2 275 000.0	(au)
A	2 074 364.26	K
α	1.886 482 51	bohr ⁻¹
β	-0.062 001 349	bohr ⁻²
b	1.948 612 95	bohr ⁻¹

The optimised parameters and dispersion coefficients employed are presented in Table 3.2. At large R this SAPT interaction energy must approach the long-range dispersion energy

$$E_{\text{Disp}} = - \sum_{n=3}^8 \frac{C_{2n}}{R^{2n}} = -\frac{C_6}{R^6} - \frac{C_8}{R^8} - \dots - \frac{C_{16}}{R^{16}}. \quad (3.17)$$

The SAPT force on nucleus A is the derivative of the interaction energy with respect to the z co-ordinate of the nucleus

$$\begin{aligned} F_{\text{SAPT}} &= -\frac{\partial E_{\text{SAPT}}}{\partial z_A} = \frac{\partial E_{\text{SAPT}}}{\partial R} \\ &= (-\alpha + 2\beta R)A \exp(-\alpha R + \beta R^2) \\ &\quad - \sum_{n=3}^8 \left[\frac{-2nC_{2n}}{R^{2n+1}} g \right] \end{aligned} \quad (3.18)$$

where

$$g = \left[\sum_{k=0}^{2n} \left(-b + \frac{(2n+k)}{R} \right) \frac{C_{2n}}{R^{2n}} \frac{(bR)^k}{k!} \exp(-bR) \right]. \quad (3.19)$$

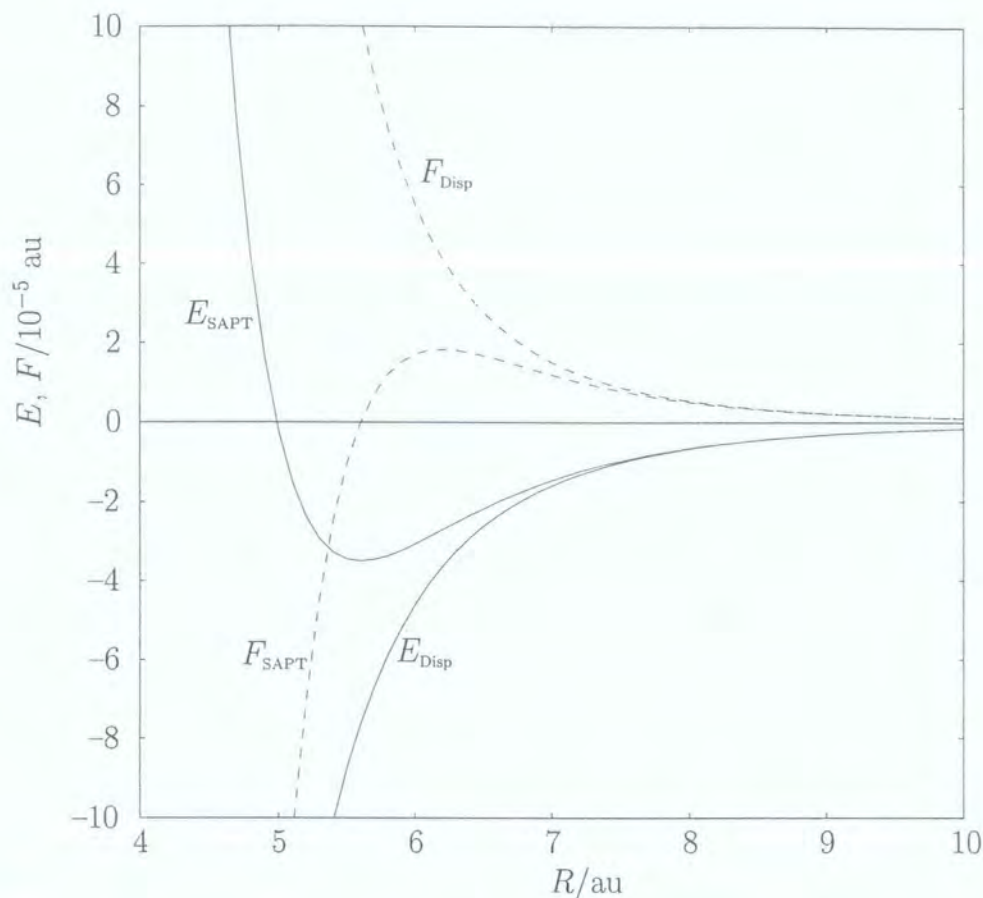


Figure 3.3: SAPT interaction energy E_{SAPT} and force F_{SAPT} , together with long-range dispersion contributions E_{disp} and force F_{disp} for He_2 .

Again, at large R this must approach the corresponding long-range dispersion force

$$F_{\text{disp}} = -\frac{\partial E_{\text{disp}}}{\partial z_A} = \frac{\partial E_{\text{disp}}}{\partial R} = \sum_{n=3}^8 \frac{2nC_{2n}}{R^{2n+1}} = \frac{6C_6}{R^7} + \frac{8C_8}{R^9} + \dots + \frac{16C_{16}}{R^{17}}. \quad (3.20)$$

A graphical comparison of the SAPT and long-range dispersion energies and forces is presented in Figure 3.3 where E_{SAPT} and F_{SAPT} are plotted as a function of R , together with the corresponding long-range dispersion contributions. Beyond $R = 7.5$ au the curves become indistinguishable, indicating that for larger internuclear separations the long-range dispersion force accurately represents the overall force due to the interaction. The implication is

Table 3.3: The force on nucleus A in He₂, in units of $\times 10^{-6} E_h$, for internuclear separations $R = 8.0, 8.5,$ and 9.0 au. All forces act along the He-He bond axis. A positive force represents an attraction between the nuclei.

R	F_{Disp}	F_{SAPT}	F_{HF}	$F_{\text{BD(T)}}$	$F_{\text{DFT}[v_{\text{C,LYP}}^{\text{Dimer}}]}$	$F_{\text{DFT}[v_{\text{C,ZMP}}^{\text{Dimer}}]}$	$F_{\text{DFT}[v_{\text{C,ZMP}}^{\text{Atoms}}]}$	$F_{\text{DFT}[v_{\text{C,ZMP}}^{\text{Int}}]}$
Total force								
8.0	5.4	5.1	-0.2	4.9	0.9	4.8	-0.3	4.8
8.5	3.4	3.3	-0.1	3.1	0.3	3.2	-0.1	3.2
9.0	2.2	2.2	-0.0	2.1	0.1	2.1	-0.0	2.1
Hellmann-Feynman contribution								
8.0	-	-	-0.1	4.8	1.0	4.5	-	-
8.5	-	-	-0.0	3.2	0.3	3.0	-	-
9.0	-	-	-0.0	2.1	0.1	2.0	-	-

that this region is dominated by the dispersion interaction, and so calculations are performed at $R = 8.0, 8.5$ and 9.0 au. In Table 3.3, F_{disp} and F_{SAPT} are presented for these three R values. The forces are close, but not identical, reflecting the fact that the atomic overlap is not zero. In this work, F_{SAPT} are regarded as near-exact reference forces.

A fundamental precept of this work is the premise that it is possible to understand the physical origin of the dispersion force in terms of distortions of atomic densities that occur when separated systems interact. The theoretical basis for this physical picture is the electrostatic theorem of Feynman [113]. The differential Hellmann-Feynman theorem [113, 118] states that the derivative of the energy E with respect to a parameter P is equal to the expectation value of the derivative of the Hamiltonian with respect to P

$$\frac{dE}{dP} = \left\langle \frac{\partial \hat{H}}{\partial P} \right\rangle. \quad (3.21)$$

Applying the Hellmann-Feynman theorem to a nuclear perturbation (i.e. a force) gives Feynman's electrostatic theorem. This states that the force on a nucleus in a molecule or extended system is just the classical electrostatic

force exerted by the other nuclei and the electron density. For the helium dimer, the force on nucleus A is thus

$$F = -\frac{4}{R^2} + 2 \int \frac{\rho(\mathbf{r}_1)}{r_{A1}^3} z_{A1} d\mathbf{r}_1 \quad (3.22)$$

where the first term is the repulsion due to the nucleus and the second term is the force due to the electron density. Feynman's electrostatic theorem does not reduce the calculation of electronic structure to a problem in classical electrostatics, as the determination of the correct charge distribution is necessary to calculate accurate forces and this step contains all the quantum mechanical complications. However, the theorem does indicate that molecular geometry may be rationalised as a balance of electrostatic forces, dependent on the charge distribution. It is thus possible to understand dispersion forces in terms of the electron density.

Consider two bare helium nuclei in an otherwise empty universe. If the internuclear separation is finite then there is a repulsive force on nucleus A due to nucleus B. Since it is known that at large internuclear separation an attractive force exists between the two nuclei (the dispersion interaction), the electron distribution in the exact case must be such that the electrostatic interaction between nucleus A and the electron density overcomes this repulsion. A spherically symmetric distribution of electrons centred about each nucleus will not achieve this, since at long-range this would become equivalent to a negative charge at the nucleus that exactly cancels the positive nuclear charge. The result would be zero force between the nuclei. By this reasoning, at large R the atomic densities must be distorted, and they must be distorted towards one another. In summary, increasing the density in the region between the nuclei would mean that the force on nucleus A (in the direction of nucleus B) due to the density is greater than the repulsion between the nuclei. Feynman described this distortion:

“The Schrödinger perturbation theory for two interacting atoms at a separation R , large compared to the radii of the atoms, leads to the result that the charge distribution of each is distorted from

central symmetry, a dipole moment of order $1/R^7$ being induced in each atom. The negative charge distribution of each atom has its centre of gravity moved slightly toward the other.”

Feynman also suggested that

“It is not the interaction of these dipoles which leads to van der Waals’ forces, but rather the attraction of each nucleus for the distorted charge distribution of its *own* electrons that gives the attractive $1/R^7$ force.”

This is generally referred to as Feynman’s conjecture.

For the case of the helium dimer this implies that the atomic electronic charge densities are distorted from spherical symmetry towards the other nucleus to form a dipole (along with the positively charged nucleus). The attraction of a given nucleus to the centre of its associated electron cloud gives rise to the leading term in the dispersion force. Hirschfelder and Eliason [119] showed that, for two hydrogen atoms, the magnitude of the distortion of the electron cloud in the vicinity of nucleus A, induced by atom B, is proportional to $1/R^7$. They thus concluded that Feynman’s conjecture was verified in this case. A more general proof has been provided by Hunt [120], who extended Hirschfelder and Eliason’s work to the case of two molecules of arbitrary symmetry at long-range and in regions of damped dispersion forces, where overlap between the charge distributions of the two systems is small but not negligible. The importance of this result is that it validates the simple physical picture of the origin of dispersion forces. Further discussion of the implications may be found in refs. [121, 122, 123].

The electrostatic theorem is only strictly valid when an infinite basis set and variational methodology are employed. This is never achieved for practical calculations, since these are always restricted to a finite basis set. However, comparison of the Hartree-Fock, BD(T) and DFT forces with Hellmann-Feynman forces (3.22) calculated using their respective densities (Table 3.3) demonstrates that it is valid to interpret the forces using the electrostatic

theorem. The force reflects the density distortion produced by the method. The density distortion is therefore quantified and visualised using a density difference function

$$\Delta\rho(\mathbf{r}) = \rho^{\text{dimer}}(\mathbf{r}) - [\rho^{\text{atom A}}(\mathbf{r}) + \rho^{\text{atom B}}(\mathbf{r})] \quad (3.23)$$

where $\Delta\rho(\mathbf{r})$ is the density of the dimer and $\rho^{\text{atom A}}(\mathbf{r})$ and $\rho^{\text{atom B}}(\mathbf{r})$ are atomic densities, each obtained from a separate calculation at the respective positions of the dimer nuclei. Note that, unlike the atomic calculations where a BSSE correction is being made, no ghost atoms are included in the atomic density calculations. The atomic densities must be spherical (as in the exact case) if the density difference comparison is to be meaningful. A positive value of $\Delta\rho(\mathbf{r})$ represents a region of density build-up, while a negative value indicates a reduction in density.

In Table 3.3 HF-SCF and BD(T) forces (denoted F_{HF} and $F_{\text{BD(T)}}$ respectively) are presented. HF-SCF fails to describe dispersion forces in the helium dimer; F_{HF} are small, repulsive rather than attractive and as overlap becomes negligible the forces vanish. BD(T) forces, however, are in good agreement with the near-exact reference values F_{SAPT} . These differences can be understood through examination of the density distortions. Figure 3.4 presents $\Delta\rho(\mathbf{r})$ for BD(T) for the three R values.

There is a positive peak on either side of the nucleus, and these are more pronounced on the side of the nucleus nearest to the other atom.² These plots are fully consistent with the Feynman distortion. Of course, we are only considering one dimension. Our plots say nothing about the distortion along a parallel line. However, as demonstrated in ref. [124] for the H_2 molecule, the behaviour along parallel directions is exactly the same. See also refs [122] and [125]. The quantitative agreement between the BD(T) and near-exact reference forces, and the fact that Hellmann-Feynman forces from BD(T) densities also agree well with the BD(T) forces, indicates that

²In order to show these peaks, a scale was chosen that means that the density differences at the nuclei are not visible. The values approach -182 , -126 and -88×10^{-7} au for $R = 8.0$, 8.5 and 9.0 respectively.

the BD(T) density distortion represents the actual distortion in all important respects.

Hartree-Fock densities, in contrast, are distorted *away* from each other. This is because of the absence of electron correlation in the HF-SCF method: the only interaction present is due to overlap (exchange) effects that must lead to a reduction in density between the nuclei. No density difference plots analogous to Figure 3.4 are presented, since at these separations the overlap is extremely small and hence the HF-SCF dimer is almost equivalent to two spherical atoms. The density difference is also, therefore, extremely small, making it difficult to distinguish real features of the distortion from numerical noise in the calculation. To demonstrate the type of distortion seen at shorter separations—where overlap is significant—Figure 3.5 presents the HF-SCF density difference for an internuclear separation of $R = 5.6$ au. The distortion of the electron densities away from one another is clear: $\Delta\rho(\mathbf{r})$ is positive on the far side of each nucleus and near the nuclei, but negative in the region between the nuclei. This leads to a repulsive interaction (exchange repulsion).

We now go on to consider forces from HFKS calculations. The only difference between the HF and HFKS equations is the correlation potential. For a HFKS calculation to yield accurate dispersion forces, therefore, the correlation potential alone must generate the density distortion.

3.5 DFT forces and correlation potentials

First, conventional DFT correlation functionals are considered. HFKS calculations are carried out using the LYP correlation functional. Eqn. (3.8) was solved with the correlation potential obtained by applying eqn. (2.40) to the LYP energy functional and this potential is denoted $v_{C,LYP}^{\text{Dimer}}(\mathbf{r})$. The forces (3.9), denoted $F_{\text{DFT}}[v_{C,LYP}^{\text{Dimer}}]$, are presented in Table 3.3. Unlike the HF-SCF forces, the LYP HFKS forces are attractive but they are still considerably too small (far smaller than those of BD(T)) and vanish as overlap

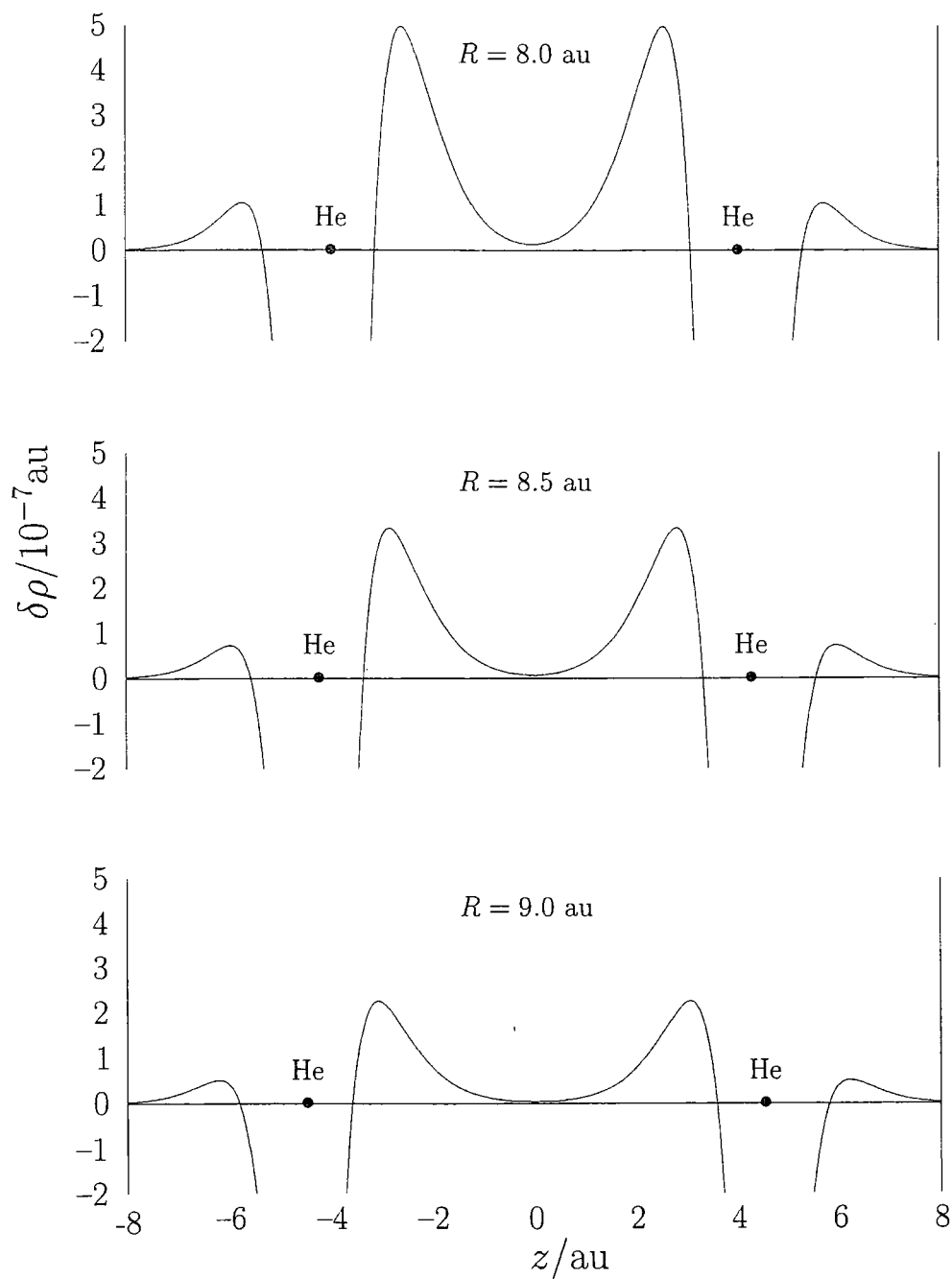


Figure 3.4: Density differences $\Delta\rho(\mathbf{r})$ determined from BD(T) densities, plotted along the He-He bond axis for the three R values. The nuclei are symmetrically placed either side of $z = 0$.

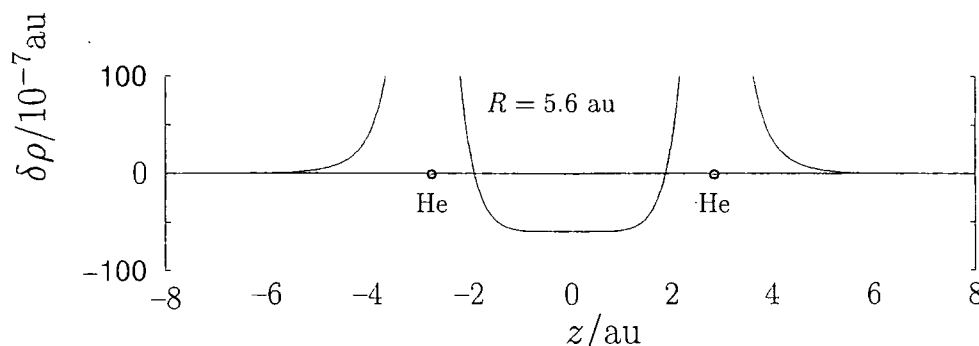


Figure 3.5: Density difference $\Delta\rho(\mathbf{r})$ determined from HF-SCF densities, plotted along the He-He bond axis for $R = 5.6$ au. The nuclei are symmetrically placed either side of $z = 0$.

reduces.

The reason for the failure of the LYP correlation functional to reproduce quantitative dispersion forces is readily apparent when the density difference calculated from HFKS LYP densities is examined. In Figure 3.6(a) $\Delta\rho(\mathbf{r})$ determined from both LYP HFKS and BD(T) densities at $R = 9.0$ au are presented. Comparing the two, it is clear that, although the LYP atomic densities are distorted towards one another, the magnitude of the distortion is far too small. This is consistent with the LYP HFKS forces, which are of the correct sign but too small by an order of magnitude.

Since the accuracy of the HFKS force depends upon the ability of the correlation potential to reproduce the density distortion, to improve upon the HFKS LYP forces the correlation potential must be improved. The ZMPX procedure was used to generate the correlation potential associated with the BD(T) density. This potential is denoted $v_{\text{C,ZMP}}^{\text{Dimer}}(\mathbf{r})$. Forces determined from eqn. (3.9) using $v_{\text{C}}(\mathbf{r}) = v_{\text{C,ZMP}}^{\text{Dimer}}(\mathbf{r})$ are denoted $F_{\text{DFT}}[v_{\text{C,ZMP}}^{\text{Dimer}}]$ in Table 3.3. They are in very good agreement with BD(T) forces; $v_{\text{C,ZMP}}^{\text{Dimer}}(\mathbf{r})$ gives rise to quantitatively correct dispersion forces. Both the agreement between the HFKS and BD(T) forces, and the fact that a HFKS calculation using $v_{\text{C,ZMP}}^{\text{Dimer}}(\mathbf{r})$ returns a density close to that of BD(T) (small differences are due to the use of finite basis set and integration grids), indicate that the atomic density distor-

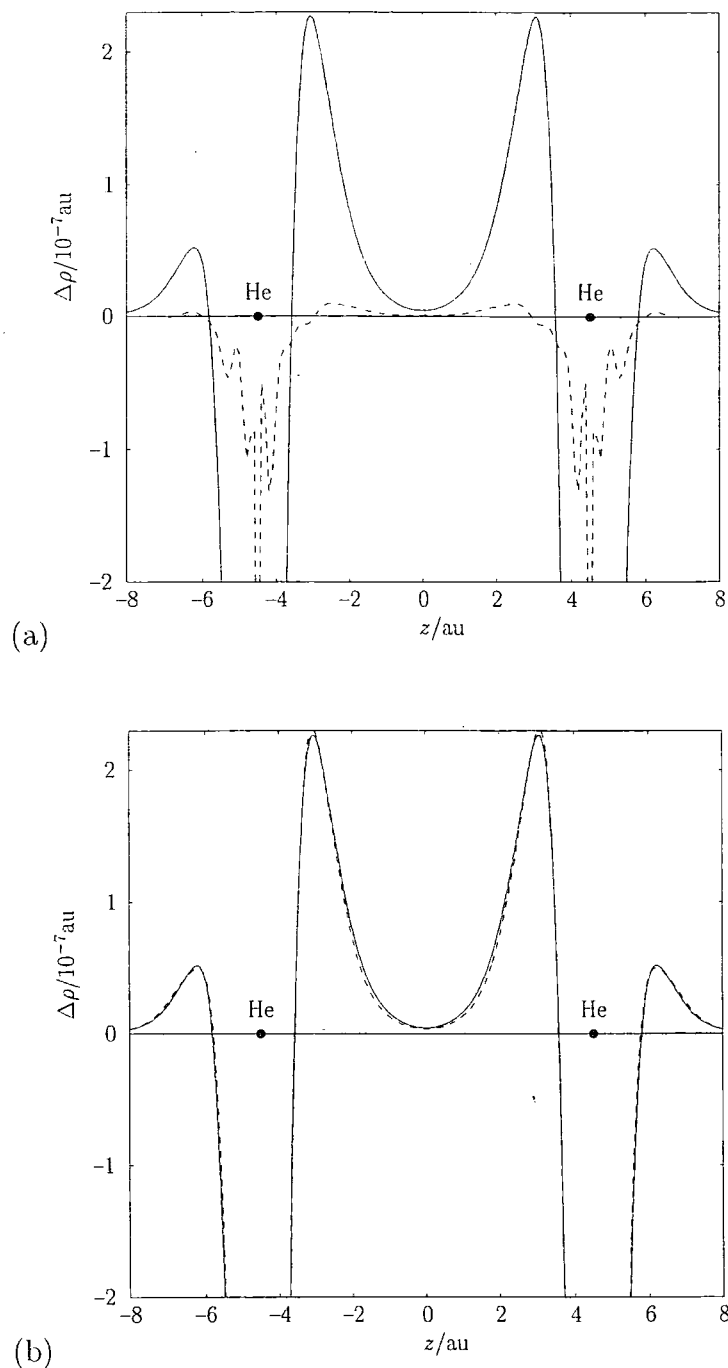


Figure 3.6: Density differences $\Delta\rho(\mathbf{r})$ determined from BD(T) densities (solid line), plotted along the He-He bond axis for $R = 9.0$ au, compared with $\Delta\rho(\mathbf{r})$ from HFKS calculations (dashed lines) using (a) LYP and (b) ZMP potentials.

tion from both calculations will be the same. Figure 3.6(b) compares $\Delta\rho(\mathbf{r})$ calculated from HFKS densities using $v_{\text{C,ZMP}}^{\text{Dimer}}(\mathbf{r})$ for the dimer and BD(T) densities, and the agreement is excellent. This agreement between the BD(T) and HFKS densities is quantified by comparing their Hellmann-Feynman forces (Table 3.3).

Figure 3.7 presents $v_{\text{C,ZMP}}^{\text{Dimer}}(\mathbf{r})$, plotted along the He-He bond axis for the three R values. The only discernible difference between the three plots is the increased separation between the atomic features. The difference between $v_{\text{C,LYP}}^{\text{Dimer}}(\mathbf{r})$ and $v_{\text{C,ZMP}}^{\text{Dimer}}(\mathbf{r})$ is demonstrated in Figure 3.8, where both dimer potentials are plotted for $R = 9.0$ au; they share virtually no common features. This is consistent with previous investigations, which have demonstrated significant discrepancies between approximate and near-exact correlation potentials [115, 126].

This is an important result, as it represents a DFT calculation that correctly describes the $1/R^7$ dispersion force without recourse to adding on a correction or exploiting fortuitous features of an exchange functional in regions of overlap of the charge densities. Although the necessity of first constructing the BD(T) density precludes the use of this method as a practical method of calculating dispersion forces in all but very simple systems, it does demonstrate that such accuracy is possible within the Kohn-Sham DFT framework, provided that a suitable correlation potential is available. The next step must be an investigation of the form of that potential, with an ultimate view to reproducing it without the need to employ the ZMP procedure.

3.6 Partitioning the correlation potential

On the scale of Figure 3.7 the dimer ZMP correlation potential $v_{\text{C,ZMP}}^{\text{Dimer}}(\mathbf{r})$ is indistinguishable from the sum of two atomic correlation potentials. This raises the question as to why $v_{\text{C,ZMP}}^{\text{Dimer}}(\mathbf{r})$ gives rise to the correct density distortion, since the atomic potentials correspond to spherically symmetric electron

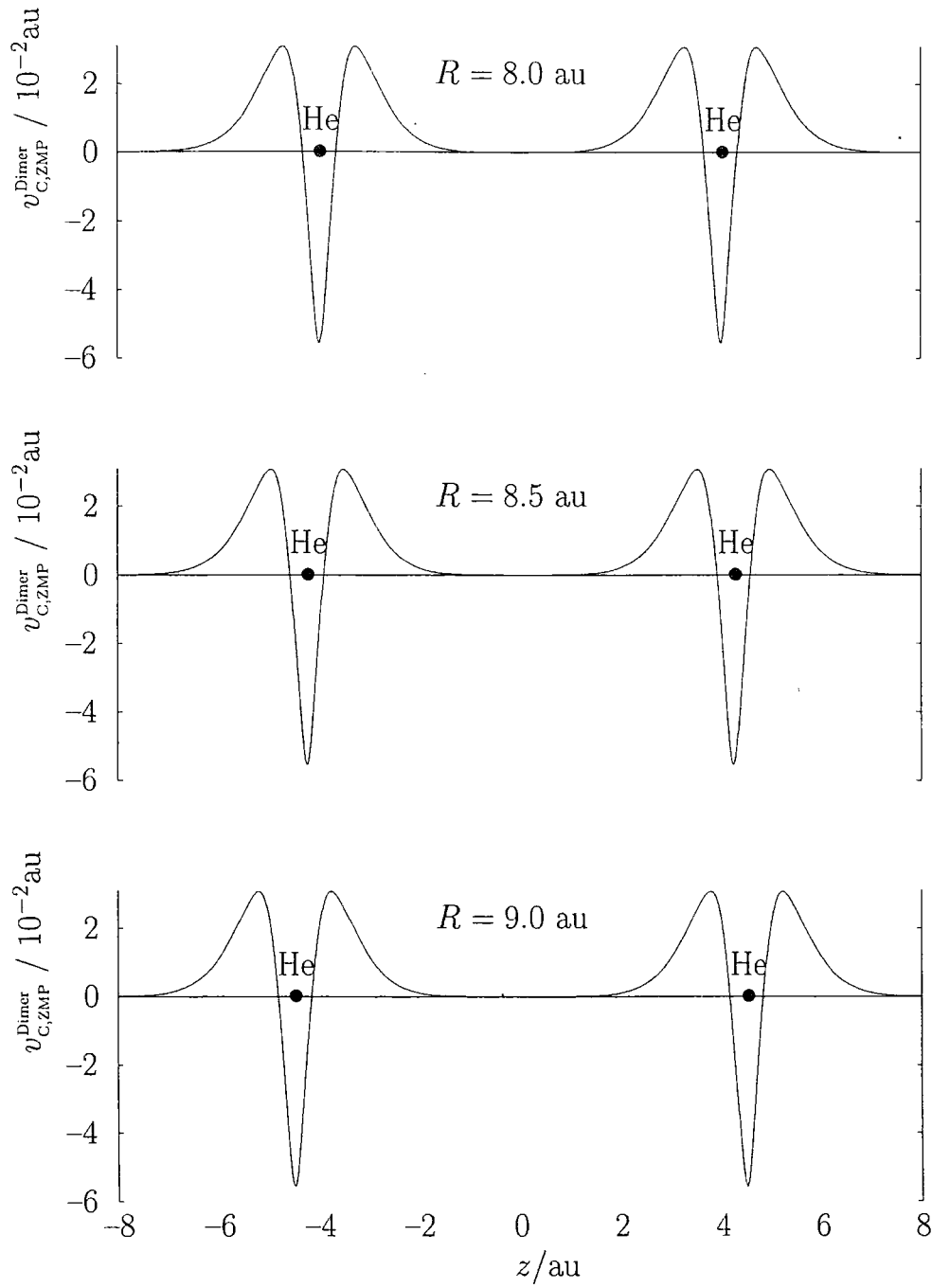


Figure 3.7: Correlation potentials $v_{C,ZMP}^{\text{Dimer}}(\mathbf{r})$ plotted along the He-He bond axis for the three R values.

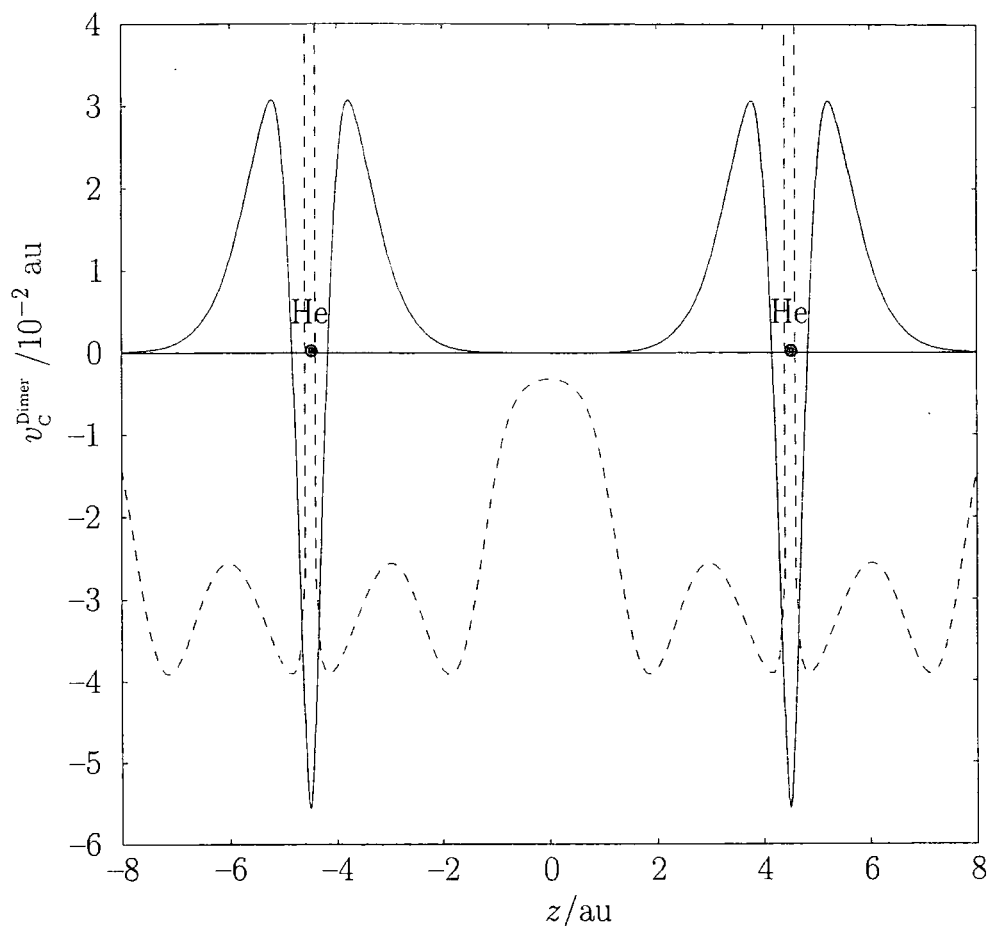


Figure 3.8: Correlation potentials $v_{C,ZMP}^{\text{Dimer}}(\mathbf{r})$ (solid curve) and $v_{C,LYP}^{\text{Dimer}}(\mathbf{r})$ (dashed curve), plotted along the He-He bond axis for $R = 9.0$ au.

densities. A partitioning of the dimer potential

$$v_{C,ZMP}^{\text{Dimer}}(\mathbf{r}) = v_{C,ZMP}^{\text{Atoms}}(\mathbf{r}) + v_{C,ZMP}^{\text{Int}}(\mathbf{r}) \quad (3.24)$$

into atomic and interaction components allows the investigation of the relationship between the correlation potential and the density distortion. Here $v_{C,ZMP}^{\text{Atoms}}(\mathbf{r})$ is the sum of two independent atomic correlation potentials, positioned at the dimer nuclear co-ordinates

$$v_{C,ZMP}^{\text{Atoms}}(\mathbf{r}) = v_{C,ZMP}^{\text{Atom A}}(\mathbf{r}) + v_{C,ZMP}^{\text{Atom B}}(\mathbf{r}) \quad (3.25)$$

and just as $\Delta\rho(\mathbf{r})$ represents the change in the density upon dimer formation, so $v_{C,ZMP}^{\text{Int}}(\mathbf{r})$ is the change in the correlation potential that occurs when the atoms interact; it is an ‘interaction correlation potential’.

In order to construct $v_{C,ZMP}^{\text{Atoms}}(\mathbf{r})$ a ZMPX calculation was used to determine the correlation potential for the BD(T) density of atom A, while including atom B as a ghost atom with an associated numerical integration grid but no basis functions. The converse procedure was then carried out for atom B with a ghost atom at A. The integration grids for the two calculations are identical, so it is straightforward to generate the sum of the potentials.

It is instructive to compare HFKS forces using $v_C(\mathbf{r}) = v_{C,ZMP}^{\text{Atoms}}(\mathbf{r})$ (denoted $F_{\text{DFT}}[v_{C,ZMP}^{\text{Atoms}}]$) and $v_C(\mathbf{r}) = v_{C,ZMP}^{\text{Int}}(\mathbf{r})$ (denoted $F_{\text{DFT}}[v_{C,ZMP}^{\text{Int}}]$) in Table 3.3. $F_{\text{DFT}}[v_{C,ZMP}^{\text{Atoms}}]$ are small and repulsive, and closely resemble HF-SCF forces. The ZMPX atomic correlation potential is short ranged, so at the separations examined the v_C of the neighbouring atom has no significant effect. This means that $v_{C,ZMP}^{\text{Atoms}}$ is spherical in the regions of the nuclei. Such a potential does not cause the atomic densities to be distorted towards one another; an examination of the density difference plots confirms this. Thus the exchange interaction dominates, giving the Hartree-Fock-like forces. The atoms themselves are correlated, but there is no correlation *between* the atoms.

$F_{\text{DFT}}[v_{C,ZMP}^{\text{Int}}]$, in contrast, are indistinguishable from forces constructed using the full dimer potential ($F_{\text{DFT}}[v_{C,ZMP}^{\text{Dimer}}]$). The fact that the interaction potential reproduces the dispersion forces of the dimer potential indicates that it alone is responsible for the dispersion force.

By examining a plot of $v_{C,ZMP}^{\text{Int}}(\mathbf{r})$ (Figure 3.9) for the three R values it is possible to understand why the potential leads to a density distortion of the correct general form. The potential is not symmetric about the nuclei (as the independent atomic potential is) but instead is greater on the side opposite the neighbouring nucleus than it is on the adjacent side. Density will tend to build up in regions where the potential is low, and therefore this asymmetry will distort the atomic densities towards one another.

The oscillatory behaviour seen near the nuclei is sensitive to basis set

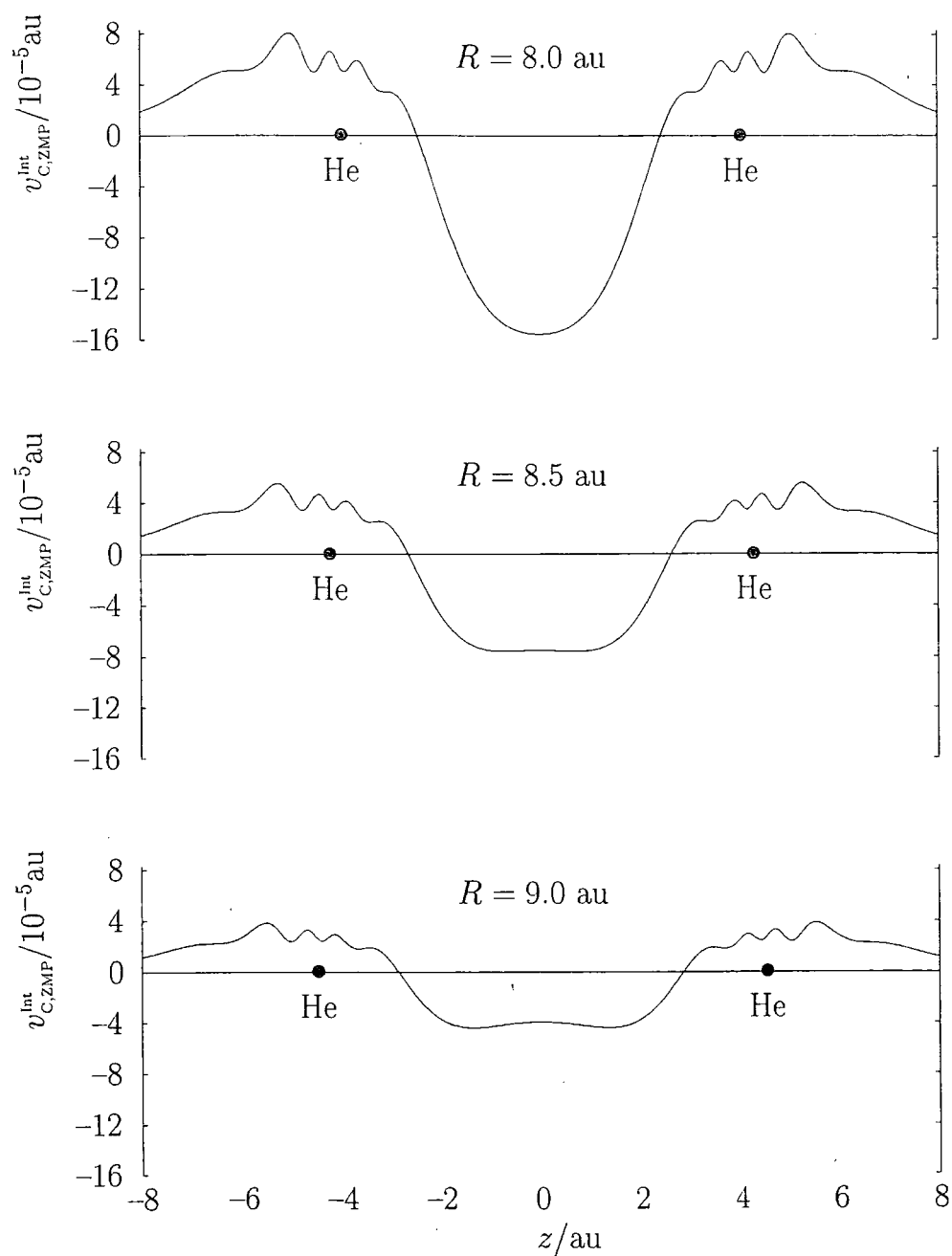


Figure 3.9: Interaction correlation potentials $v_{C,ZMP}^{int}(\mathbf{r})$ plotted along the He-He bond axis for the three R values.

and other convergence criteria, and it is possible that it does not represent physical features of the interaction correlation potential. The major features of the potential are not sensitive to the precise details of the computation, and we are confident of their accuracy.

Despite giving essentially identical dispersion forces, HFKS calculations using $v_{C,ZMP}^{\text{Int}}(\mathbf{r})$ and $v_{C,ZMP}^{\text{Dimer}}(\mathbf{r})$ are fundamentally different. At large R

$$\lim_{R \rightarrow \infty} v_{C,ZMP}^{\text{Int}}(\mathbf{r}) = 0 \quad (3.26)$$

but

$$\lim_{R \rightarrow \infty} v_{C,ZMP}^{\text{Dimer}}(\mathbf{r}) = v_{C,ZMP}^{\text{Atoms}}(\mathbf{r}) \quad (3.27)$$

and so, asymptotically, the former yields two Hartree-Fock atoms whereas the latter yields two BD(T)-like atoms. Quantitatively similar dispersion forces can therefore be obtained through a minor distortion of Hartree-Fock or BD(T)-like atoms. It is the distortion that matters, not the underlying atom.

3.7 The hydrogen molecule

One of the key findings of this work is the structure of the He_2 asymmetric interaction correlation potentials in Figure 3.9. Before concluding the chapter, we demonstrate that similar potentials also arise in the H_2 molecule.

Figure 3.10 presents the potential energy curve of H_2 determined using restricted Hartree-Fock (RHF), compared with the near-exact BD curve. As noted in Chapter 1, RHF is reasonable near the equilibrium geometry, but breaks down as the internuclear separation increases. This is often termed left-right correlation. Unlike the He_2 case, it is possible to include an additional curve: unrestricted Hartree-Fock (UHF). By breaking the spin-symmetry, UHF dissociates correctly.

Therefore, it is possible to calculate HFKS correlation potentials v_c that lead to UHF and BD densities. We have used the ZMPX procedure to calculate these potentials using the doubly augmented pV6Z basis set with f , g and

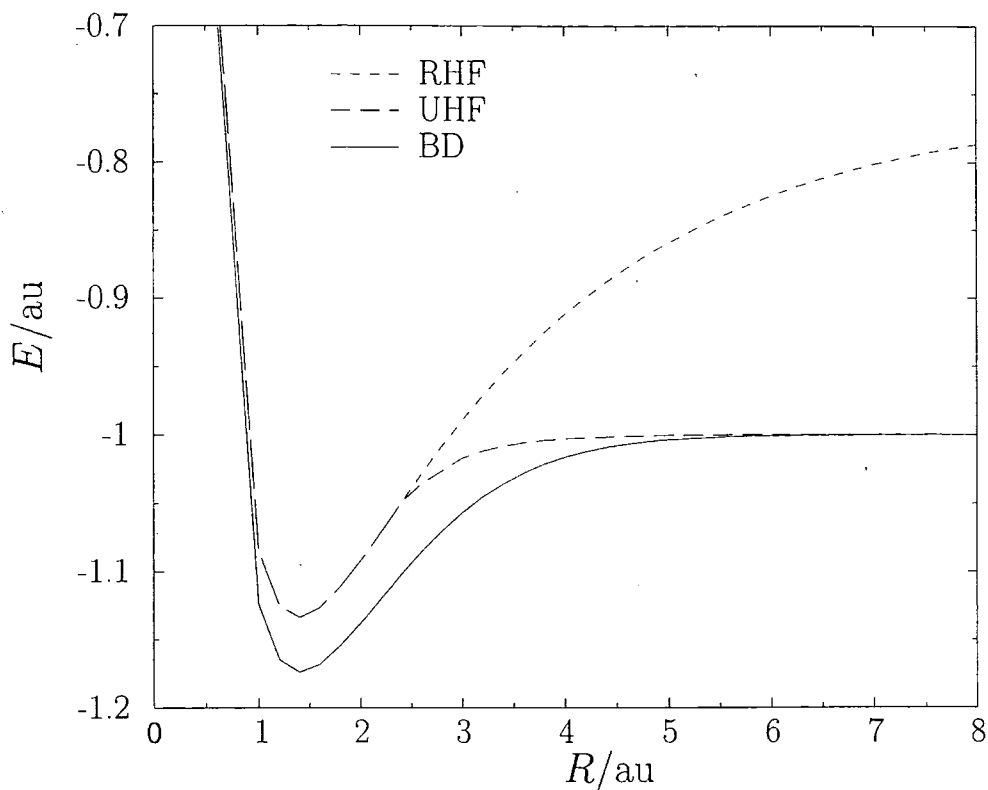


Figure 3.10: Potential energy curves of H_2 .

h functions removed. A Lagrange multiplier $\lambda = 900$ was used. We denote these potentials v_c^{UHF} and v_c^{BD} . Such potentials are presented in Figure 3.11 for two internuclear separations: the dashed curves are UHF potentials and solid curves BD potentials. The shorter distance (3.78 au) is slightly beyond the Coulson-Fischer point [127]. The longer distance (9.45 au) is closer to dissociation. At 3.78 au there is a noticeable difference between the two curves. This reflects the fact that the UHF and BD descriptions are not the same. However, at 9.45 au the two curves become indistinguishable. UHF is now near-exact.

At large distances the principle deficiency with UHF is the lack of dispersion. We therefore expect the difference between v_c^{UHF} and v_c^{BD} to resemble the interaction correlation potentials. Figure 3.12 presents the differences at the two internuclear separations. The general structure closely resembles

that of Figure 3.9.

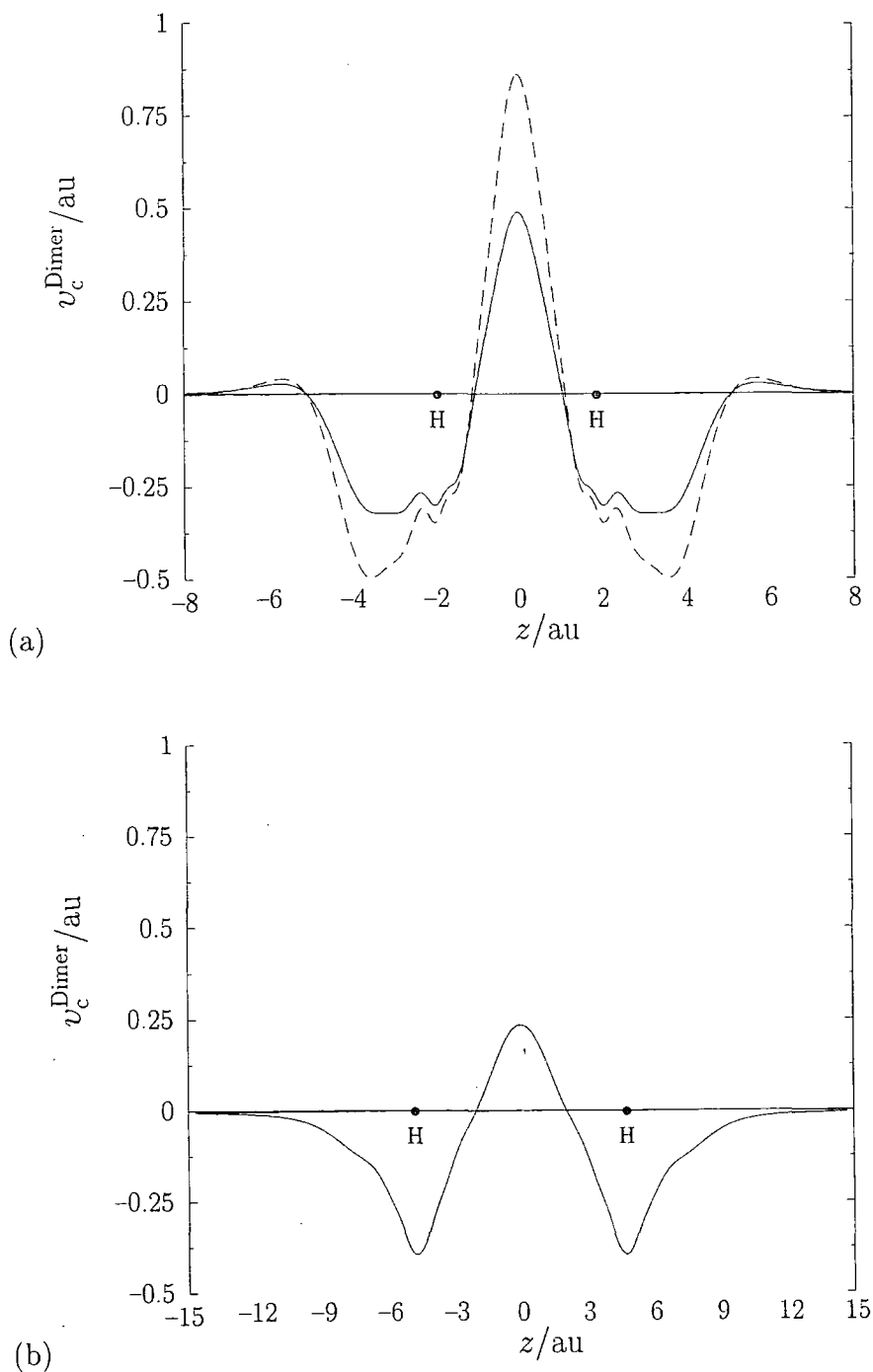


Figure 3.11: H_2 correlation potentials v_c^{BD} (solid curves) and v_c^{UHF} (dashed curves), (a) $R = 3.78$ bohr and (b) $R = 9.45$ bohr.

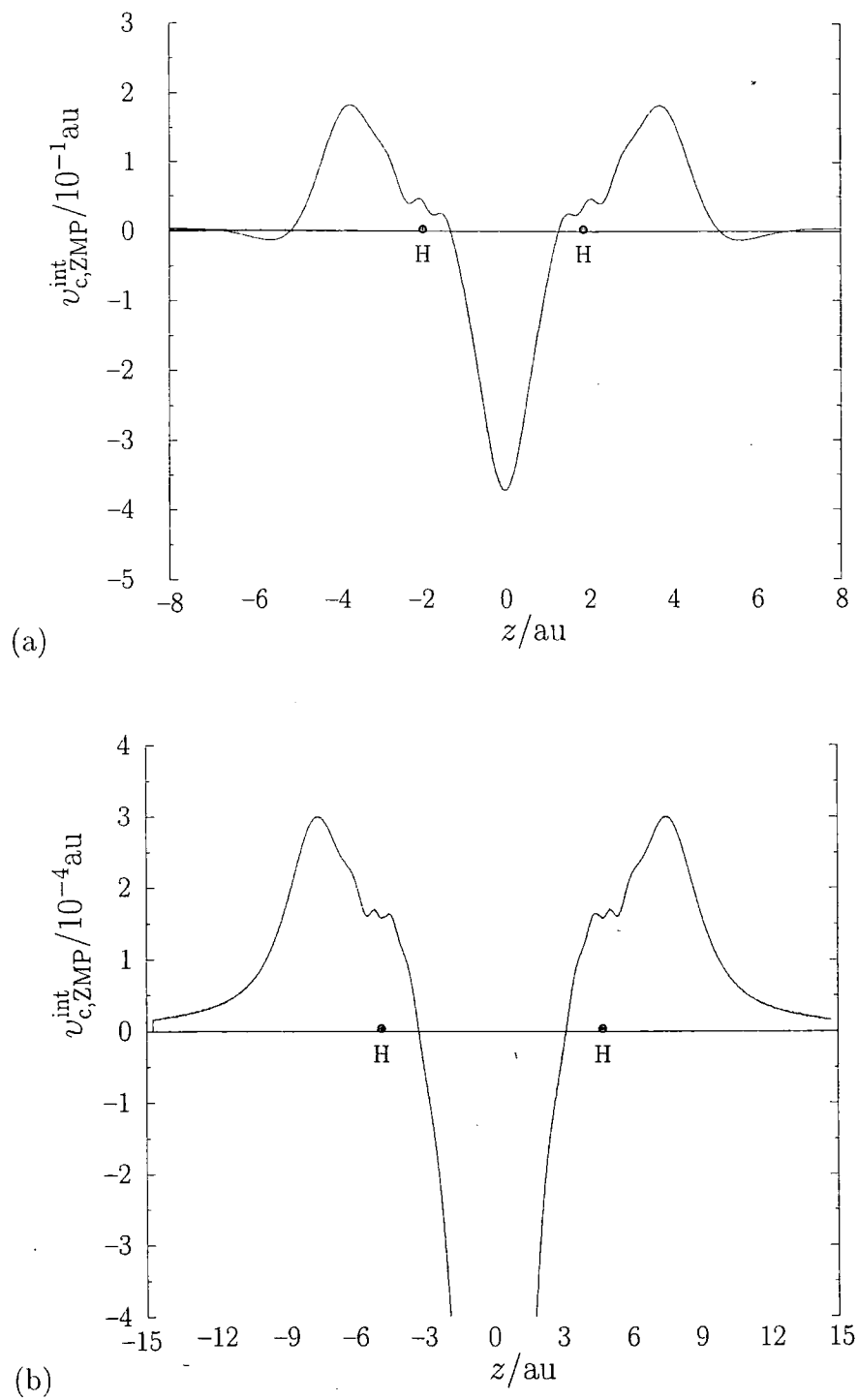


Figure 3.12: H_2 interaction potentials, (a) $R = 3.78$ bohr and (b) $R = 9.45$ bohr. Note different scales.

3.8 Summary

We have used high quality electron densities to learn about DFT dispersion interactions in the helium dimer. We have highlighted the importance of the density distortion and the correlation potential. A knowledge of the structure of the potential may aid the development of new energy functionals that correctly describe dispersion. It may also help develop pragmatic schemes for correcting existing potentials. We have also highlighted similar structures in the potentials of the H_2 molecule.

Remaining within the HFKS scheme, the requirement is for a correlation functional that produces the correct distortion: the associated functional must exhibit the asymmetric structure about the nuclei (in the case of a diatomic). It is doubtful if this could be achieved with a local correlation functional. A possible route to functionals that have associated asymmetrical potentials might be the use of non-local functionals (though an associated rise in computational effort might make this uneconomic).

Chapter 4

Magnetic and electric response properties

DFT response properties depend to a large extent on the Kohn-Sham orbitals and eigenvalues. It has previously been shown that improved orbitals and eigenvalues, determined from high quality electron densities, can improve magnetic response properties [69], including NMR shielding constants. In this chapter, this approach to the calculation of magnetic properties is extended to chemical shifts, and comparisons are made with orbital dependent methods and functionals optimised for shielding constants. Kohn-Sham orbitals and eigenvalues determined from electron densities are then used in electric response property calculations. Wavefunction and DFT densities are employed to calculate static polarisabilities and vertical excitation energies. The explicit dependence of electric response properties on the exchange-correlation functional derivative (which is not the case for corresponding magnetic properties) leads naturally to an investigation of its role in such calculations.

4.1 Kohn-Sham magnetic response theory

The calculation of magnetic response properties in DFT is especially important for the determination of nuclear magnetic resonance (NMR) chemical shifts. NMR is perhaps the single most important characterisation tool in modern organic chemistry, and finds wide application in all branches of chemistry. The ability to calculate spectra from theoretical methods is therefore extremely valuable, provided that reasonable accuracy can be obtained. Comparison with experimental spectra can aid in the interpretation of such, and even allow the identification of unknown compounds.

NMR depends on the resonant absorption of radio frequency radiation by magnetic nuclei in the presence of an externally applied magnetic field. A magnetic nucleus has a nuclear spin quantum number $I \neq 0$ (each nucleus has a fixed value of I , integral or half-integral, and positive). A nucleus of spin I has $2I + 1$ permitted orientations relative to an applied magnetic field and each orientation has a different energy. It is this energy difference that can be detected and, because it varies not only with the nucleus but also with the chemical environment around the nucleus, this is a powerful tool for characterisation.

The field at the magnetic nucleus is not necessarily that of the applied field, B . The applied field induces electronic currents that circulate throughout the framework of the molecule, and these currents give rise to an additional field at the nuclei. The additional field, B_{ind} is proportional to the applied field and it is usual to express it in terms of a dimensionless quantity, the shielding constant, σ

$$B_{ind} = -\sigma B \quad (4.1)$$

Thus the total local field at the nucleus becomes

$$B_{loc} = B + B_{ind} = (1 - \sigma)B \quad (4.2)$$

It would be feasible to report the different resonant frequencies in terms of shielding constants, but it is more usual to quote values in terms of the chemical shift, which is the difference between the resonance frequency of

the nucleus in question and that of a reference system. The separation is proportional to the strength of the applied field, but if chemical shifts are reported on the δ scale

$$\delta = \frac{\nu - \nu^\circ}{\nu^\circ} \times 10^6 \quad (4.3)$$

the chemical shifts are independent of the strength of the applied field.

NMR shielding constants can be expressed as a mixed second derivative of the total electronic energy with respect to the magnetic field B and the nuclear magnetic moment μ

$$\sigma = I + \left. \frac{\partial^2 E}{\partial B \partial \mu} \right|_{B=\mu=0} \quad (4.4)$$

Stationary perturbation theory may be applied to this problem. In conventional HF-SCF this leads to the coupled perturbed Hartree-Fock equations, which describe the linear response of the molecular orbitals (which define the Slater determinant of the corresponding Hartree-Fock ground state) to the external perturbation. However, Hartree-Fock calculations do not generate shielding constants of sufficient accuracy for useful comparison with experiment, and the inclusion of correlation is generally necessary. Because of this, expensive post Hartree-Fock methods must be employed, and the cost associated with these techniques limit their applicability. The relatively inexpensive inclusion of correlation effects in DFT suggests that it might be a more general route to the calculation of shielding constants.

Both GGA and hybrid functionals (containing a fraction ξ of orbital exchange) can be represented in a general form

$$E_{\text{xc}}[\rho] = E_{\text{xc}}^{\text{GGA}}[\rho] - \frac{\xi}{4} \int \int \frac{\rho_1(\mathbf{r}, \mathbf{r}')^2}{|\mathbf{r} - \mathbf{r}'|} d\mathbf{r} d\mathbf{r}' \quad (4.5)$$

Minimisation of the total electronic energy with respect to the Kohn-Sham orbitals gives

$$\left[-\frac{1}{2} \nabla^2 + v_{\text{ext}}(\mathbf{r}) + v_{\text{J}}(\mathbf{r}) + v_{\text{xc}}^{\text{GGA}}(\mathbf{r}) - \frac{\xi}{2} \int \frac{\rho_1(\mathbf{r}, \mathbf{r}')}{|\mathbf{r} - \mathbf{r}'|} P_{\text{rr}'} d\mathbf{r}' - \epsilon_i \right] \varphi_i(\mathbf{r}) = 0 \quad (4.6)$$

where $v_{\text{XC}}^{\text{GGA}}(\mathbf{r})$ is the multiplicative potential associated with $E_{\text{XC}}^{\text{GGA}}[\rho]$ and $P_{\text{rr}'}$ is the electron interchange operator. The Kohn-Sham orbitals $\varphi_i(\mathbf{r})$ and eigenvalues ϵ_i then appear in the diamagnetic contribution to the shielding tensor

$$\sigma_d^{A\alpha\beta} = \sum_j (j | (\mathbf{r} \cdot \mathbf{r}_A \delta^{\alpha\beta} - r_A^\alpha r_A^\beta) r_A^{-3} | j) \quad (4.7)$$

and also the paramagnetic contribution [128]

$$\sigma_p^{A\alpha\beta} = - \sum_{bj} C_{bj}^\alpha [(j | l_A^\beta r_A^{-3} | b) + (b | l_A^\alpha r_A^{-3} | j)] \quad (4.8)$$

The overall shielding tensor is simply

$$\sigma^{A\alpha\beta} = \sigma_d^{A\alpha\beta} + \sigma_p^{A\alpha\beta} \quad (4.9)$$

C_{bj}^α represents the linear response of the Kohn-Sham orbitals to the external static magnetic field and is determined from a set of coupled-perturbed equations [128]

$$\sum_{bj} (H_2)_{ai,bj} C_{bj}^\alpha = -l_{ai}^\alpha \quad (4.10)$$

$(H_2)_{ai,bj}$ is the magnetic Hessian matrix

$$(H_2)_{ai,bj} = (\epsilon_a - \epsilon_i) \delta_{ai,bj} + \xi [(aj|bi) - (ab|ji)] \quad (4.11)$$

and l_{ai}^α is the angular momentum index matrix.

The functional does not appear explicitly in the shielding tensor; its importance is due to it determining the orbitals and eigenvalues that do appear in the expression.

If a GGA functional is employed ($\xi = 0$) then the coupled-perturbed equations have a simple solution

$$C_{bj}^\alpha = \frac{-l_{bi}^\alpha}{(\epsilon_b - \epsilon_j)} \quad (4.12)$$

and the paramagnetic contribution becomes

$$\sigma_p^{A\alpha\beta} = - \sum_{bj} \frac{(b | l_A^\alpha | j) (j | l_A^\beta r_A^{-3} | b) + (b | l_A^\alpha r_A^{-3} | j) (j | l^\beta | b)}{\epsilon_b - \epsilon_j} \quad (4.13)$$

For hybrid functionals (where $\xi \neq 0$) the magnetic Hessian matrix (eqn. (4.11)) is not diagonal and hence the coupled-perturbed equations (eqn. (4.10)) must be solved. This is a consequence of the presence of the non-local exchange operator, meaning that the response of a particular orbital is dependent on the linear response of all the occupied orbitals. The approach is often termed “coupled” because of this. This does not imply that the hybrid functionals explicitly include current dependence; it is the inclusion of the fraction of exact (HF-SCF) exchange that means the approach must be coupled.

Most GGAs perform poorly for the calculation of shielding constants and chemical shifts of main group nuclei (an exception is the KT2 functional [51], whose form was chosen in order that its potential should closely mimic high-quality potentials, with the aim of improving the description of shielding constants). The inclusion of a fraction of exact exchange (hybrid functionals) does not generally improve this situation. Both approximations tend to give shieldings that are too deshielded.

Several procedures have been advanced with the aim of improving accuracy within the DFT framework. Malkin et al. [129], working within the uncoupled sum-over states density functional perturbation theory (SOS-DFPT) formalism, explicitly corrected occupied-virtual eigenvalue differences; ref. [130] presents an investigation of such a correction, denoted Loc.3. Wilson et al. [128] have obtained high quality shielding constants using a hybrid Kohn-Sham calculation that includes only a small fraction of orbital exchange. Patchkovskii et al. [131] have applied an optimised effective potential approach to the self-interaction corrected (SIC) LDA functional; the approach (denoted SIC-VWN) gives high quality chemical shifts. Poater et al. [132] have demonstrated that the statistical average of different model orbital potentials (SAOP) is another route to high quality chemical shifts. Keal and Tozer [51] have presented a GGA functional denoted KT2 (see Section 2.8.7), designed specifically to provide high quality shielding constants. Results are 2–3 times more accurate than other, commonly used GGAs for main group nuclei [51].

Wilson and Tozer [69] have also proposed the Multiplicative Kohn-Sham (MKS) approach, which is now discussed.

4.1.1 MKS magnetic response properties

The ZMP method can be used for the evaluation of shielding constants. The most straightforward approach would be to solve the ZMP equations (eqn. (2.83)) for the occupied and virtual orbitals and eigenvalues associated with a reference density, and substitute these into equation (4.9). However, an alternative method was employed in order to allow flexibility in the basis sets employed.

Wilson and Tozer [69] have shown that NMR shielding constants can be successfully determined from ZMP orbitals and eigenvalues. Their method for determining orbitals and eigenvalues can be summarised as follows:

1. The first step is the calculation of a relaxed density matrix¹ for a particular basis set and theoretical method.
2. This density matrix is used to solve the ZMP equations using the same basis set that was used in the calculation of the density matrix. A finite value of λ is used ($\lambda = 900$) because of the finite basis set. The ZMP potential is written to disk.
3. A conventional Kohn-Sham calculation is performed, but the ZMP potential is read from the disk, rather than explicitly calculating the potential. The basis set used for the Kohn-Sham calculation is not restricted to the basis used in the calculation of the density matrix.

If the same basis set is used throughout then the orbitals and eigenvalues will be identical (within numerical integration error) to those calculated analytically in the ZMP approach. The advantage of the above method is that it allows the use of a large basis set for the shielding calculations while the ZMP

¹relaxed density defined as one for which the finite field dipole corresponds to the expectation value using that density

calculations can employ a smaller basis. Because the densities used included expensive correlated wavefunction methods the use of large, diffuse basis sets would severely constrain the size of the systems that could be considered. In this work, for the determination of chemical shifts, the less extensive basis set TZ2P was employed for the ZMP calculations.

This method is denoted MKS (for Multiplicative Kohn-Sham, as it returns a multiplicative potential from a reference density), and the specific notation used is MKS followed by the method used to determine the reference density in parenthesis, e.g. MKS(BD).

4.2 Chemical shifts

We now apply the MKS method to the study of chemical shifts for the first time. To a good approximation the chemical shift δ is related to the absolute shielding constant σ by

$$\delta = \sigma_{\text{ref}} - \sigma \quad (4.14)$$

where σ_{ref} is the shielding constant of an appropriate reference system. Because the chemical shift is a shielding constant difference, it could benefit from a cancellation of errors. However, both shielding constants and chemical shifts are poorly described with DFT.

Patchkovskii et al. [131] and Poater et al. [132] have calculated isotopic chemical shifts of 44 molecules that consist of the elements H, C, N, O and F. These previous studies use the Amsterdam Density Functional program [133, 134, 135, 136] (ADF) and both use Slater basis sets. It is not possible to employ an identical basis set for comparison purposes, since the present version of CADPAC uses Gaussian basis sets only.

Poater et al. [132] quote LDA absolute shielding constants for 8 small molecules using 5 of the standard ADF basis sets. The results for ADF V (the TZ2P quality Slater basis employed by Patchkovskii et al.) and ADF VII (the 8s6p3d3f/6s3p basis used by Poater et al. [132] in their main study) are reproduced in Table 4.1. This allows preliminary comparison with LDA

Table 4.1: LDA isotropic shielding constants in ppm. Calculations are performed at TZP BP86 geometries.

Molecule	Nucleus	ADF ¹		CADPAC			Expt ²
		ADF V	ADF VII	TZ2P	HuzIV	8s6p3d	
CH ₄	C	194.6	189.6	193.4	190.7	190.3	198.7
	H	30.9	30.8	31.2	30.9	30.9	30.61
NH ₃	N	266.6	261.6	261.8	266.9	265.8	264.54
	H	31.3	31.0	30.8	30.3	30.3	31.2
H ₂ O	O	329.1	325.2	310.5	326.0	321.6	344.0
	H	30.7	30.1	31.1	30.4	30.4	30.052
HF	F	408.2	406.7	394.4	408.1	405.2	410.0
	H	29.3	28.4	33.7	28.9	28.9	28.5
N ₂	N	-94.5	-100.4	-93.6	-96.5	-98.1	-61.6
CO	C	-23.0	-29.0	-20.8	-25.8	-26.3	3.0
	O	-90.4	-102.3	-94.1	-99.2	-100.8	-42.3
CH ₂ NN	C	163.4	159.5	169.4	166.9	166.6	164.5
	N(middle)	-60.6	-70	-54.0	-65.7	-66.9	-42.3
	N(terminal)	-175.7	-184.4	-172.4	-179.8	-182.6	-149.0
	H	27.7	27.6	29.1	29.0	28.9	
O ₃	O(terminal)	-1647.0	-1674	-1675.5	-1665.0	-1695.3	-1290.0
	O(middle)	-987.0	-989.2	-974.9	-982.0	-988.8	-724.0

¹ The Amsterdam Density Functional program [133, 134, 135, 136]

² Ref. [131]

chemical shifts computed using the CADPAC program, using three different basis sets (TZ2P, Huzinaga IGLO IV [137, 138] and a standard CADPAC 8s6p3d/6s3p basis set) which are also presented in Table 4.1. The CADPAC basis 8s6p3d/6s3p gives results closest to Poater's ADF7 basis set, so would appear to be the most appropriate for the present study.

Note that our NMR calculations use the LORG formalism [139] and, following Patchkovskii et al. and Poater et al., reference shielding constants are not used to determine chemical shifts, since, as the authors of both studies point out, this is liable to bias the comparison of theoretical methods by

placing too much emphasis on their performance for the reference systems. Instead, σ_{ref} is treated as an adjustable parameter that is chosen to minimise the average signed error for the calculated chemical shifts. A consequence of this definition of the reference shieldings is that the chemical shifts depend (to a small degree) on the set of systems chosen.

Due to a limitation on the number of basis functions allowed in a shielding constant calculation in the CADPAC program, it is only possible to include a subset of 36 of the 44 systems considered in the previous studies. Chemical shifts calculated using this subset are not directly comparable with those published in refs. [131, 132]. To allow comparison with the previous results, it was necessary to recalculate the chemical shifts from [131, 132] for the subset of 36 molecules. Absolute shielding constants were not quoted by these authors, but can be recovered using eqn. (4.14).

Table 4.2 compares our LDA reference shieldings and mean absolute errors, determined using the 8s6p3d/6s3p basis, with those recalculated from the data of Patchkovskii et al. and Poater et al. Following [131, 132], calculations were performed at TZP-quality BP86 geometries, taken from reference 63 in the bibliography of [131] and reproduced in Appendix C. Dirac exchange [25] was combined with Vosko-Wilk-Nusair (VWN) correlation [30]. The errors demonstrate the poor performance of LDA for chemical shifts. Our values are in good agreement with those of Poater et al., and this justifies a direct comparison between their high quality SAOP results and calculations performed using the 8s6p3d/6s3p basis set in this work. This is not the case for the high quality SIC-VWN results of Patchkovskii et al.: the poor agreement between their LDA values and those calculated using the 8s6p3d/6s3p basis mean that a direct comparison is not warranted. The slightly smaller errors of Patchkovskii et al. reflect their use of a less extensive basis set.

Table 4.3 presents isotropic chemical shifts from HCTH, B97-2, SAOP, MKS(B97-2) and KT2. The same TZP-BP86 geometries were used as for the LDA calculations. Following previous work [59, 69], B97-2 electron densities and exchange-correlation potentials were determined using a TZ2P basis set

Table 4.2: LDA reference shieldings σ_{ref} and mean absolute errors in isotropic chemical shifts for the 36 molecules in Table 4.3. Values for Poater *et al.* [132] and Patchkovskii *et al.* [131] have been re-calculated from the data in the original references. All quantities are in ppm.

		^{13}C	^1H	^{15}N	^{17}O	^{19}F
This work						
	σ_{ref}	175.1	30.57	-112.9	173.3	302.6
	Mean abs. error	9.2	0.41	57.3	138.5	31.1
Poater <i>et al.</i> [132]						
	σ_{ref}	173.8	30.43	-114.3	176.6	306.2
	Mean abs. error	9.4	0.41	56.1	133.1	30.1
Patchkovskii <i>et al.</i> [131]						
	σ_{ref}	179.3	30.45	-106.6	192.6	314.7
	Mean abs. error	7.8	0.41	53.5	124.6	24.7

and a Lagrange multiplier of 900. All chemical shift calculations used the full 8s6p3d/6s3p basis set. The experimental values are taken from [131]. Corresponding reference shieldings and mean absolute errors are presented in Table 4.4.

Table 4.3: Isotropic chemical shifts in ppm. SAOP values have been re-calculated from the data in Ref. [132]. Unless otherwise stated, calculations are performed at TZP BP86 geometries.

Molecule	Nucleus	HCTH	B97-2	SAOP	MKS (B97-2)	KT2	KT2 ¹	Expt ²
CO	C	195.6	202.0	192.0	192.6	188.8	188.6	194.2
	O	296.0	272.0	313.4	345.4	330.8	354.3	386.3
CO ₂	C	127.7	131.7	128.6	129.6	130.1	131.0	136.4
	O	11.4	-20.3	44.8	73.4	50.2	74.5	100.6
F ₂	F	629.3	618.2	638.6	585.8	573.6	536.1	596.0
OF ₂	O	967.9	869.1	952.6	905.6	910.5	853.3	817.1
	F	457.8	446.4	455.1	424.0	446.3	420.4	426.0
HOF	O	399.4	365.5	443.5	431.6	400.0	389.2	
	H	12.6	12.6	13.4	12.1	11.8	11.4	12.1
	F	206.9	187.8	191.4	203.2	197.8	186.8	194.0
NF ₃	N	108.8	99.3	110.4	106.5	112.0	103.3	
	F	357.0	353.1	343.3	338.1	364.1	358.4	312.8
H ₂ O	O	-96.8	-130.8	-71.6	-27.4	-55.4	-35.7	0.0
	H	0.2	0.4	0.8	0.4	0.2	0.0	0.55
H ₂ O ₂	O	154.3	109.7	177.4	204.7	181.2	184.6	210.6
	H	7.1	6.9	7.5	6.9	6.8	6.5	
HCN	C	108.1	111.5	111.1	108.5	106.2	108.1	113.0
	N	-60.0	-54.5	-54.5	-53.1	-54.9	-44.8	-41.3
	H	2.6	2.6	2.2	2.7	3.0	2.9	2.83
N ₂	N	-12.5	-4.4	-8.4	-8.4	-10.8	-3.1	0.0
N ₂ O	N(terminal)	-180.4	-171.9	-168.1	-167.5	-168.0	-162.5	-161.1
	N(middle)	-98.3	-87.2	-86.3	-81.6	-82.7	-74.8	-72.9
	O	61.5	32.2	100.8	117.3	104.4	123.1	141.5
N ₂ O ₃	N(NO)	654.6	544.9	541.5	520.3	535.6	466.0	366.0
	N(NO ₂)	89.1	115.0	112.1	108.8	103.3	100.5	138.0
	O(NO)	1217.7	1089.5	1068.1	1069.0	1088.2	1036.0	891.0
	O(NO ₂)	347.3	344.0	398.8	407.8	388.4	395.6	461.0
O ₃	O(terminal)	1803.5	2047.1	1755.2	1566.8	1664.6	1587.0	1634.0
	O(middle)	1137.3	1387.9	1193.3	1122.1	1126.3	1116.2	1068.0
HF	F	-89.5	-74.3	-74.0	-64.3	-79.5	-66.2	-46.9
	H	1.7	2.1	3.3	2.1	1.5	1.4	2.10
NH ₃	N	-350.0	-352.6	-349.0	-332.5	-335.9	-330.5	-326.2
	H	-0.4	-0.3	-0.5	-0.3	-0.4	-0.5	-0.09
CH ₄	C	-3.5	-4.7	-5.7	-1.4	-1.1	-2.1	0.0
	H	-0.1	-0.1	-0.4	-0.1	-0.1	-0.1	0.00
C ₂ H ₆	C	13.6	10.8	11.8	14.8	15.9	14.6	14.2
	H	0.7	0.6	0.4	0.7	0.8	0.8	0.74
C ₂ H ₄	C	131.3	131.9	133.2	130.5	129.8	130.2	130.5
	H	5.5	5.4	5.2	5.4	5.4	5.6	5.18
CH ₂ CCH ₂	C(middle)	225.0	228.3	227.5	222.7	222.0	223.4	224.3
	C(terminal)	77.8	77.9	77.7	77.7	77.7	77.6	79.7
	H	4.7	4.6	4.2	4.6	4.7	4.8	

Table 4.3: (continued)

Molecule	Nucleus	HCTH	B97-2	SAOP	MKS (B97-2)	KT2	KT2 ¹	Expt ²
C ₂ H ₂	C	71.2	72.8	74.6	72.7	71.5	73.4	77.9
	H	1.2	1.2	0.7	1.3	1.5	1.4	1.33
H ₂ CO	O	640.7	628.0	616.0	650.7	657.1	681.9	590.0
	C	204.2	204.3	205.6	201.8	199.5	200.1	195.2
CH ₃ CHO	H	10.2	9.9	9.8	9.7	10.0	10.2	9.5
	C(C(O)H)	207.9	209.1	210.8	207.4	203.7	204.1	201.7
	C(CH ₃)	37.2	34.7	36.3	38.8	39.8	39.2	38.0
	O	568.7	555.2	548.9	586.4	591.4	613.7	628.0
	H(C(O)H)	10.2	9.9	9.9	9.8	10.1	10.4	
	H(CH ₃)	1.8	1.8	1.6	2.0	1.8	2.1	1.79
CH ₂ CO	C(CO)	200.0	203.8	200.4	198.1	198.6	198.3	201.0
	C(CH ₂)	1.9	1.8	2.3	3.7	3.3	2.2	9.5
	O	240.3	217.2	255.0	287.0	277.0	299.3	
	H	2.2	2.3	1.7	2.2	2.3	2.3	
CH ₂ CHCHO	O	572.2	550.0	542.2	580.9	588.7	611.5	615.1
	C(C(O)H)	201.3	203.0	202.7	198.4	197.7	198.5	201.2
	C(CH)	148.8	149.1	150.1	147.8	148.2	148.5	145.8
	C(CH ₂)	146.9	147.3	149.7	145.6	144.0	145.6	144.6
	H(C(O)H)	9.9	9.7	9.5	9.5	9.8	10.1	
	H(CH)	6.3	6.4	6.2	6.3	6.4	6.6	
	H(CH ₂ ,cis)	6.5	6.5	5.9	6.1	6.5	6.8	
	H(CH ₂ ,trans)	6.2	6.2	6.3	6.4	6.1	6.3	
(CH ₂) ₂ O	C	49.0	45.5	49.9	51.1	50.4	49.6	47.6
	O	-101.6	-144.9	-83.8	-34.9	-66.7	-44.2	-13.0
	H	2.4	2.3	2.1	2.4	2.4	2.4	
C ₃ O ₂	C(middle)	-14.0	-16.7	-13.4	-14.8	-13.0	-12.6	-7.6
	C(terminal)	119.7	125.2	121.1	122.1	120.9	122.2	136.7
CH ₃ NH ₂	O	89.2	58.3	121.5	148.0	125.0	150.8	
	C	37.3	34.0	36.6	38.4	40.1	39.1	36.8
	N	-325.6	-332.3	-326.6	-311.0	-312.2	-307.4	-311.7
	H(CH ₃)	2.2	2.1	2.0	2.1	2.3	2.3	
CH ₂ NN	H(NH ₂)	0.0	0.0	-0.2	0.1	0.1	0.0	0.27
	C	25.4	25.6	28.2	26.8	28.3	26.7	30.1
	N(middle)	-38.5	-40.8	-23.3	-27.7	-28.8	-21.7	-16.2
	N(terminal)	75.8	102.1	79.5	72.2	76.6	78.1	90.4
CH ₃ CN	H	3.1	3.2	2.7	3.1	3.3	3.4	
	C(CH ₃)	5.1	2.9	3.5	6.5	8.0	7.4	7.4
	C(CN)	119.1	121.5	121.8	118.8	117.1	118.9	121.3
	N	-69.2	-63.5	-64.1	-62.6	-61.5	-52.7	-52.8
CH ₃ NC	H	1.6	1.6	1.2	1.6	1.8	1.8	1.53
	C(CH ₃)	30.6	28.6	29.8	32.1	33.9	33.4	33.8
	C(NC)	173.9	179.7	175.9	172.8	168.9	170.3	165.2
	N	-181.0	-180.2	-178.1	-169.8	-172.0	-162.2	-141.0
	H	2.9	2.8	2.5	2.9	3.0	3.1	

Table 4.3: (continued)

Molecule	Nucleus	HCTH	B97-2	SAOP	MKS (B97-2)	KT2	KT2 ¹	Expt ²
CH ₃ NO ₂	C	68.1	66.9	68.7	68.5	70.7	68.9	68.4
	N	42.2	71.4	71.2	58.7	57.1	61.1	74.7
	O	589.1	580.5	613.5	601.4	609.5	617.4	639.0
CH ₃ F	H	4.1	4.0	3.7	4.0	4.2	4.1	3.91
	C	80.9	77.1	82.1	81.5	82.5	81.6	78.9
	F	-133.3	-127.4	-130.0	-111.0	-128.4	-114.0	-107.7
CH ₂ F ₂	H	4.1	4.0	4.1	4.1	4.2	4.4	4.00
	C	124.8	119.5	123.6	124.2	126.5	125.4	117.6
	F	5.8	5.5	5.6	5.7	5.9	6.1	
CHF ₃	F	4.3	7.7	6.6	19.5	17.6	32.5	24.1
	C	136.8	131.6	131.2	135.7	138.4	137.0	126.7
	H	6.7	6.4	6.4	6.5	6.8	7.0	
CF ₄	F	71.0	76.3	73.3	84.9	87.1	100.9	89.1
	C	143.2	138.0	132.7	141.5	145.0	144.0	130.7
	F	88.1	96.6	89.5	103.6	102.3	115.1	104.2
COF ₂	C	147.0	147.2	141.2	147.3	148.6	149.3	141.1
	O	202.4	180.4	216.5	255.0	237.6	258.2	
	F	141.5	148.7	139.4	149.3	152.3	163.2	141.5

¹ Evaluated at KT2 optimised geometries² Ref. [131]

When considering the performance of the various methods for calculating chemical shifts, ¹⁵N, ¹⁷O and ¹⁹F are the most diagnostic nuclei, since these vary most. All methods considered are consistent for the ¹³C chemical shifts and the description is in good agreement with experiment (note that this still represents an improvement of more than 50% over LDA, with mean absolute errors reducing from ~ 9.5 to ~ 4.5 ppm). ¹H chemical shifts span the range of 1–10 ppm and vibrational corrections are likely to be of comparable magnitude to these results. A more rigorous study—correcting for rovibrational effects—would be required to make a detailed analysis of these results meaningful.

HCTH represents a significant improvement over LDA for ¹⁵N, ¹⁷O and ¹⁹F. The reduction in the errors is reasonably uniform, approximately 25% in each case. The B97-2 hybrid functional improves upon HCTH for ¹⁵N and ¹⁹F, but is poor for ¹⁷O (a mean absolute error of 136.2 ppm is similar to the LDA value of 138.5 ppm). The erratic performance of hybrid functionals

Table 4.4: Reference shieldings σ_{ref} and mean absolute errors in isotropic chemical shifts for the 36 molecules in Table 4.3. SAOP values have been recalculated from the data in Ref. [132]. Unless otherwise stated, calculations are performed at TZP BP86 geometries. All quantities are in ppm.

	^{13}C	^1H	^{15}N	^{17}O	^{19}F
HCTH					
σ_{ref}	182.9	31.15	-95.6	216.1	309.7
Mean abs. error	4.5	0.26	44.4	102.3	24.4
B97-2					
σ_{ref}	184.0	31.16	-96.8	184.3	327.0
Mean abs. error	4.7	0.17	29.3	136.2	18.1
SAOP					
σ_{ref}	181.7	30.83	-94.2	249.4	337.2
Mean abs. error	4.1	0.45	27.0	78.0	20.4
MKS(B97-2)					
σ_{ref}	186.5	31.14	-76.1	290.4	340.4
Mean abs. error	4.0	0.14	23.8	50.8	8.5
KT2					
σ_{ref}	191.6	31.19	-76.5	260.4	321.0
Mean abs. error	4.4	0.25	26.1	59.5	17.3
KT2 ¹					
σ_{ref}	194.0	31.69	-65.6	289.7	342.8
Mean abs. error	4.0	0.35	16.1	42.8	19.7

¹ Evaluated at KT2 optimised geometries

for shielding constants of first and second row elements has been previously described [140]. Chemical shifts were also calculated using two other hybrid functionals, B3LYP and PBE0; though the results are not presented in Table 4.3 they confirm that functionals including exact exchange do not present a direct route to high accuracy conventional shieldings. For ^{15}N , ^{17}O and ^{19}F the B3LYP errors are 33.6, 146.1 and 22.0 ppm, respectively. The corresponding PBE0 errors are 30.3, 153.4 and 19.2 ppm. Both functionals are therefore less accurate than B97-2. The SAOP results are of good quality; errors are notably smaller than those of HCTH. MKS(B97-2) is significantly more accurate. Finally, the KT2 functional gives errors that are intermediate between those of SAOP and MKS(B97-2).

MKS(B97-2) clearly provides the best performance, but the requirement to generate the multiplicative exchange-correlation potential associated with the B97-2 density makes it more computationally demanding than a conventional DFT calculation, and more difficult to implement. Thus KT2 is the best compromise between accuracy and simplicity. It improves over the other methods, including SAOP, and is trivial to implement. It is no more computationally expensive than any other GGA DFT functional.

KT2 has a further advantage over SAOP. The strong dependence of calculated chemical shifts on geometries is well established. Calculated chemical shifts have been used as a criteria to assess molecular geometries [141]. KT2 is a well-defined functional, and can therefore be used to optimise geometries, making it possible to perform a consistent calculation where both geometry and chemical shifts are determined using the same functional. SAOP, being a model potential, is not suitable for geometry optimisations because its potential is not a functional derivative. Unphysical nuclear forces will arise unless the optimisation is performed in internal coordinates, in which case the geometry will then depend on the coordinate system chosen [142].

To complete this study we therefore performed consistent calculations where KT2 chemical shifts are determined for the 36 molecules at geometries optimised using KT2 and the 8s6p3d/6s3p basis set. Chemical shifts, refer-

ence shieldings and mean absolute errors are presented in Tables 4.3 and 4.4. The geometry dependence is particularly evident in the improvement of the ^{15}N and ^{17}O chemical shifts. ^{19}F shifts become slightly less accurate in moving to KT2 geometries. Rovibrational corrections were not included in the experimental values, and these are significant for the F_2 molecule; inclusion of the correction for this molecule alone means that the KT2 errors at the BP86 and optimised geometries are essentially identical, at 16.2ppm. The small number of ^{19}F results will also make the statistical analysis less meaningful.

4.3 Kohn-Sham electric response theory

We now go on to consider the application of the MKS approach to electronic response properties; specifically, we consider static isotropic and anisotropic polarisabilities and vertical excitation energies. Previous studies have shown that it is possible to achieve reasonable accuracy for isotropic polarisabilities within the DFT framework [59], and that vertical excitation energies can also be computed accurately, provided that some form of asymptotic correction is made to the potential in order to describe the Rydberg excitations correctly [143, 144, 145]. While we do not, therefore, expect the dramatic reduction in errors seen with chemical shifts, this new work allows direct comparison between the MKS properties determined from a particular density and the conventional polarisabilities and excitation energies from the method used to generate that density.

The dependence of electric response properties on Kohn-Sham orbitals and eigenvalues has been investigated in previous work. Van Gisbergen et al. [146] have determined isotropic polarisabilities using the Kohn-Sham orbitals and eigenvalues associated with exchange-correlation potentials determined from wavefunction densities. Using high quality densities and the LDA exchange-correlation integrand, their polarisabilities were close to the best estimates. The new work presented here compliments the previous study

in several ways: it extends the number of systems considered; it considers excitation energies as well as polarisabilities; it makes use of potentials from both wavefunction and DFT electron densities; it makes direct comparison between the MKS results and the corresponding conventional results and it investigates the dependence of the results on the exchange-correlation integrand. Before presenting our results we review the appropriate theory.

The variation of the electronic energy, E with an applied electric field, ε gives the dipole moment

$$\mu = -\frac{\partial E}{\partial \varepsilon} \quad (4.15)$$

the polarisability

$$\alpha = -\frac{\partial^2 E}{\partial \varepsilon^2} \quad (4.16)$$

and the hyperpolarisability

$$\beta = -\frac{\partial^3 E}{\partial \varepsilon^3}. \quad (4.17)$$

The determination of the response of an interacting many-particle system to a time-dependent external field can be accomplished through time-dependent density functional theory (TDDFT). This determination of response properties has been extensively reviewed [147, 148, 149, 150].

If the unrestricted time-dependent Kohn-Sham equations are written

$$\hat{K}_\sigma \varphi_{i\sigma} = i\hbar \frac{\partial \varphi_{i\sigma}}{\partial t}, \quad (4.18)$$

where \hat{K}_σ is the σ spin Kohn-Sham operator and $\varphi_{i\sigma}$ is an occupied σ spin orbital, then the first order expansion of the Kohn-Sham orbitals, in the presence of a time-dependent electric field with λ component $\varepsilon^\lambda \cos \omega t$, is

$$\varphi_{i\sigma}^\varepsilon = \varphi_{i\sigma} + \frac{1}{2} \varepsilon^\lambda (U_{ri\sigma}^\lambda(+)) e^{-i\omega t} + U_{ri\sigma}^\lambda(-) e^{-i\omega t} \varphi_{r\sigma}. \quad (4.19)$$

Here r denotes both occupied and virtual orbitals. The frequency dependent polarisability can now be obtained by considering the first-order response of the electric dipole [151], thus

$$\alpha_{\lambda\mu}(-\omega; \omega) = -2 \sum_{1,a,\sigma} Z_{ai\sigma}^\lambda P_{ai\sigma}^\mu \quad (4.20)$$

where P^μ is the dipole integral matrix

$$P_{ai\sigma}^\mu = (\varphi_{a\sigma} | r_\mu | \varphi_{i\sigma}) \quad (4.21)$$

and

$$Z_{ai\sigma}^\lambda = U_{ai\sigma}^\lambda (+) + U_{ai\sigma}^{\lambda*} (-) \quad (4.22)$$

(in each case the subscript a indicates virtual (unoccupied) orbitals.) This quantity is the solution to a set of coupled perturbed equations

$$(\mathbf{H}_2\mathbf{H}_1 - \omega^2\mathbf{I})\mathbf{Z} = -\mathbf{H}_2\mathbf{P} \quad (4.23)$$

where \mathbf{H}_1 and \mathbf{H}_2 are the electric and magnetic Hessian matrices respectively.

The frequency dependent polarisability is an important quantity because it allows the calculation of both static polarisabilities and vertical excitation energies. This is because it has the important properties that it gives the static polarisabilities when $\omega = 0$ and it diverges at the electronic excitation energies. This divergence is especially useful as it allows the calculation of single photon vertical electronic excitation energies from a description of the ground state energy only.

If a gradient-corrected exchange-correlation functional is written as

$$E_{\text{XC}}[\rho_\alpha, \rho_\beta] = \int F_{\text{XC}}(\rho_\alpha, \rho_\beta, \zeta_{\alpha\alpha}, \zeta_{\beta\beta}) d\mathbf{r} \quad (4.24)$$

where ρ_σ are the spin densities and $\zeta_{\sigma\sigma} = \nabla\rho_\sigma \cdot \nabla\rho_\sigma$, then if current dependence is ignored the electric Hessian matrix is

$$\begin{aligned} (\mathbf{H}_1)_{ai\alpha, bj\alpha} &= (\epsilon_{a\alpha} - \epsilon_{i\alpha})\delta_{ai, bj} + 2(a\alpha i\alpha | b\alpha j\alpha) \\ &+ 2 \int \varphi_{a\alpha}\varphi_{i\alpha} \frac{\partial^2 F_{\text{XC}}}{\partial\rho_\alpha^2} \varphi_{b\alpha}\varphi_{j\alpha} d\mathbf{r} \\ &+ 8 \int \nabla(\varphi_{a\alpha}\varphi_{i\alpha}) \cdot \nabla\rho_\alpha \frac{\partial^2 F_{\text{XC}}}{\partial\zeta_{\alpha\alpha}^2} \nabla\rho_\alpha \cdot \nabla(\varphi_{b\alpha}\varphi_{j\alpha}) d\mathbf{r} \\ &+ 4 \int \varphi_{a\alpha}\varphi_{i\alpha} \frac{\partial^2 F_{\text{XC}}}{\partial\rho_\alpha\partial\zeta_{\alpha\alpha}} \nabla\rho_\alpha \cdot \nabla(\varphi_{b\alpha}\varphi_{j\alpha}) d\mathbf{r} \\ &+ 4 \int \nabla\rho_\alpha \cdot \nabla(\varphi_{a\alpha}\varphi_{i\alpha}) \frac{\partial^2 F_{\text{XC}}}{\partial\rho_\alpha\partial\zeta_{\alpha\alpha}} \varphi_{b\alpha}\varphi_{j\alpha} d\mathbf{r} \\ &+ 4 \int \nabla(\varphi_{a\alpha}\varphi_{i\alpha}) \cdot \nabla(\varphi_{b\alpha}\varphi_{j\alpha}) \frac{\partial F_{\text{XC}}}{\partial\zeta_{\alpha\alpha}} d\mathbf{r} \end{aligned} \quad (4.25)$$

and

$$\begin{aligned}
(\mathbf{H}_1)_{ai\alpha,bj\beta} &= 2(a\alpha i\alpha|b\beta j\beta) + 2 \int \varphi_{a\alpha}\varphi_{i\alpha} \frac{\partial^2 F_{xc}}{\partial\rho_\alpha\partial\rho_\beta} \varphi_{b\beta}\varphi_{j\beta} d\mathbf{r} \\
&+ 8 \int \nabla(\varphi_{a\alpha}\varphi_{i\alpha}) \cdot \nabla\rho_\alpha \frac{\partial^2 F_{xc}}{\partial\zeta_{\alpha\alpha}\partial\zeta_{\beta\beta}} \nabla\rho_\beta \cdot \nabla(\varphi_{b\beta}\varphi_{j\beta}) d\mathbf{r} \\
&+ 4 \int \varphi_{a\alpha}\varphi_{i\alpha} \frac{\partial^2 F_{xc}}{\partial\rho_\alpha\partial\zeta_{\beta\beta}} \nabla\rho_\beta \cdot \nabla(\varphi_{b\beta}\varphi_{j\beta}) d\mathbf{r} \\
&+ 4 \int \nabla\rho_\alpha \cdot \nabla(\varphi_{a\alpha}\varphi_{i\alpha}) \frac{\partial^2 F_{xc}}{\partial\rho_\beta\partial\zeta_{\alpha\alpha}} \varphi_{b\beta}\varphi_{j\beta} d\mathbf{r}
\end{aligned} \tag{4.26}$$

where $(p\sigma q\sigma|r\sigma's\sigma')$ denotes a two electron integral. In contrast, the magnetic Hessian matrix is diagonal (assuming that there is no current dependence)

$$(\mathbf{H}_2)_{ai\sigma,bj\sigma} = (\epsilon_{a\sigma} - \epsilon_{i\sigma})\delta_{ai,bj} \tag{4.27}$$

Thus, unlike the magnetic case, electric response properties are not determined solely by the orbitals and eigenvalues. Instead, there is an explicit dependence on the exchange-correlation integrand F_{xc} which must be considered.

4.3.1 MKS electric response properties

MKS polarisabilities and excitation energies are calculated by evaluating eqn. (4.20) using ZMP orbitals and orbital energies, generated as in the magnetic case (Section 4.1.1). Since \mathbf{H}_1 explicitly depends upon the exchange-correlation integrand F_{xc} it is possible to investigate the effect of varying the F_{xc} . Therefore the notation is extended such that the functional of the density used to generate the integrand is appended in square brackets. For example, an MKS calculation using a Brueckner Doubles density with the HCTH integrand is denoted MKS(BD)[HCTH].

Unlike the MKS calculations for magnetic response, for electric response calculations one basis set was used consistently for all parts of the calculations. The basis sets employed for polarisability and excitation energy

calculations are rather more modest than those required to generate accurate shielding constants and consequently there was no advantage in using a smaller basis for the ZMP calculations.

4.4 MKS polarisabilities

Static electric polarisabilities are quantifications of the ease of distortion of charge density by an external electric field. The calculation of polarisabilities is of considerable importance owing to their use in the understanding of molecular interactions and the properties of dimers.

Static electric polarisabilities were calculated for 14 small molecules. All polarisability calculations were carried out at the near experimental geometries listed in Appendix C and used the Sadlej basis set [152, 153].

4.4.1 Analytical versus numerical calculations

There are two possible ways of determining a static polarisability; the finite field method (numerical differentiation) or solving the coupled-perturbed Kohn-Sham equations (computing the derivative analytically). Both approaches are equivalent, but analytical evaluation—while more difficult to implement—is numerically more stable. Analytical derivatives were used for all methods except BD and BD(T) for which the procedure is not available in CADPAC. For these, numerical differentiation was necessary.

In numerical polarisability calculations, the components of the polarisability tensor are constructed through a series of calculations with applied electric fields

$$\alpha_{\alpha\beta} = \frac{\mu_{\alpha}(+\delta E_{\beta}) - \mu_{\alpha}(-\delta E_{\beta})}{2\delta E_{\beta}} \quad (4.28)$$

where μ_{α} is the dipole moment component in the direction α and δE_{β} is the magnitude of the applied field in the direction β . Then, for a polarisability

tensor

$$\begin{pmatrix} \alpha_{xx} & \alpha_{xy} & \alpha_{xz} \\ \alpha_{yx} & \alpha_{yy} & \alpha_{yz} \\ \alpha_{zx} & \alpha_{zy} & \alpha_{zz} \end{pmatrix} \quad (4.29)$$

the isotropic polarisability is [154]

$$\alpha = \frac{1}{3} (\alpha_{xx} + \alpha_{yy} + \alpha_{zz}) \quad (4.30)$$

and the anisotropic polarisability $\Delta\alpha$ is defined by [154]

$$(\Delta\alpha)^2 = \frac{1}{2} [(\alpha_{xx} - \alpha_{yy})^2 + (\alpha_{xx} - \alpha_{zz})^2 + (\alpha_{yy} - \alpha_{zz})^2] \quad (4.31)$$

For all calculations an electric field strength of 0.001 au was used.

4.4.2 Error analysis and vibrational corrections

When considering the results of calculations of molecular polarisabilities, it is important to note that calculated values correspond to static polarisabilities, while experimental values relate to molecules that are vibrating. Unless vibrational corrections are introduced, a comparison between experimental and calculated values is not valid. To make error analysis meaningful, comparison with high accuracy correlated *ab initio* methods, rather than experimental values, avoids this problem. Even if vibrational effects are eliminated however, it is not true that the highest level correlated method is necessarily the most accurate, since cancellation of errors may mean that simpler methods yield more accurate results for a given basis (errors due to decreasing the order of correlation and reducing the size of the basis may have opposite sign, and hence cancel each other). As an example, to assess the accuracy of the BD and BD(T) methods (the best wavefunction methods available within the CADPAC program) the vibrational corrections of Russell and Spackman [155, 156] were added to the calculated values for the 7 molecules CH₄, H₂O, H₂S, HCl, HF, NH₃ and PH₃ and the resulting polarisabilities were compared with experimental values. For this procedure, BD has a mean absolute error of 0.09 au compared with the BD(T) value of 0.22, so adding the

perturbative triplet excitations seems to reduce the accuracy. However, to compare with BD values, as those which get closest to experimental values neglecting vibrational effects, begs the question as to how good the vibrational correction actually is, and what effect basis set truncation has. We consider it more sensible to compare with BD(T) values, since this is the highest order correlated method available to us within the approximation of the basis set and neglect of vibration.

4.4.3 Isotropic and anisotropic polarisabilities

In Table 4.5 we present isotropic polarisabilities of 14 small molecules, calculated using DFT methods, wavefunction methods and multiplicative Kohn-Sham potentials built from DFT and wavefunction densities. DFT methods and densities are denoted by the exchange-correlation functional. All MKS calculations used the LDAX F_{xc} (Local Density Approximation for exchange only).

Table 4.5: Static isotropic polarisabilities (in atomic units), determined using the Sadlej basis set. MKS calculations use the LDAX F_{xc}

	HCTH	B97-1	B97-2	HF-SCF	MP2	BD	BD(T)	MKS (HCTH)	MKS (B97-1)	MKS (B97-2)	MKS (HF-SCF)	MKS (MP2)	MKS (BD)	MKS (BD(T))	Expt. ¹
C ₂ H ₄	27.96	27.92	27.56	27.77	27.26	26.74	26.91	27.33	27.31	26.79	26.72	27.73	27.05	27.30	27.70
CH ₄	17.08	16.86	16.64	15.88	16.51	16.29	16.43	16.71	16.58	16.28	15.78	16.69	16.42	16.54	17.27
Cl ₂	30.89	30.91	30.46	29.89	30.56	30.47	30.71	30.18	30.45	29.75	29.36	31.14	30.78	31.10	30.35
CO	13.33	13.05	12.96	12.23	13.09	12.91	13.04	13.04	12.92	12.72	12.31	13.21	12.95	13.10	13.08
CO ₂	17.42	17.17	16.99	15.81	17.82	17.39	17.56	17.08	17.01	16.68	15.82	17.44	17.03	17.27	17.51
F ₂	8.69	8.62	8.53	8.58	8.22	8.31	8.45	8.49	8.37	8.20	7.60	8.63	8.43	8.58	8.38
H ₂ O	10.25	9.81	9.70	8.50	9.79	9.48	9.71	9.97	9.69	9.46	8.58	9.81	9.45	9.64	9.64
H ₂ S	25.18	24.99	24.61	23.78	24.71	24.44	24.67	24.56	24.58	24.04	23.92	25.13	24.78	25.01	24.71
HCl	17.84	17.74	17.42	16.67	17.37	17.26	17.43	17.40	17.52	17.07	16.92	17.78	17.61	17.77	17.39
HF	6.02	5.75	5.68	4.89	5.67	5.51	5.64	5.86	5.70	5.55	4.95	5.71	5.52	5.64	5.60
N ₂	11.94	11.84	11.71	11.43	11.46	11.59	11.75	11.71	11.72	11.50	11.39	11.89	11.77	11.89	11.74
NH ₃	15.07	14.53	14.34	12.93	14.42	14.04	14.33	14.68	14.33	13.98	13.01	14.57	14.08	14.33	14.56
PH ₃	31.30	30.99	30.76	29.91	30.68	30.29	30.45	30.53	30.44	29.98	29.76	30.97	30.52	30.73	30.90
SO ₂	25.95	25.50	25.26	23.73	26.15	25.66	26.06	25.50	25.27	24.81	23.48	26.31	25.44	25.95	25.61
Errors relative to experimental values															
mean	0.32	0.09	-0.13	-0.89	-0.05	-0.29	-0.11	-0.10	-0.18	-0.55	-1.06	0.18	-0.19	0.03	
mean abs.	0.36	0.22	0.19	0.93	0.24	0.31	0.28	0.22	0.24	0.55	1.06	0.28	0.30	0.28	
Errors relative to BD(T) values															
mean	0.43	0.20	-0.02	-0.77	0.06	-0.18		0.02	-0.07	-0.43	-0.95	0.30	-0.07	0.14	
mean abs.	0.47	0.34	0.24	0.92	0.17	0.19		0.24	0.20	0.43	0.95	0.31	0.21	0.22	

¹CO from Ref. [157]; all others from Ref. [154]

When comparing results with those from BD(T), MP2 performs best overall, while BD is very close. The best MKS results are for B97-1, BD and BD(T) densities, and all these give mean absolute errors which are comparable with the best wavefunction methods. MKS(BD) and MKS(BD(T)) mean absolute errors are very close to those of BD and BD(T). This is very encouraging, as it means it is possible to obtain correlated wavefunction type accuracy for polarisabilities without differentiating the wavefunction energy twice. The fact that this accuracy can be achieved using wavefunction densities in a DFT calculation also shows that inclusion of the current dependence in response property calculations is not necessary for the DFT model to equal the best *ab initio* performance; improving the description of the orbitals and eigenvalues is sufficient.

Even more important, from the point of view of practical calculations, is the performance of MKS(B97-1). Here again, the performance of the correlated wavefunction calculations is equalled, but no wavefunction calculations is performed, and hence the N^7 scaling that limits coupled cluster calculations is avoided. Although the MKS procedure is less efficient than a standard DFT calculation it will scale in a similar way (N^4).

Noting that calculating errors with respect to experimental values is not strictly valid, the comparison is nonetheless interesting since the pattern seen is similar to the comparison with BD(T). B97-2 has the lowest mean absolute error overall, while MP2 is the best wavefunction method. MKS(HCTH) and MKS(B97-1) are comparable with the best DFT and wavefunction methods. Also, MKS(BD) and MKS(BD(T)) have mean absolute errors very close to BD and BD(T) respectively.

Similarly, anisotropic polarisabilities are presented in Table 4.6. Note that, in the case of the errors compared to experimental values, this is only for the 10 systems for which experimental values are available. Comparing with BD(T), BD performs the best by a considerable margin. This seems to be because of the close agreement between BD and BD(T) on the value for SO_2 . There is little variation in the errors of the other methods, except



for the HF-SCF and MKS(HF-SCF), both of which are extremely poor. In comparing with experiment there are no clear winners, although conventional B97-1 and B97-2 perform best overall.

An important point to note is the seeming disparity in the errors for the B97-1 and B97-2 DFT methods and the MKS results using B97-1 and B97-2 densities. For conventional DFT calculations, B97-2 outperforms B97-1. However, when using these two functionals in MKS calculations B97-1 gives better results than B97-2. This can be understood by considering the densities associated with the two functionals. In order to assess the quality of the densities dipole moments were calculated (see Table 4.7). Dipole moments are a good indication of the quality of a density and B97-1 outperforms B97-2. Since the values of properties calculated using the MKS method depend on the quality of the density, it might be predicted that MKS(B97-1) would outperform MKS(B97-2).

The question remains: why is conventional B97-2 better at calculating polarisabilities than B97-1? B97-2 is fitted to exchange-correlation potentials, and consequently is more likely to describe the long-range region well: more physics is included in the functional. This region is important for the accurate calculation of polarisabilities. B97-1 does better at short range, which accounts for its performance on dipole moment calculations. The issue is the emphasis of different regions of space.

Table 4.6: Static anisotropic polarisabilities (in atomic units), determined using the Sadlej basis set. MKS calculations use the LDAX F_{XC}

	HCTH	B97-1	B97-2	HF-SCF	MP2	BD	BD(T)	MKS (HCTH)	MKS (B97-1)	MKS (B97-2)	MKS (HF-SCF)	MKS (MP2)	MKS (BD)	MKS (BD(T))	Expt. ¹
C ₂ H ₄	11.78	11.84	11.91	12.98	10.61	11.02	10.86	11.32	10.85	10.86	9.04	10.68	10.74	10.91	11.40
CH ₄	0.00	0.00	0.00	0.00	0.00	0.00	0.00	0.00	0.00	0.00	0.00	0.00	0.00	0.00	
Cl ₂	16.23	16.62	16.58	18.30	16.56	16.78	16.61	15.85	15.90	15.73	15.26	16.00	15.77	15.83	17.53
CO	3.75	3.65	3.63	3.36	3.91	4.00	3.94	3.66	3.54	3.47	2.91	3.41	3.18	3.25	
CO ₂	13.65	13.44	13.34	12.04	14.93	14.37	14.38	13.48	13.08	12.90	10.96	12.93	12.35	12.67	14.17
F ₂	5.62	6.27	6.24	9.01	4.92	5.75	5.70	5.44	5.54	5.50	5.60	5.39	5.46	5.46	
H ₂ O	0.30	0.60	0.59	1.14	0.42	0.48	0.41	0.32	0.54	0.56	0.84	0.16	0.31	0.25	0.66
H ₂ S	1.21	0.89	0.77	0.31	0.82	0.77	0.91	1.06	0.86	0.70	0.65	0.93	0.73	0.82	0.65
HCl	1.44	1.55	1.57	1.87	1.87	1.68	1.66	1.47	1.49	1.53	1.50	1.50	1.57	1.55	1.45
HF	1.12	1.19	1.18	1.29	1.10	1.17	1.16	1.10	1.13	1.13	1.12	0.83	0.90	0.88	1.33
N ₂	5.06	5.03	5.06	5.38	4.44	4.82	4.87	4.92	4.71	4.70	4.18	4.85	4.63	4.65	4.70
NH ₃	2.52	1.82	1.79	0.51	1.93	1.65	1.87	2.44	1.88	1.77	1.03	2.30	1.89	2.07	1.94
PH ₃	2.09	1.78	1.70	0.96	1.68	1.43	1.56	2.08	1.97	1.85	2.05	2.05	1.66	1.72	
SO ₂	13.23	13.02	12.99	12.50	13.68	10.73	10.80	13.07	12.62	12.51	10.69	12.78	12.08	12.44	13.00
Errors relative to experimental values															
mean	-0.03	-0.08	-0.11	-0.06	-0.05	-0.34	-0.33	-0.32	-0.38	-0.44	-1.16	-0.39	-0.59	-0.48	
mean abs.	0.45	0.31	0.33	0.83	0.45	0.47	0.50	0.42	0.43	0.47	1.20	0.55	0.63	0.56	
Errors relative to BD(T) values															
mean	0.23	0.21	0.19	0.35	0.11	-0.01		0.11	-0.04	-0.11	-0.64	-0.06	-0.25	-0.16	
mean abs.	0.48	0.41	0.43	1.13	0.39	0.08		0.47	0.38	0.42	0.77	0.48	0.45	0.45	

¹Ref. [158]

Table 4.7: Dipole moments (in atomic units) determined using the Sadlej basis set

	B97-1	B97-2	MKS (B97-1)	MKS (B97-2)	BD	BD(T)	Expt. ¹
CO	0.044	0.041	0.043	0.041	0.040	0.056	0.043
H ₂ O	0.726	0.727	0.726	0.727	0.731	0.722	0.727
H ₂ S	0.401	0.409	0.401	0.409	0.391	0.384	0.401
HCl	0.441	0.444	0.441	0.444	0.440	0.433	0.441
HF	0.705	0.706	0.705	0.706	0.708	0.702	0.707
NH ₃	0.598	0.598	0.598	0.598	0.601	0.592	0.603
PH ₃	0.258	0.272	0.258	0.272	0.231	0.228	0.226
SO ₂	0.641	0.632	0.641	0.632	0.679	0.644	0.640
Errors relative to experimental values($\times 10^{-3}$)							
mean	3.11	5.19	3.13	5.20	4.07	-3.42	
mean abs.	5.23	9.23	5.15	9.34	8.05	8.06	
Errors relative to BD(T) values($\times 10^{-2}$)							
mean	0.65	0.86	0.66	0.86	0.75		
mean abs.	1.03	1.52	1.05	1.54	1.14		

¹Ref. [158]

4.4.4 Variation of isotropic polarisabilities with F_{xc}

Next the effect of varying F_{xc} on the MKS isotropic polarisability calculations is considered. In Tables 4.8 to 4.11 are presented isotropic polarisabilities from MKS calculations with a range of densities using the LDAX+VWN, BLYP, HCTH and $1/4 F_{xc}$ approximations respectively. Also presented is a summary of the mean errors cf. BD(T) in Table 4.12. Overall, the LDAX F_{xc} performs best, giving the smallest mean error for HCTH, B97-1, BD and BD(T) densities. Only B97-2 and HF-SCF perform better with another F_{xc} , specifically the HCTH F_{xc} . Note that the B97-1 density coupled with the BLYP F_{xc} gives a mean error comparable with those termed ‘best’.

Table 4.8: MKS static isotropic polarisabilities (in atomic units) determined using the Sadlej basis and the LDAX+VWN F_{xc}

	MKS (HCTH)	MKS (B97-1)	MKS (B97-2)	MKS (HF-SCF)	MKS (MP2)	MKS (BD)	MKS (BD(T))	BD(T)	Expt. ¹
C ₂ H ₄	27.73	27.71	27.17	27.10	28.13	27.43	27.68	26.91	27.70
CH ₄	16.96	16.82	16.52	16.00	16.93	16.65	16.78	16.43	17.27
Cl ₂	30.57	30.84	30.12	29.72	31.54	31.17	31.50	30.71	30.35
CO	13.21	13.08	12.87	12.46	13.37	13.11	13.26	13.04	13.08
CO ₂	17.25	17.18	16.84	15.96	17.60	17.19	17.43	17.56	17.51
F ₂	8.57	8.45	8.27	7.66	8.71	8.51	8.66	8.45	8.38
H ₂ O	10.13	9.83	9.60	8.69	9.95	9.58	9.78	9.71	9.64
H ₂ S	25.00	25.01	24.45	24.33	25.57	25.21	25.44	24.33	24.71
HCl	17.68	17.80	17.33	17.18	18.05	17.88	18.05	17.43	17.39
HF	5.93	5.77	5.62	5.01	5.78	5.59	5.71	5.69	5.60
N ₂	11.84	11.85	11.63	11.51	12.02	11.90	12.02	11.75	11.74
NH ₃	14.94	14.57	14.21	13.21	14.82	14.31	14.56	14.33	14.56
PH ₃	31.07	30.98	30.50	30.28	31.51	31.05	31.26	30.64	30.57
SO ₂	25.78	25.53	25.07	23.71	26.59	25.71	26.22	26.06	25.61
Errors relative to experimental values									
mean	0.16	0.07	-0.30	-0.83	0.44	0.06	0.28	-0.11	
mean abs.	0.24	0.19	0.31	0.83	0.49	0.28	0.36	0.28	
Errors relative to BD(T) values									
mean	0.27	0.18	-0.19	-0.72	0.55	0.18	0.39		
mean abs.	0.38	0.31	0.26	0.74	0.55	0.31	0.41		

¹CO from Ref. [157]; all others from Ref. [154]

Table 4.9: MKS static isotropic polarisabilities (in atomic units) determined using the Sadlej basis set and the BLYP F_{XC}

	MKS (HCTH)	MKS (B97-1)	MKS (B97-2)	MKS (HF-SCF)	MKS (MP2)	MKS (BD)	MKS (BD(T))	BD(T)	Expt. ¹
C ₂ H ₄	27.43	27.42	26.89	26.84	27.84	27.18	27.42	26.91	27.70
CH ₄	16.75	16.62	16.33	15.83	16.74	16.47	16.60	16.43	17.27
Cl ₂	30.18	30.46	29.76	29.38	31.15	30.80	31.11	30.71	30.35
CO	13.02	12.90	12.70	12.30	13.19	12.94	13.09	13.04	13.08
CO ₂	17.02	16.96	16.63	15.78	17.39	16.99	17.22	17.56	17.51
F ₂	8.48	8.36	8.19	7.59	8.64	8.43	8.58	8.45	8.38
H ₂ O	9.92	9.65	9.41	8.55	9.78	9.42	9.61	9.71	9.64
H ₂ S	24.55	24.59	24.04	23.94	25.14	24.80	25.02	24.33	24.71
HCl	17.35	17.48	17.03	16.89	17.74	17.58	17.73	17.43	17.39
HF	5.81	5.66	5.51	4.92	5.67	5.49	5.61	5.69	5.60
N ₂	11.66	11.67	11.46	11.35	11.85	11.73	11.85	11.75	11.74
NH ₃	14.65	14.30	13.96	13.00	14.56	14.07	14.31	14.33	14.56
PH ₃	30.64	30.57	30.10	29.91	31.11	30.67	30.87	30.45	30.90
SO ₂	25.43	25.20	24.75	23.45	26.25	25.40	25.90	26.06	25.61
Errors relative to experimental values									
mean	-0.11	-0.19	-0.55	-1.05	0.19	-0.18	0.03	-0.11	
mean abs.	0.21	0.22	0.55	1.05	0.28	0.29	0.26	0.28	
Errors cf. BD									
mean	0.00	-0.07	-0.43	-0.94	0.30	-0.06	0.15		
mean abs.	0.27	0.23	0.43	0.94	0.33	0.24	0.25		

¹CO from Ref. [157]; all others from Ref. [154]

Table 4.10: MKS static isotropic polarisabilities (in atomic units) determined using the Sadlej basis set and the HCTH F_{XC}

	MKS (HCTH)	MKS (B97-1)	MKS (B97-2)	MKS (HF-SCF)	MKS (MP2)	MKS (BD)	MKS (BD(T))	BD(T)	Expt. ¹
C ₂ H ₄	27.91	27.93	27.37	27.37	28.39	27.70	27.95	26.91	27.70
CH ₄	17.02	16.91	16.60	16.11	17.05	16.77	16.90	16.43	17.27
Cl ₂	30.88	31.19	30.45	30.07	31.90	31.53	31.86	30.71	30.35
CO	13.30	13.19	12.98	12.59	13.50	13.24	13.39	13.04	13.08
CO ₂	17.40	17.35	17.00	16.15	17.81	17.39	17.63	17.56	17.51
F ₂	8.68	8.56	8.38	7.77	8.85	8.64	8.79	8.45	8.38
H ₂ O	10.19	9.91	9.67	8.78	10.07	9.70	9.89	9.71	9.64
H ₂ S	25.14	25.20	24.62	24.53	25.77	25.41	25.64	24.33	24.71
HCl	17.81	17.95	17.47	17.33	18.22	18.05	18.21	17.43	17.39
HF	5.98	5.82	5.67	5.07	5.85	5.67	5.78	5.69	5.60
N ₂	11.91	11.93	11.70	11.61	12.11	12.00	12.12	11.75	11.74
NH ₃	15.01	14.66	14.30	13.33	14.95	14.44	14.69	14.33	14.56
PH ₃	31.27	31.23	30.73	30.56	31.80	31.33	31.54	30.45	30.90
SO ₂	25.91	25.71	25.24	23.94	26.81	25.93	26.44	26.06	25.61
Errors relative to experimental values									
mean	0.28	0.22	-0.16	-0.66	0.62	0.24	0.46	-0.11	
mean abs.	0.33	0.30	0.20	0.66	0.65	0.34	0.51	0.28	
Errors relative to BD(T) values									
mean	0.40	0.33	-0.05	-0.55	0.73	0.35	0.57		
mean abs.	0.44	0.42	0.23	0.66	0.73	0.40	0.57		

¹CO from Ref. [157]; all others from Ref. [154]

Table 4.11: MKS static isotropic polarisabilities (in atomic units) determined using the Sadlej basis set and the $1/4 F_{xc}$

	MKS (HCTH)	MKS (B97-1)	MKS (B97-2)	MKS (HF-SCF)	MKS (MP2)	MKS (BD)	MKS (BD(T))	BD(T)	Expt. ¹
C ₂ H ₄	27.74	27.73	27.19	27.16	28.18	27.49	27.74	26.91	27.70
CH ₄	16.96	16.83	16.53	16.03	16.95	16.68	16.80	16.43	17.27
Cl ₂	30.65	30.94	30.22	29.83	31.65	31.28	31.61	30.71	30.35
CO	13.21	13.09	12.89	12.49	13.39	13.14	13.28	13.04	13.08
CO ₂	17.25	17.19	16.86	16.00	17.64	17.23	17.46	17.56	17.51
F ₂	8.57	8.45	8.28	7.67	8.73	8.52	8.67	8.45	8.38
H ₂ O	10.10	9.81	9.58	8.69	9.96	9.59	9.78	9.71	9.64
H ₂ S	25.01	25.05	24.48	24.38	25.61	25.26	25.49	24.33	24.71
HCl	17.68	17.81	17.35	17.20	18.08	17.91	18.07	17.43	17.39
HF	5.91	5.75	5.61	5.01	5.77	5.59	5.70	5.69	5.60
N ₂	11.83	11.84	11.62	11.52	12.02	11.90	12.02	11.75	11.74
NH ₃	14.89	14.54	14.19	13.21	14.81	14.31	14.56	14.33	14.56
PH ₃	31.14	31.07	30.59	30.40	31.63	31.17	31.38	30.45	30.90
SO ₂	25.77	25.54	25.08	23.77	26.62	25.75	26.25	26.06	25.61
Errors relative to experimental values									
mean	0.16	0.09	-0.29	-0.79	0.47	0.10	0.31	-0.11	
mean abs.	0.24	0.21	0.29	0.79	0.52	0.30	0.39	0.28	
Errors relative to BD(T) values									
mean	0.27	0.20	-0.17	-0.68	0.59	0.21	0.43		
mean abs.	0.37	0.33	0.27	0.72	0.59	0.34	0.44		

¹CO from Ref. [157]; all others from Ref. [154]

Table 4.12: Summary of variation of mean errors with F_{xc} cf. BD(T)

	MKS (HCTH)	MKS (B97-1)	MKS (B97-2)	MKS (HF-SCF)	MKS (MP2)	MKS (BD)	MKS (BD(T))
LDAX	0.25	0.20	0.43	0.95	0.31	0.21	0.22
LDAX+VWN	0.38	0.31	0.26	0.74	0.55	0.31	0.41
BLYP	0.27	0.23	0.43	0.94	0.33	0.24	0.25
HCTH	0.44	0.42	0.23	0.66	0.73	0.40	0.57
1/4	0.37	0.33	0.27	0.72	0.59	0.34	0.44

4.4.5 The HCTH[LDAX] method

In Table 4.13 the performance of another procedure, termed HCTH[LDAX], is assessed. This is a standard HCTH calculation with the F_{xc} replaced by that of the LDAX. With this it is hoped to reproduce the performance of MKS(HCTH)[LDAX] without the cost of the separate density and potential calculations. We include standard HCTH and MKS(HCTH)[LDAX] results for comparison. Since the only difference between the HCTH[LDAX] and MKS(HCTH)[LDAX] procedures should be the asymptotic correction introduced by the Fermi-Amaldi term in the ZMP method, asymptotically corrected HCTH [143] results (denoted HCTH(AC)) are also presented.

Replacing the F_{xc} to give HCTH[LDAX] does produce results very close to those of the MKS(HCTH)[LDAX] procedure. The MKS(HCTH)[LDAX] results are slightly lower; since the effect of the asymptotic correction is to lower polarisabilities, this is consistent.

4.5 MKS excitation energies

Excitation energies for CO, N₂, H₂CO and C₂H₄ were calculated at near experimental geometries. The Sadlej basis set was used with additional diffuse functions to ensure good description of the virtual orbitals. Geometries and additional functions used are summarised in Table C.2.

Table 4.13: HCTH[LDAX] static isotropic polarisabilities (in atomic units) determined using the Sadlej basis set

	HCTH	MKS(HCTH)	HCTH	HCTH	BD(T)	Expt ¹
		[LDAX]	[LDAX]	(AC)		
C ₂ H ₄	27.96	27.33	27.38	26.64	26.91	27.70
CH ₄	17.08	16.71	16.77	16.15	16.43	17.27
Cl ₂	30.89	30.18	30.20	30.74	30.71	30.35
CO	13.33	13.04	13.08	12.84	13.04	13.08
CO ₂	17.42	17.08	17.11	16.93	17.56	17.51
F ₂	8.69	8.49	8.51	8.28	8.45	8.38
H ₂ O	10.25	9.97	10.04	9.40	9.71	9.64
H ₂ S	25.18	24.56	24.61	24.71	24.33	24.71
HCl	17.84	17.40	17.44	17.64	17.43	17.39
HF	6.02	5.86	5.90	5.44	5.69	5.60
N ₂	11.94	11.71	11.75	11.52	11.75	11.74
NH ₃	15.07	14.68	14.76	13.88	14.33	14.56
PH ₃	31.30	30.53	30.57	30.73	30.45	30.93
SO ₂	25.95	25.50	25.55	25.51	26.06	25.61
Errors relative to experimental values						
mean	0.32	-0.10	-0.06	-0.29	-0.11	
mean abs.	0.36	0.22	0.21	0.38	0.28	
Errors relative to BD(T) values						
mean	0.43	0.02	0.07	-0.17		
mean abs.	0.47	0.25	0.27	0.30		

¹CO from Ref. [157]; all others from Ref. [154]

Knowing that there is an explicit dependence on F_{xc} in the electric Hessian matrix it was anticipated that varying F_{xc} would have an effect on calculated electric response properties. We have shown that this is the case for polarisabilities. We note that MKS(BD)[LDAX] performs much better than MKS(BD)[HCTH] for polarisabilities. Since the procedure for determining Kohn-Sham orbitals and eigenvalues, MKS(BD), is constant between the two methods the orbitals and eigenvectors themselves will be constant. Thus the difference between the two methods is due to the F_{xc} .

Vertical excitation energies were calculated for CO, N₂, H₂CO and C₂H₄. The singlet excitations for these molecules are presented in Tables 4.14 to 4.17. We compare a standard KS-DFT calculation using the HCTH exchange-correlation functional with an MKS calculation using a BD density with both the HCTH and LDAX F_{xc} and the HCTH[LDAX] method (described above). In comparing the MKS(BD)[HCTH] and MKS(BD)[LDAX] results it can be seen that the choice of F_{xc} has relatively little effect on the mean absolute errors: Rydberg excitations are insensitive to F_{xc} . This is consistent with the observation that Rydbergs may be improved by improving eigenvalue differences (via an asymptotic correction which leaves F_{xc} unchanged). In effect, the eigenvalue differences dominate the electric Hessian matrix. In contrast, the valence excitations are much more sensitive to F_{xc} , changing by up to 0.2 eV. This suggests that accurately representing F_{xc} is important for the evaluation of low lying excitations, a class that is problematic for Kohn-Sham theory.

4.6 Summary

We have considered response properties using the MKS procedure. Previous studies have shown a dramatic improvement for shielding constants when going from conventional B97-2 to MKS(B97-2) [59, 69]: similar results are seen here for chemical shifts. MKS(B97-2) chemical shift errors are the lowest of the methods considered in this study, though KT2 is the best practical

Table 4.14: Vertical excitation energies of CO (in eV), computed using the augmented Sadlej basis set.

State	Transition	HCTH	MKS(BD) [HCTH]	MKD(BD) [LDAX]	HCTH [LDAX]	Expt ¹
$F \ ^1\Sigma^+$	$\sigma \rightarrow 3d\sigma$	9.58	11.69	11.70	9.59	12.4
$E \ ^1\Pi$	$\sigma \rightarrow 3p\pi$	9.48	10.87	10.88	9.53	11.53
$C \ ^1\Sigma^+$	$\sigma \rightarrow 3p\sigma$	9.41	10.82	10.82	9.43	11.40
$B \ ^1\Sigma^+$	$\sigma \rightarrow 3s$	8.94	10.19	10.19	8.96	10.78
$D \ ^1\Delta$	$\pi \rightarrow \pi^*$	10.19	10.39	10.62	10.41	10.23
$I \ ^1\Sigma^-$	$\pi \rightarrow \pi^*$	9.92	10.13	10.13	9.92	9.88
$A \ ^1\Pi$	$\sigma \rightarrow \pi^*$	8.31	8.55	8.71	8.44	8.51
Mean abs. error		1.13	0.39	0.46	1.11	

¹Ref [159]Table 4.15: Vertical excitation energies of N₂ (in eV), computed using the augmented Sadlej basis set.

State	Transition	HCTH	MKS(BD) [HCTH]	MKD(BD) [LDAX]	HCTH [LDAX]	Expt ¹
$^1\Pi_u$	$\pi_u \rightarrow 3s\sigma_g$	11.11	13.12	13.14	11.08	13.24
$^1\Sigma_u^+$	$\sigma_g \rightarrow 3p\sigma_u$	10.48	12.13	12.10	10.48	12.98
$^1\Pi_u$	$\sigma_g \rightarrow 3p\pi_u$	10.49	12.07	12.06	10.50	12.90
$^1\Sigma_g^+$	$\sigma_g \rightarrow 3s\sigma_g$	10.19	11.48	11.47	10.20	12.2
$^1\Delta_u$	$\pi_u \rightarrow \pi_g$	10.08	10.09	10.34	10.33	10.27
$^1\Sigma_u^-$	$\pi_u \rightarrow \pi_g$	9.73	9.75	9.75	9.73	9.92
$^1\Pi_g$	$\sigma_g \rightarrow \pi_g$	9.15	9.40	9.53	9.27	9.31
Mean abs. error		1.25	0.38	0.39	1.27	

¹Ref [160]

Table 4.16: Vertical excitation energies of H₂CO (in eV), computed using the Sadlej basis set.

State	Transition	HCTH	MKS(BD) [HCTH]	MKD(BD) [LDAX]	HCTH [LDAX]	Expt ¹
¹ A ₂	$n \rightarrow 3db_1$	7.11	9.21	9.22	7.11	9.22
¹ A ₂	$n \rightarrow 3pb_1$	6.54	8.25	8.26	6.55	8.38
¹ B ₁	$\sigma \rightarrow \pi^*$	8.98	9.32	9.42	9.08	8.68
¹ B ₂	$n \rightarrow 3pa_1$	6.38	7.84	7.86	6.39	8.12
¹ A ₁	$n \rightarrow 3pb_2$	6.33	7.97	8.01	6.32	7.97
¹ B ₂	$n \rightarrow 3sa_1$	5.69	7.05	7.07	5.68	7.09
¹ A ₂	$n \rightarrow \pi^*$	3.92	4.42	4.50	4.00	3.94
Mean abs. error		1.29	0.23	0.25	1.31	

¹Ref [161]

choice as it provides excellent results at a low computational cost.

MKS(BD) and MKS(BD(T)) polarisabilities are close to those of conventional BD and BD(T) calculations respectively. MKS(B97-2) does not reduce errors in polarisabilities as was seen for magnetic response properties. The best polarisabilities used the LDAX F_{xc} . For vertical excitations, Rydberg excitations are relatively insensitive to F_{xc} . Valence excitations are more sensitive, and the accuracy of the F_{xc} is important, but no calculations performed as part of this work showed a substantial gain in accuracy.

Table 4.17: Vertical excitation energies of C_2H_4 (in eV), for states formed by single excitations from the $b_{3u} = \pi$ orbital (molecule lies in yz plane), computed using the augmented Sadlej basis set.

State	Transition	HCTH	MKS(BD) [HCTH]	MKD(BD) [LDAX]	HCTH [LDAX]	Expt ¹
$^1B_{1u}$	$3d\pi = b_{2g}$	7.82	9.09	9.12	8.09	9.33
$^1B_{2u}$	$3d\delta = b_{1g}$	7.37	8.83	8.85	7.58	9.05
$^1B_{3u}$	$3d\delta = a_g$	7.29	8.74	8.75	7.45	8.90
$^1B_{3u}$	$3d\sigma = a_g$	6.86	8.53	8.55	6.98	8.62
1A_g	$3p\pi = b_{3u}$	6.94	8.15	8.14	7.05	8.28
$^1B_{1u}$	$\pi^* = b_{2g}$	7.18	7.57	7.72	7.30	8.0
$^1B_{2g}$	$3p\sigma = b_{1u}$	6.68	7.71	7.72	6.71	7.90
$^1B_{1g}$	$3p\sigma = b_{2u}$	6.69	7.67	7.68	6.73	7.80
$^1B_{3u}$	$3s = a_g$	6.24	7.07	7.07	6.24	7.11
Mean abs. error		1.32	0.18	0.15	1.21	

¹Ref [162]

Chapter 5

Eigenvalues, integer discontinuities and NMR shieldings

In this chapter, high quality electron densities are used to investigate Kohn-Sham eigenvalues and related properties. First, Kohn-Sham HOMO-LUMO eigenvalue differences are considered. GGA values are compared with values determined from coupled-cluster densities; the influence on NMR shielding constants is investigated. Next, eigenvalues calculated from electron densities are used to investigate the integer discontinuity. This leads to a consideration of the HOMO eigenvalue. GGA HOMO eigenvalues are compared with ionisation potentials and eigenvalues calculated from a continuum functional that averages over the integer discontinuity. Further investigation of NMR shielding constants is presented, and the study is extended to excitation energies.

5.1 HOMO-LUMO eigenvalue differences

Kohn-Sham eigenvalues are extremely important [65, 163, 164, 165, 166, 167, 168, 169, 170, 171, 172, 173, 174, 21], both intrinsically, since there is controversy over the physical significance (if any) of Kohn-Sham orbitals and eigenvalues, and practically, because of the importance of eigenvalue differences in the calculation of response properties.

The ZMP method was used to calculate Kohn-Sham orbitals and eigenvalues from Brueckner Doubles electron densities. A Lagrange multiplier value of $\lambda = 900$ was employed. An extensive preliminary investigation into the effect of the use of different basis sets was carried out. Diffuse functions were found to be important, as the calculations require a good description of high-lying orbitals. Unless otherwise stated, the aug-cc-PVTZ basis set [175], with d and f functions removed (for technical reasons) from hydrogen and non-hydrogen atoms respectively, was used. Near experimental geometries used are listed in Table C.3. Experimental vertical ionisation potentials (I) and electron affinities (A) are listed in Table C.4.

In Table 5.1 HOMO-LUMO eigenvalue differences from the ZMP procedure are compared with those from conventional GGA functionals. Although HCTH (Section 2.8.4) is fitted to thermochemical data and ZMP potentials, while PBE (Section 2.8) is non-empirical and developed from theoretical considerations, the two functionals give very similar results. (Note that although HCTH used ZMP(BD) potentials in the fitting procedure, it was not explicitly fitted to BD densities and other data were also fitted to. Thus we do not expect HCTH to necessarily reproduce the ZMP(BD) values.) Eigenvalue differences from both HCTH and 1/4 are below those from the ZMP calculations. The 1/4 functional (Section 2.8.5) shares a functional form with HCTH, but it was fitted to ZMP potentials only, with no explicit thermochemical information supplied. This emphasis on ZMP potentials might be expected to improve 1/4 HOMO-LUMO eigenvalue differences, and the 1/4 results are closer to those calculated using the ZMP approach than HCTH or PBE. However, the improvement is small, and the 1/4 values are still lower

Table 5.1: HOMO-LUMO eigenvalue differences $\Delta\epsilon = \epsilon_{\text{LUMO}} - \epsilon_{\text{HOMO}}$ determined from the ZMP approach, compared to those from the HCTH, PBE, and 1/4 functionals. Experimental values of $I - A$ and calculated $\Delta_{\text{XC}} = I - A - \Delta\epsilon^{\text{ZMP}}$ are also presented. All values are in au.

System	$\Delta\epsilon^{\text{ZMP}}$	$\Delta\epsilon^{\text{HCTH}}$	$\Delta\epsilon^{\text{PBE}}$	$\Delta\epsilon^{1/4}$	$I - A$	Δ_{XC}
H ₂ O	0.28	0.23	0.23	0.24	0.70	0.42
NH ₃	0.24	0.20	0.20	0.21	0.60	0.37
CH ₄	0.37	0.33	0.33	0.35	0.79	0.42
HF	0.38	0.32	0.32	0.33	0.81	0.43
PH ₃	0.24	0.22	0.22	0.23	0.46	0.22
CO	0.27	0.26	0.26	0.26	0.58	0.31
N ₂	0.32	0.31	0.31	0.31	0.65	0.34
H ₂ S	0.22	0.20	0.20	0.21	0.46	0.24
HCN	0.30	0.29	0.29	0.29	0.58	0.29
C ₂ H ₂	0.26	0.25	0.25	0.25	0.52	0.26
C ₂ H ₄	0.21	0.21	0.21	0.21	0.46	0.24
H ₂ CO	0.15	0.14	0.13	0.13	0.46	0.30

than those from ZMP.

5.1.1 NMR shielding constants

Molecular response properties are highly sensitive to eigenvalue differences. This has been demonstrated for the case of NMR shielding constants by the work of Malkin et al. [129], where it was shown that correction of Kohn-Sham eigenvalue differences significantly improved calculated shielding constants. In this section we consider the effect on NMR shielding constants of the aforementioned discrepancy between GGA and ZMP HOMO-LUMO eigenvalues differences.

As discussed in Chapter 4, for a GGA functional the shielding tensor for

nucleus A takes the form [128]

$$\begin{aligned} \sigma_{\alpha\beta}^A &= \sum_j (j | (\mathbf{r} \cdot \mathbf{r}_A \delta^{\alpha\beta} - r_A^\alpha r_A^\beta) r_A^{-3} | j) \\ &- \sum_{bj} \frac{(b | l^\alpha | j)(j | l_A^\beta r_A^{-3} | b) + (b | l_A^\alpha r_A^{-3} | j)(j | l^\beta | b)}{\epsilon_b - \epsilon_j} \end{aligned} \quad (5.1)$$

where l^α and l^β are angular momentum operators; j and b denote occupied and virtual Kohn-Sham orbitals, respectively; and ϵ_j and ϵ_b denote occupied and virtual Kohn-Sham eigenvalues, respectively.

The latter term in eqn. (5.1) is the paramagnetic contribution to the shielding tensor and it involves contributions from all occupied-virtual excitations. However, it is reasonable to suppose that excitations to spatially diffuse high-lying virtual orbitals are relatively unimportant due to the presence of the r^{-3} term in the numerator matrix elements and the relatively large eigenvalue differences in the denominator; this is indeed the case [69, 128].

The underestimation of the HOMO-LUMO gap by conventional functionals seen in Table 5.1 would be expected to reduce calculated shielding constants by increasing the magnitude of the negative paramagnetic term; it is well known that NMR shielding constants calculated from conventional GGA functionals are significantly too deshielded [176]. Previous work by Wilson and Tozer [69] has shown that when eqn. (5.1) is evaluated using ZMP orbitals and eigenvalues determined from Brueckner Doubles densities the resulting shielding constants approach *ab initio* quality. The improvement over conventional GGA shielding constants by this method (MKS(BD)) is due to the improvement of all the orbitals and eigenvalues, but it must arise primarily from low-lying excitations (as high-lying excitations are relatively unimportant) and of these the HOMO-LUMO is likely to be significant. This is because it involves relatively compact orbitals and, of all the excitations, has the smallest eigenvalue difference.

To quantify the effect of excitations to the LUMO, shielding constants were calculated using the HCTH and 1/4 functionals but with their respective

LUMO eigenvalues explicitly replaced by

$$\begin{aligned}\epsilon_{\text{LUMO}}^{\text{HCTH}} &\rightarrow \epsilon_{\text{LUMO}}^{\text{MKS(BD)}} - \epsilon_{\text{HOMO}}^{\text{MKS(BD)}} + \epsilon_{\text{HOMO}}^{\text{HCTH}} \\ \epsilon_{\text{LUMO}}^{1/4} &\rightarrow \epsilon_{\text{LUMO}}^{\text{MKS(BD)}} - \epsilon_{\text{HOMO}}^{\text{MKS(BD)}} + \epsilon_{\text{HOMO}}^{1/4}\end{aligned}\quad (5.2)$$

In other words, the HCTH and 1/4 HOMO-LUMO eigenvalue differences are forced to equal the ZMP differences. The results are denoted HCTH(LC1) and 1/4(LC1) respectively, for ‘LUMO Correction 1’. The results are presented in Table 5.2, together with conventional HCTH and 1/4 shielding constants and the MKS(BD) results from [69]. The deshielding of the conventional functionals and the great improvement of the MKS(BD) results are evident. For both HCTH and 1/4 the LUMO correction reduces the mean absolute errors compared to MKS(BD) (denoted $\Delta^{\text{MKS(BD)}}$) by increasing the shielding constants. In fact, over two-thirds of the error is corrected simply by correcting the LUMO eigenvalue (for HCTH the mean absolute error reduces from 37.5 to 11.9 ppm, while in the case of 1/4 there is a corresponding reduction from 47.4 to 15.1 ppm).

In Table 5.3 anisotropic shieldings for a series of small molecules are presented. Similar results are obtained as with the isotropic shieldings; the LUMO correction reduces the mean absolute errors by more than half.

5.1.2 The integer discontinuity

Using an ensemble treatment, Perdew et al. [171] have demonstrated that the exact exchange-correlation potential is discontinuous as the number of electrons passes through an integer. The limiting potentials from above and below the integer N differ by an amount Δ_{xc}

$$\lim_{\delta \rightarrow 0} v_{\text{xc}}(N + \delta) - \lim_{\delta \rightarrow 0} v_{\text{xc}}(N - \delta) = \Delta_{\text{xc}} \quad (5.3)$$

and give LUMO and HOMO eigenvalues of [171]

$$\begin{aligned}\epsilon_{\text{LUMO}}(N + \delta) &= -A \\ \epsilon_{\text{HOMO}}(N - \delta) &= -I\end{aligned}\quad (5.4)$$

Table 5.2: Isotropic NMR shieldings (in ppm) at near-experimental geometries, determined using the Huzinaga IGLO IV basis set.

Mol.	Nucl.	HCTH	1/4	HCTH (LC1)	1/4 (LC1)	HCTH (LC2)	1/4 (LC2)	MKS (BD)	Expt
HF	F	411.5	413.1	417.9	418.7	412.2	420.5	416.3	419.7 ¹
H ₂ O	O	327.6	329.5	330.3	331.7	331.5	336.0	331.1	357.6 ¹
CH ₄	C	189.3	189.7	189.3	189.7	189.3	189.7	189.9	198.4 ¹
CO	C	-7.5	-15.6	-4.0	-8.5	-49.7	-5.6	0.2	2.8 ¹
	O	-66.8	-74.7	-61.1	-63.6	-134.8	-58.9	-42.9	-36.7 ¹
N ₂	N	-76.9	-84.6	-69.3	-73.7	-132.7	-67.5	-64.4	-59.6 ¹
F ₂	F	-269.9	-278.6	-200.4	-196.8	-	-	-190.9	-192.8 ¹
	O'OO'	O'	-1438.2	-1486.0	-1105.3	-1117.2	-	-	-1063.9
PN	O	-859.4	-886.5	-680.5	-688.3	-	-	-729.4	-724 ¹
	P	-7.6	-41.9	22.4	-1.3	-	-	42.0	53 ²
H ₂ S	N	-378.5	-393.3	-354.2	-360.7	-	-	-346.1	-349 ²
	S	720.1	718.7	724.9	723.6	593.3	690.8	723.4	752 ³
NH ₃	N	259.8	261.0	260.1	261.3	260.5	262.5	261.2	273.3 ¹
HCN	C	75.7	70.4	76.8	71.6	53.3	74.9	79.3	82.1 ¹
	N	-33.4	-43.2	-30.5	-40.2	-89.8	-32.1	-22.0	-20.4 ¹
C ₂ H ₂	C	112.2	107.2	112.7	107.7	95.3	108.1	113.8	117.2 ⁴
C ₂ H ₄	C	53.4	47.5	54.7	49.3	26.3	54.8	56.1	64.5 ⁵
	H ₂ CO	C	-17.7	-27.6	-2.9	-8.5	-38.3	5.2	-8.6
N'NO	O	-406.7	-437.0	-330.6	-340.1	-518.4	-273.7	-331.6	-375 ¹
	N'	94.9	90.4	100.8	97.2	-	-	100.9	99.5 ⁶
	N	8.5	4.0	14.9	11.1	-	-	11.3	11.3 ⁶
CO ₂	O	174.8	175.4	179.1	180.3	-	-	203.3	200.5 ⁶
	C	57.5	53.4	58.0	57.3	57.0	63.1	61.6	58.8 ⁵
	O	215.3	212.2	214.1	217.3	216.9	225.1	235.0	243.4 ⁷
OF ₂	O	-610.9	-637.2	-544.7	-559.5	-	-	-458.5	-473.1 ⁷
H ₂ CNN'	C	161.8	161.3	162.1	161.4	-	-	164.6	164.5 ¹
	N	-51.0	-56.7	-40.8	-45.5	-	-	-39.7	-43.4 ¹
	N'	-155.6	-164.8	-125.2	-130.9	-	-	-124.9	-149.0 ¹
HCl	Cl	949.4	949.9	953.2	952.8	-	-	951.2	952 ⁸
SO ₂	S	-183.9	-212.2	-143.8	-169.3	-	-	-150.5	-126 ³
	O	-260.6	-268.6	-226.0	-232.4	-	-	-180.8	-205 ³
PH ₃	P	576.6	571.6	579.7	575.6	438.0	537.0	577.6	599.9 ⁸
$\Delta^{\text{MKS(BD)}}$		37.5	47.4	11.9	15.1				

¹ Ref. [177]; ² Ref. [178]; ³ Ref. [179]; ⁴ Ref. [180]; ⁵ Ref. [181]; ⁶ Ref. [182]; ⁷ [183]; ⁸ Ref. [184]

Table 5.3: Anisotropic NMR shieldings (in ppm) at near-experimental geometries, determined using the Huzinaga IGLO IV basis set.

Mol.	Nucl.	HCTH	1/4	HCTH	1/4	HCTH	1/4	MKS	Expt
				(LC1)	(LC1)	(LC2)	(LC2)		
HF	F	105.3	101.9	95.7	93.4	104.3	90.7	97.6	93.8 ¹
CO	C	420.9	432.4	415.6	421.9	484.2	417.4	408.7	406.1 ¹
	O	716.0	726.8	707.3	710.2	817.9	703.0	679.3	676.1 ¹
N ₂	N	625.1	635.9	613.7	619.6	708.8	610.3	605.7	603 ¹
F ₂	F	1137.2	1149.2	1033.0	1026.5	-	-	1018.3	1050 ¹
PN	P	1461.7	1511.6	1416.7	1450.7	-	-	1385.9	1376 ²
	N	1081.0	1102.6	1044.5	1053.7	-	-	1031.7	1048 ²
NH ₃	N	-47.9	-48.4	-48.4	-48.8	-49.0	-50.5	-48.5	-40.3 ³
H ₂ CO	C	167.1	179.3	144.9	150.6	198.1	130.1	161.9	158.8 ¹
HCl	Cl	300.1	297.6	294.4	293.3	-	-	296.0	298 ³
PH ₃	P	-64.5	-69.3	-65.2	-70.1	-24.8	-61.4	-50.8	-64.5 ³
$\Delta^{\text{MKS(BD)}}$		31.2	42.8	12.5	17.5				

¹ Ref. [177]; ² Ref. [178]; ³ Ref. [184]

In the case of the exact ZMP potential (where the reference density is equal to the exact density) the potential vanishes asymptotically and

$$\epsilon_{\text{HOMO}}^{\text{ZMP}} = -I \quad (5.5)$$

Eqn. (5.5) can be considered an exact Koopmans' theorem (see Section 1.3.3) for the HOMO eigenvalue. Thus Hartree-Fock has an approximate Koopmans' theorem for all eigenvalues and DFT has an exact Koopmans' theorem for one eigenvalue, that of the HOMO.

It follows, given that the potential in the electron deficient limit has a HOMO eigenvalue equal to $-I$ (eqn. (5.4)), that the exact ZMP potential is the electron deficient limit of the exact exchange-correlation potential

$$v_{\text{ZMP}} = \lim_{\delta \rightarrow 0} v_{\text{XC}}(N - \delta) \quad (5.6)$$

and if we substitute eqn. (5.6) into eqn. (5.3) we see that the ZMP potential and the limiting potential on the electron abundant side differ only by the constant Δ_{XC}

$$v_{\text{ZMP}} = \lim_{\delta \rightarrow 0} v_{\text{XC}}(N + \delta) - \Delta_{\text{XC}} \quad (5.7)$$

Hence the ZMP LUMO eigenvalue is obtained by subtracting Δ_{xc} from the $v_{\text{xc}}(N + \delta)$ LUMO eigenvalue which, using the relation in eqn. (5.4), gives

$$\epsilon_{\text{LUMO}}^{\text{ZMP}} = -A - \Delta_{\text{xc}} \quad (5.8)$$

From eqn. (5.5) and eqn. (5.8) it follows that [185]

$$\epsilon_{\text{LUMO}}^{\text{ZMP}} - \epsilon_{\text{HOMO}}^{\text{ZMP}} = I - A - \Delta_{\text{xc}} \quad (5.9)$$

Thus the discontinuity can be approximated from ZMP HOMO-LUMO eigenvalue differences, provided that values for I and A are available. In Table 5.1 experimental values of $I - A$ and values of the discontinuity Δ_{xc} determined from eqn. (5.9) are presented; the discontinuity is of the order of 6 to 11 eV. These calculated values are consistent with previous studies [173] and their significance will be seen when the relationship between the GGA HOMO eigenvalue and the ionisation potential is considered in the next section.

5.2 HOMO eigenvalues

It is generally assumed that, since GGA potentials vanish asymptotically (i.e. the magnitude of the potential at infinity is zero), from eqn. (5.5) the HOMO eigenvalue associated with a GGA functional should satisfy

$$\epsilon_{\text{HOMO}}^{\text{GGA}} = -I \quad (5.10)$$

but in practice this is not found to be the case. In Table 5.4 HOMO eigenvalues determined using HCTH, PBE, 1/4 and ZMP are compared with $-I$ (experimental values). In line with eqn. (5.5), the agreement between the ZMP HOMO eigenvalues and $-I$ is good, and any discrepancies are attributable to errors in the BD densities and the use of finite basis sets and Lagrange multipliers. However, in all cases the GGA HOMO eigenvalue lies well above $-I$. This is well known. It will now be argued that these HOMO eigenvalues are completely appropriate for a GGA and that it is incorrect to assume that the HOMO should equal $-I$.

Table 5.4: HOMO eigenvalues from ZMP, HCTH, PBE, and 1/4, compared to $-I$ and the average HOMO $\epsilon_{\text{HOMO}}^{\text{average}}$ defined in Eqn. (5.13). All values are in au.

System	$\epsilon_{\text{HOMO}}^{\text{ZMP}}$	$-I$	$\epsilon_{\text{HOMO}}^{\text{HCTH}}$	$\epsilon_{\text{HOMO}}^{\text{PBE}}$	$\epsilon_{\text{HOMO}}^{1/4}$	$\epsilon_{\text{HOMO}}^{\text{average}}$
H ₂ O	-0.48	-0.46	-0.27	-0.27	-0.29	-0.25
NH ₃	-0.40	-0.40	-0.23	-0.23	-0.25	-0.21
CH ₄	-0.51	-0.50	-0.35	-0.35	-0.38	-0.29
HF	-0.61	-0.59	-0.36	-0.35	-0.39	-0.38
PH ₃	-0.38	-0.39	-0.25	-0.25	-0.27	-0.28
CO	-0.50	-0.51	-0.33	-0.33	-0.36	-0.36
N ₂	-0.56	-0.57	-0.38	-0.38	-0.41	-0.40
H ₂ S	-0.37	-0.39	-0.23	-0.23	-0.26	-0.26
HCN	-0.49	-0.50	-0.33	-0.33	-0.36	-0.36
C ₂ H ₂	-0.41	-0.42	-0.26	-0.26	-0.29	-0.29
C ₂ H ₄	-0.39	-0.39	-0.25	-0.25	-0.27	-0.27
H ₂ CO	-0.40	-0.40	-0.23	-0.23	-0.26	-0.25

GGAs functionals are continuum functionals and, as such, cannot (by definition) exhibit the discontinuity of the true potential as the number of electrons passes through integer. The best that can be achieved [170, 185] is to approximately average over the integer discontinuity such that

$$v_{\text{XC}}^{\text{average}} = \frac{1}{2} (v_{\text{XC}}(N + \delta) + v_{\text{XC}}(N - \delta)) = v_{\text{ZMP}} + \frac{\Delta_{\text{XC}}}{2} \quad (5.11)$$

Since the average potential is shifted from the ZMP potential by $\Delta_{\text{XC}}/2$ the HOMO eigenvalue associated with the average potential is similarly shifted

$$\epsilon_{\text{HOMO}}^{\text{average}} = \epsilon_{\text{HOMO}}^{\text{ZMP}} + \frac{\Delta_{\text{XC}}}{2} \quad (5.12)$$

and from eqn. (5.5) this is

$$\epsilon_{\text{HOMO}}^{\text{average}} = -I + \frac{\Delta_{\text{XC}}}{2} \quad (5.13)$$

Thus given values for I and Δ_{XC} we can calculate $\epsilon_{\text{HOMO}}^{\text{average}}$. We have performed calculations using experimental I and the Δ_{XC} values in Table 5.1 and the results are compared with HCTH, PBE and 1/4 HOMO eigenvalues in Table 5.4. HOMO eigenvalues from HCTH, PBE and 1/4 are in fact much closer to $\epsilon_{\text{HOMO}}^{\text{average}}$ than they are to $-I$. It has previously been observed [172] that GGA HOMO eigenvalues are close to $-(I + A)/2$, and we note that, for open-shell systems in a restricted formalism, $\epsilon_{\text{HOMO}}^{\text{average}}$ reduces to this value. For the heavier systems (those with more than one first row non-hydrogen atom, or those with a second row atom) the 1/4 functional performs better than HCTH and PBE (the results of which are very similar). For the lighter systems the opposite is observed (HF is an interesting exception). This is consistent with previous studies which show that 1/4 performs especially well for heavier systems [49].

We rationalise the agreement between GGA HOMO eigenvalues and $\epsilon_{\text{HOMO}}^{\text{average}}$ in the following manner. The HOMO eigenvalue is largely determined by the potential in regions where there is significant density. Conventional GGA functionals describe the average potential (eqn. (5.11)) reasonably well in such regions, and so correctly shift the HOMO eigenvalue from $-I$ by approximately $\Delta_{\text{XC}}/2$. At long range the potential should approach a system dependent constant, Δ_{XC} . The fact that the potentials from GGA functionals do not do so, but instead vanish at long range, indicates that the approximation breaks down in this region; see ref. [186] for illustration. This failure leads to inaccurate asymptotic densities and a consequent poor description of Rydberg electronic excitation energies [143], but it does not significantly impact the HOMO eigenvalue. This breakdown is also consistent with underestimated HOMO-LUMO eigenvalue differences (Section 5.1).

5.2.1 NMR shielding constants

The above analysis of the HOMO eigenvalue suggests another approach for correcting the LUMO eigenvalue. By analogy with eqn. (5.12) the potential

that averages over the discontinuity has an associated LUMO eigenvalue

$$\epsilon_{\text{LUMO}}^{\text{average}} = \epsilon_{\text{LUMO}}^{\text{ZMP}} + \frac{\Delta_{\text{XC}}}{2} \quad (5.14)$$

and from (5.8) this is

$$\epsilon_{\text{LUMO}}^{\text{average}} = -A - \frac{\Delta_{\text{XC}}}{2} \quad (5.15)$$

Combining (5.13) and (5.15) gives [185]

$$\epsilon_{\text{HOMO}}^{\text{average}} + \epsilon_{\text{LUMO}}^{\text{average}} = -(I + A) \quad (5.16)$$

It follows from (5.16) that if $\epsilon_{\text{HOMO}}^{\text{average}}$, I and A are known then it is possible to calculate $\epsilon_{\text{LUMO}}^{\text{average}}$. For the HCTH and 1/4 functionals, the new correction of the LUMO takes the form

$$\begin{aligned} \epsilon_{\text{LUMO}}^{\text{HCTH}} &\rightarrow -(I + A) - \epsilon_{\text{HOMO}}^{\text{HCTH}} \\ \epsilon_{\text{LUMO}}^{1/4} &\rightarrow -(I + A) - \epsilon_{\text{HOMO}}^{1/4} \end{aligned} \quad (5.17)$$

respectively. The corrected methods are denoted HCTH(LC2) and 1/4(LC2) (for LUMO Correction 2). To assess this correction, isotropic and anisotropic shielding constants were calculated for the subset of systems for which reliable experimental vertical I and A values are available. The results are presented in Tables 5.2 and 5.3.

For the majority of systems the HCTH(LC2) results are less accurate than conventional HCTH. In contrast, 1/4(LC2) shielding constants are an improvement over conventional 1/4 results for many of the systems. These results can be understood because of the way the HOMO-LUMO gap depends on how well the HOMO eigenvalue averages over the discontinuity. There is an implicit assumption in the LC2 correction that the potential associated with the GGA functional employed is a good approximation to the potential that averages over the discontinuity. In other words, the calculated LUMO (and hence the gap) depends on the value of the HOMO. Eqn. (5.16) constrains the sum of the HOMO and LUMO eigenvalues to be a constant, therefore since HCTH HOMO eigenvalues are too high, calculated LUMOs are too low, leading to an underestimation of the HOMO-LUMO eigenvalue

difference. The improved average 1/4 HOMO eigenvalues (Table 5.4) are reflected in the improved 1/4(LC2) shielding constants, an indication that the gaps have opened.

5.2.2 Excitation energies

Having considered the explicit correction of the LUMO eigenvalue on the calculation of magnetic response properties, the next logical step is to extend this to electrical properties. Vertical electronic excitation energies were calculated for CO, N₂, H₂CO and C₂H₄ at near experimental geometries. The Sadlej basis set [152, 153] was used with additional diffuse functions to ensure good description of the virtual orbitals. Geometries and additional functions used are summarised in Table C.2. Results are presented for the LDA, HCTH and 1/4 exchange-correlation functionals, and for the LUMO corrected (LC2) counterparts (as described in Section 5.2.1) in Tables 5.5 to 5.8.

In calculating excitation energies using the LC2 procedure, it was found that in almost all cases the mean absolute error compared to experiment increased relative to the uncorrected values. This is consistent with the poor description of the HOMO eigenvalue by the GGA functionals compromising the calculated gaps. For the LDA and HCTH functionals, for all molecules the—already too low—excitation energies were further reduced by the correction of the LUMO eigenvalue. Although the better description of the HOMO eigenvalue by the 1/4 functional led to an increase in excitation energies for all affected values, this generally over compensated, and again the mean errors increased. The only exception was the 1/4 C₂H₄ values, where the LUMO correction reduced the mean error. Note that for CO and N₂ (Tables 5.5 and 5.6) the 1/4 mean error increased less than those of LDA and HCTH when the LUMO correction was applied (approximately 0.1 eV as compared to the order of 0.5 eV). The reverse is true for H₂CO (Table 5.7), and there is no obvious pattern in the average HOMO eigenvalues (Table 5.4) that would account for this. The conclusion is that the excitation energies

Table 5.5: Vertical excitation energies of CO (in eV), computed using the augmented Sadlej basis set.

State	Transition	LDA	LDA (LC2)	HCTH	HCTH (LC2)	1/4	1/4 (LC2)	Expt ¹
<i>F</i> ${}^1\Sigma^+$	$\sigma \rightarrow 3d\sigma$	9.70	9.70	9.58	9.58	10.22	10.22	12.4
<i>E</i> ${}^1\Pi$	$\sigma \rightarrow 3p\pi$	9.65	9.65	9.48	9.47	10.09	10.10	11.53
<i>C</i> ${}^1\Sigma^+$	$\sigma \rightarrow 3p\sigma$	9.56	9.56	9.41	9.41	10.03	10.03	11.40
<i>B</i> ${}^1\Sigma^+$	$\sigma \rightarrow 3s$	9.08	9.50	8.94	8.93	9.54	9.54	10.78
<i>D</i> ${}^1\Delta$	$\pi \rightarrow \pi^*$	10.32	9.50	10.19	9.03	10.27	10.68	10.23
<i>I</i> ${}^1\Sigma^-$	$\pi \rightarrow \pi^*$	9.84	9.03	9.92	8.76	9.91	10.33	9.88
<i>A</i> ${}^1\Pi$	$\sigma \rightarrow \pi^*$	8.18	7.36	8.31	7.15	8.28	8.70	8.51
Mean abs. error		1.09	1.42	1.13	1.70	0.82	0.94	

¹Ref [159]Table 5.6: Vertical excitation energies of N₂ (in eV), computed using the augmented Sadlej basis set.

State	Transition	LDA	LDA (LC2)	HCTH	HCTH (LC2)	1/4	1/4 (LC2)	Expt ¹
${}^1\Pi_u$	$\pi_u \rightarrow 3s\sigma_g$	11.81	11.80	11.48	11.47	12.15	12.15	13.24
${}^1\Sigma_u^+$	$\sigma_g \rightarrow 3p\sigma_u$	10.62	10.62	10.48	10.48	11.46	11.20	12.98
${}^1\Pi_u$	$\sigma_g \rightarrow 3p\pi_u$	10.61	10.61	10.49	10.49	11.23	11.23	12.90
${}^1\Sigma_g^+$	$\sigma_g \rightarrow 3s\sigma_g$	10.39	10.39	10.19	10.19	10.85	10.85	12.2
${}^1\Delta_u$	$\pi_u \rightarrow \pi_g$	10.22	9.43	10.08	8.90	10.16	10.61	10.27
${}^1\Sigma_u^-$	$\pi_u \rightarrow \pi_g$	9.64	8.85	9.73	8.55	9.70	10.16	9.92
${}^1\Pi_g$	$\sigma_g \rightarrow \pi_g$	9.04	8.25	9.15	7.96	9.12	9.57	9.31
Mean abs. error		1.14	1.59	1.25	1.79	0.84	0.92	

¹Ref [160]

Table 5.7: Vertical excitation energies of H₂CO (in eV), computed using the Sadlej basis set.

State	Transition	LDA	LDA (LC2)	HCTH	HCTH (LC2)	1/4	1/4 (LC2)	Expt ¹
¹ A ₂	<i>n</i> → 3 <i>db</i> ₁	7.23	7.23	7.11	7.11	7.81	7.81	9.22
¹ A ₂	<i>n</i> → 3 <i>pb</i> ₁	6.69	6.69	6.54	6.54	7.19	7.19	8.38
¹ B ₁	σ → π*	8.79	8.62	8.98	8.47	8.93	10.05	8.68
¹ B ₂	<i>n</i> → 3 <i>pa</i> ₁	6.46	6.46	6.38	6.38	6.96	6.96	8.12
¹ A ₁	<i>n</i> → 3 <i>pb</i> ₂	6.50	6.50	6.33	6.33	6.92	6.92	7.97
¹ B ₂	<i>n</i> → 3 <i>sa</i> ₁	5.83	5.83	5.69	5.69	6.14	6.14	7.09
¹ A ₂	<i>n</i> → π*	3.68	3.51	3.92	3.40	3.84	4.92	3.94
Mean abs. error		1.21	1.22	1.29	1.35	0.87	1.16	

¹Ref [161]

are very sensitive to the HOMO-LUMO gap and that it is not possible to account for anything beyond broad trends. All results were consistent with our above conclusions: that correcting the LUMO eigenvalue in terms of the HOMO eigenvalue is limited by the ability of the GGA under consideration to average over the discontinuity, that the poor performance of the GGA functionals tested is consistent with their inability to reproduce $\epsilon_{\text{HOMO}}^{\text{average}}$ and that, in general, the 1/4 functional performs better than HCTH, as might be expected from their respective HOMO eigenvalues.

5.3 Summary

We have generated eigenvalues associated with coupled-cluster BD electron densities via the ZMP procedure. A comparison was made between HOMO-LUMO eigenvalue differences from conventional GGA functionals and those from the ZMP procedure. GGA eigenvalue differences are all smaller than those of ZMP. Forcing GGA HOMO-LUMO eigenvalue differences to equal

Table 5.8: Vertical excitation energies of C_2H_4 (in eV), for states formed by single excitations from the $b_{3u} = \pi$ orbital (molecule lies in yz plane), computed using the augmented Sadlej basis set.

State	Transition	LDA	LDA (LC2)	HCTH	HCTH (LC2)	1/4	1/4 (LC2)	Expt ¹
$^1B_{1u}$	$3d\pi = b_{2g}$	8.00	7.91	7.82	7.60	8.34	8.44	9.33
$^1B_{2u}$	$3d\delta = b_{1g}$	7.72	7.72	7.37	7.37	8.10	8.10	9.05
$^1B_{3u}$	$3d\delta = a_g$	7.63	7.63	7.29	7.29	7.99	7.99	8.90
$^1B_{3u}$	$3d\sigma = a_g$	7.11	7.11	6.86	6.86	7.57	7.57	8.62
1A_g	$3p\pi = b_{3u}$	7.31	7.31	6.94	6.94	7.62	7.62	8.28
$^1B_{1u}$	$\pi^* = b_{2g}$	7.39	6.92	7.18	6.34	7.51	7.86	8.0
$^1B_{2g}$	$3p\sigma = b_{1u}$	7.04	7.04	6.68	6.68	7.27	7.27	7.90
$^1B_{1g}$	$3p\sigma = b_{2u}$	7.04	7.05	6.69	6.67	7.27	7.27	7.80
$^1B_{3u}$	$3s = a_g$	6.56	6.56	6.24	6.24	6.75	6.75	7.11
Mean abs. error		1.02	1.08	1.32	1.44	0.73	0.65	

¹Ref [162]

those of ZMP significantly improves isotropic and anisotropic NMR shielding constants.

The magnitude of the integer discontinuity was approximated using ZMP eigenvalue differences. HOMO eigenvalues from GGAs are not close to $-I$, but they are close to $\epsilon_{\text{HOMO}}^{\text{average}}$. This suggested another approach to correcting the HOMO-LUMO eigenvalue differences, under the assumption that the potential approximately averages over the integer discontinuity. This correction was used to determine NMR shielding constants and excitation energies. These results are dependent upon the accuracy of the calculated HOMO eigenvalue from a particular functional.

Chapter 6

The *gauche* effect

This thesis has considered the use of high quality electron densities within DFT. Broadly, these densities have been used to explore the likely implications for DFT if high-accuracy approximations for $E_{xc}[\rho]$ were available. This is possible because exchange-correlation potentials $v_{xc}(\mathbf{r})$ can be generated from electron densities rather than exchange-correlation functionals. In principle the accuracy is limited only by the quality of the supplied electron density (though at a much higher computational cost than conventional DFT).

However, there is another way in which electron densities can be employed in DFT calculations: they can be used in the development of functionals. B97-2 is a hybrid exchange-correlation functional that was developed in this way. In this chapter, the B97-2 functional is used to study the *gauche* effect in 2-fluoroethylamine, 2-fluoroethanol and their protonated analogues.

6.1 The *gauche* effect

The *gauche* effect [187] describes the tendency for certain molecules to adopt a particular conformation in preference to other dynamically available spatial arrangements. This interaction is stereoelectronic in origin and is noteworthy because it overcomes unfavourable steric interactions¹ and results in structures that defy a simplistic conformational analysis.

In this study the extent of any *gauche* effect in 2-fluoroethylamine, 2-fluoroethanol and their protonated analogues will be investigated using theoretical calculations and X-ray analysis of solid-state structures. These studies were prompted by observations made by O'Hagan and co-workers [188, 189] of a fluorine-amide *gauche* effect and a study comprising solid-state investigations and theoretical calculations that reported a fluorine-ester *gauche* effect [190, 191].

6.2 Conformational preference of substituted ethanes

Consider rotation about the carbon-carbon bond in ethane. There are two extreme conformations, staggered and eclipsed (see Figure 6.1). Rotation about the C-C bond is free, meaning that although a barrier to rotation exists, it is low (for ethane, about 3 kcal mol⁻¹). This barrier to rotation exists because when a methyl group is rotated about the C-C axis, starting from the staggered conformation, the hydrogen-hydrogen distances decrease to a minimum at the eclipsed conformation and the potential energy increases as the H-H distances decrease. This increase in potential energy also means that the staggered conformation is energetically preferred.

Moving from ethane to propane (by substituting a methyl group for one of the hydrogen atoms, see Figure 6.2), the barrier to rotation increases because

¹to a first approximation, steric interactions can be equated with the *bulk* of a group: two substituents cannot occupy the same region of space

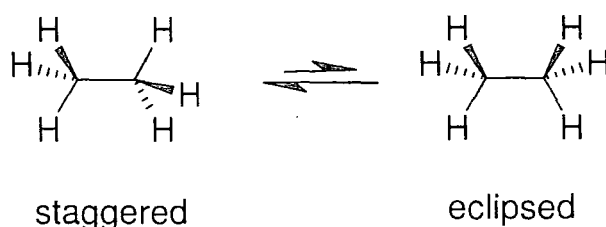


Figure 6.1: Ethane staggered and eclipsed conformations

of the greater steric bulk of the methyl group, relative to a hydrogen atom.

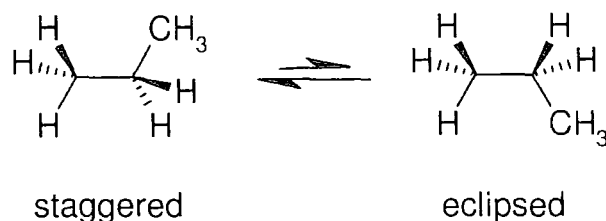
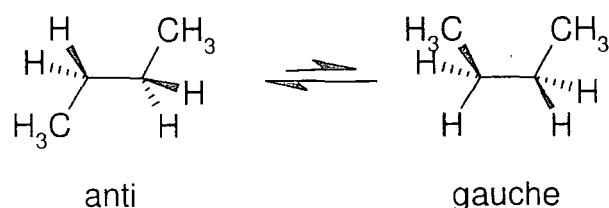


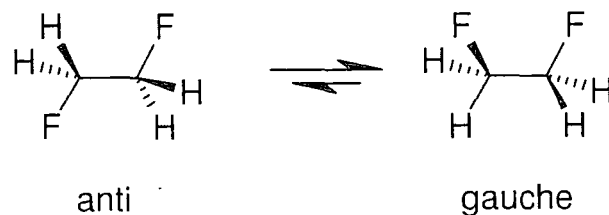
Figure 6.2: Propane staggered and eclipsed conformations

Further substitution to give butane not only increases the barrier to rotation over propane, it also means that there are two distinct staggered conformations, referred to as *anti* and *gauche* (see Figure 6.3). Because the *anti* conformation maximises the separation between the bulky methyl groups it is lower in energy than the *gauche* conformation. Thus the *anti* structure is more stable than the *gauche*.

For some systems there is a counterintuitive conformational preference for the *gauche* structure. The canonical example is 1,2-difluoroethane (Fig-

Figure 6.3: Butane *anti* and *gauche* conformations

ure 6.4). Here, the *gauche* structure is energetically preferred by 0.5-1.0 kcal mol⁻¹ [192, 193, 194], despite the fact that this brings the bulky F atoms into closer proximity with one another than they are in the *anti* structure.

Figure 6.4: 1,2-difluoroethane *anti* and *gauche* conformations

This *gauche* preference is a consequence of a *gauche* effect. It is important to differentiate these two terms, as the *gauche* conformer may be stabilised relative to its *anti* equivalent by means of an intramolecular hydrogen bond or other structural elements that do not induce an appeal to a separate *gauche* effect. A *gauche* preference refers to the tendency to adopt the *gauche* conformer, while the *gauche* effect is a specific mechanism that promotes this stabilisation relative to the *anti* conformer. The stabilisation has been

attributed to a $\sigma \rightarrow \sigma^*$ donation [195, 196, 197, 198]. In the case of 1,2-difluoroethane the C-H bonds (those *anti* to the C-F bonds) are the donors and the C-F bonds the acceptors. The *gauche* structure is the most stable because the molecule adopts a conformation that places the best σ -donor bond *anti* to the best σ -acceptor bond.

6.3 Theoretical studies

The B97-2 functional (Section 2.9.4) was used for all calculations. A TZ2P basis augmented with diffuse *s* and *p* function on non-hydrogen atoms (a simple geometric progression was used to determine the exponents) was employed. As part of preliminary investigations, calculations were also performed using the HCTH, B3LYP and B97-1 functionals and the MP2 method. Similar trends to those seen with the B97-2 functional were observed. Minimum energy structures for each conformation were determined using analytic first derivatives (forces). Harmonic vibrational frequencies were determined from finite differences of analytic first derivatives at perturbed geometries and these were used to (1) confirm that the stationary points represented real minima on the potential energy surface and (2) to determine zero-point vibrational energies. All relative energies presented include zero-point vibrational corrections. Calculated energies of systems are given in E_h , while energy differences are given in kcal mol^{-1} for ease of comparison with literature values.

Calculations on 2-fluoroethylamine and 2-fluoroethylammonium

Figure 6.5 presents geometries of *gauche* ((a) - (c)) and *anti* ((d) - (f)) conformers of 2-fluoroethylamine. The calculated energies of these optimised geometries are presented, along with the energy differences of the *gauche* relative to the *anti*, in Table 6.1.

The *gauche* conformers 6.5(a) and 6.5(c) are 0.9 and 1.0 kcal mol^{-1} lower in energy than the corresponding *anti* conformers 6.5(d) and 6.5(f). However,

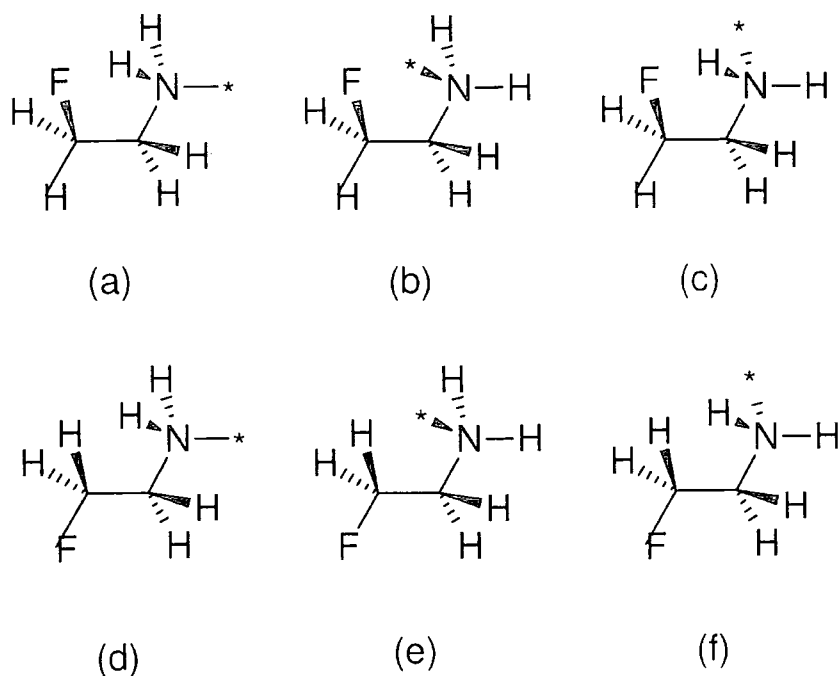


Figure 6.5: Minimum conformations of 2-fluoroethylamine. The stars denote lone pairs

in both these cases it is possible that the *gauche* structure is stabilised by an $F \cdots H$ intramolecular hydrogen bond. The pair of structures 6.5(b) and 6.5(e), for which such a hydrogen bond is not possible, displays no preference for the *gauche* conformer; instead the *anti* conformer is $0.9 \text{ kcal mol}^{-1}$ lower in energy. This suggests that any *gauche* effect is not responsible for the stabilisation, but rather that it depends on intramolecular hydrogen bonding.

The F-C-C-H dihedral angles of the *gauche* structures 6.5 (a), (b) and (c) are 175.9, 165.3 and 174.8 degrees respectively. Clearly, the presence or absence of hydrogen bonding affects the F-C-C-H dihedral.

In 2-fluoroethylammonium (protonated 2-fluoroethylamine, see Figure 6.6) the three-fold radial symmetry of the NH_3 group means that there is only one *gauche* and one *anti* conformer. The protonation of the nitrogen atom has two important effects on the conformation adopted by 2-fluoroethylammonium,

Table 6.1: F-C-C-N dihedral angles, absolute energies and *gauche anti* energy differences of 2-fluoroethylamine and 2-fluoroethylammonium

<i>gauche</i>	Dihedral angle (degrees)	Total energy (Hartrees)	<i>anti</i>	Dihedral angle (degrees)	Total energy (Hartrees)	<i>gauche - anti</i> (kcal mol ⁻¹)
NH ₂			NH ₂			
6.5(a)	61.5	-234.342092	6.5(d)	180.0	-234.340615	-0.9
6.5(b)	69.8	-234.338996	6.5(e)	178.3	-234.340450	+0.9
6.5(c)	66.7	-234.342000	6.5(f)	181.7	-234.340450	-1.0
NH ₃ ⁺			NH ₃ ⁺			
6.6(a)	52.7	-234.685112	6.6(b)	180.0	-234.675825	-5.8

both related to the fact that the nitrogen acquires a positive charge relative to the equivalent atom in 2-fluoroethylamine. The increased electronegative character of the nitrogen atom will further polarise the H-N⁺ bond, promoting the intramolecular hydrogen bond. Similarly, the C-N⁺ bond will also become more polarised, and this will heighten the *gauche* effect.

The combination of these two effects predicts a strong *gauche* preference for 2-fluoroethylammonium. The calculated energies of the optimised geometries are presented in Table 6.1. The *gauche* structure is stabilised relative to the *anti* by 5.8 kcal mol⁻¹. However, there is no simple way to separate this *gauche* preference into components relating to intramolecular F...H hydrogen bonding and a stereoelectronic *gauche* effect. The F-C-C-H dihedral is now 172.5 degrees.

Calculations on 2-fluoroethanol and protonated 2-fluoroethanol

Having considered fluoroethylamine and fluoroethylammonium, calculations were performed on the corresponding oxygen analogues. A stronger *gauche* effect was anticipated for these compounds, since the greater electronegativity of oxygen relative to nitrogen will create a more polarised C-O bond. Also, as discussed above, the electronegativity of oxygen will promote in-

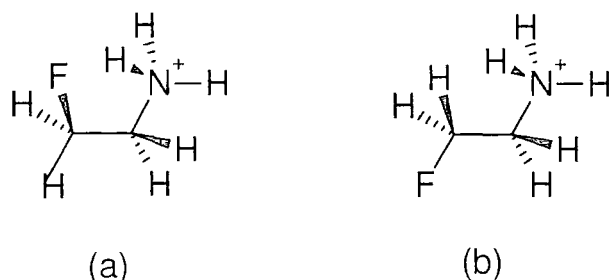


Figure 6.6: Minimum conformations of 2-fluoroethylammonium

tramolecular hydrogen bonding, in structures where the conformation makes such bonding possible.

2-fluoroethanol has been considered in a previous study by Dixon and Smart [199] allowing comparison with calculations presented here. Structures are shown in Figure 6.7 and calculated energies are presented in Table 6.2. Examining the *gauche* structures, 6.7(a) has the potential to be stabilised via intramolecular hydrogen bonding, while 6.7(b) and 6.7(c) do not. Where the intramolecular $F \cdots H$ bond is present the *gauche* structure is stabilised relative to the corresponding *anti* (Figure 6.7(d)). The *gauche* preference is approximately $2.0 \text{ kcal mol}^{-1}$. The *gauche* structures 6.7(b) and 6.7(c) do exhibit a *gauche* preference over their *anti* analogues (unlike the case of 2-fluoroethylamine where, in the absence of an intramolecular hydrogen bond, the *anti* energy is lower), though the stabilisation is only of the order of $0.1\text{--}0.2 \text{ kcal mol}^{-1}$. Any *gauche* effect in 2-fluoroethanol is small, and the stabilisation of 6.7(a) is largely due to the $F \cdots H$ bonding. These results are in agreement with the previously published work [199].

The F-C-C-H dihedral angles of the *gauche* structures 6.7 (a), (b) and (c) are 176.5 , 166.3 and 170.5 degrees respectively. Again, the orientation of the OH_2 group affects the F-C-C-H dihedral.

In protonated 2-fluoroethanol, as with protonated 2-fluoroethylamine, the increased polarisation of the bonds to the oxygen atom are expected to increase the *gauche* preference by enhancing the intramolecular hydrogen bond-

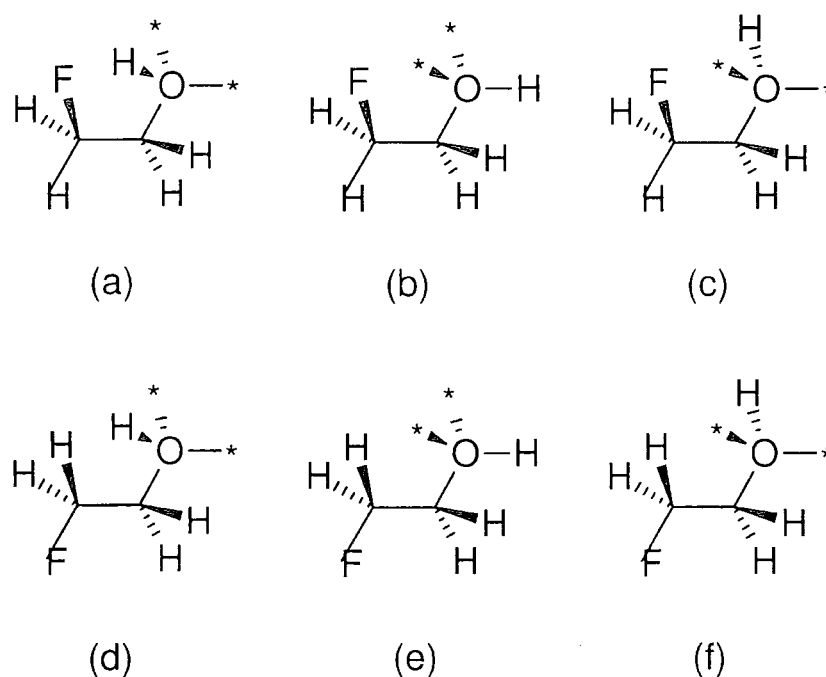


Figure 6.7: Minimum conformations of 2-fluoroethanol

ing and *gauche* preference. In contrast to 2-fluoroethylammonium, however, *gauche* conformers of protonated 2-fluoroethanol exist that do not exhibit intramolecular hydrogen bonding, allowing the separation of any *gauche* preference into contributions from hydrogen bonding and a *gauche* effect.

Figure 6.8 shows optimised structures for protonated 2-fluoroethanol, and total energies and energy differences are presented in Table 6.2. In all cases the *gauche* structure is stabilised relative to the *anti*. Where there is no intramolecular hydrogen bonding (structures 6.8(b) and 6.8(e)) the energy difference is $4.4 \text{ kcal mol}^{-1}$, which can be attributed to a stereoelectronic *gauche* effect. Compare the free amide analogues (6.5(b) and 6.5(e)), where steric repulsion dominates in the absence of intramolecular hydrogen bonding.

When conformers that display intramolecular hydrogen bonding are considered (6.8(a)/6.8(d) and 6.8(c)/6.8(f)) the stabilisation is increased, and

Table 6.2: F-C-C-O dihedral angles, absolute energies and *gauche anti* energy differences of 2-fluoroethanol and protonated 2-fluoroethanol

<i>gauche</i>	Dihedral angle (degrees)	Total energy (Hartrees)	<i>anti</i>	Dihedral angle (degrees)	Total energy (Hartrees)	<i>gauche - anti</i> (kcal mol ⁻¹)
OH			OH			
6.7(a)	65.3	-254.225123	6.7(d)	178.5	-254.222006	-2.0
6.7(b)	72.8	-254.222654	6.7(e)	180.0	-254.222198	-0.3
6.7(c)	64.9	-254.222054	6.7(f)	181.5	-254.222006	-0.0
OH ₂ ⁺			OH ₂ ⁺			
6.8(a)	48.2	-254.512994	6.8(d)	180.0	-254.501790	-7.0
6.8(b)	63.5	-254.509319	6.8(e)	175.9	-254.502339	-4.4
6.8(c)	50.5	-254.513888	6.8(f)	184.1	-254.502339	-7.2

the *gauche* structures are lower in energy by 7.0 and 7.2 kcal mol⁻¹. On the assumption that the contribution from the *gauche* effect is constant across all the conformers, this large *gauche* preference consists of a stereoelectronic *gauche* effect of approximately 4.4 kcal mol⁻¹ and an intramolecular hydrogen bond that contributes between 2.6 and 2.8 kcal mol⁻¹.

The F-C-C-H dihedral angles of the *gauche* structures 6.8 (a), (b) and (c) are 165.7, 178.1 and 164.7 degrees respectively.

6.4 Solid state studies

It is important to investigate whether our theoretical results are consistent with experimental observations. To this end, O'Hagan and co-workers [200] have determined X-ray crystal structures for the 2-fluoroethylammonium derivative systems presented in Figure 6.9 (for details of synthesis and other experimental details, see ref. [200]). Figures 6.10, 6.12, 6.14, 6.16 and 6.18 show the structures of the molecules in the solid-state. In all cases there is a clear *gauche* preference, as was observed in the molecular calculations.

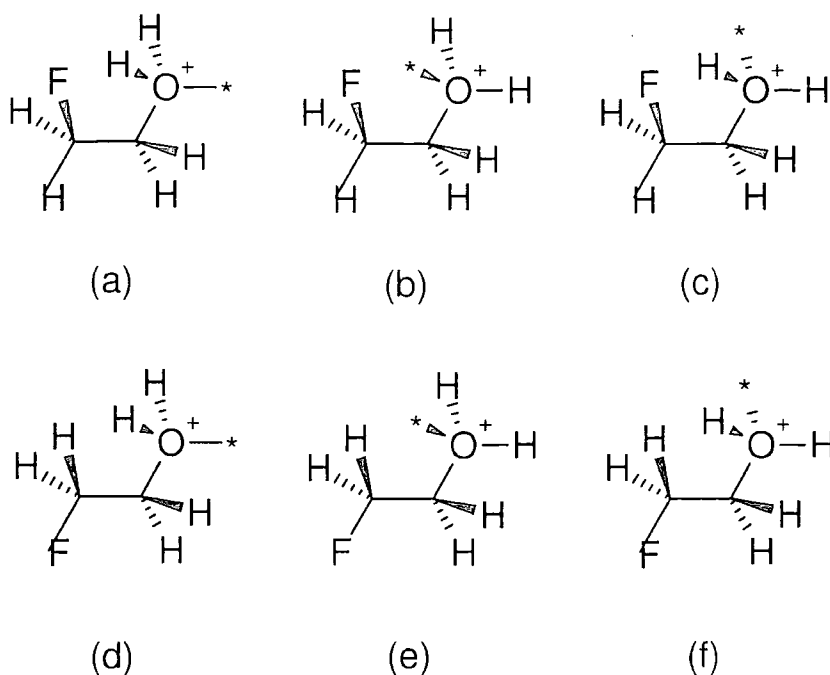
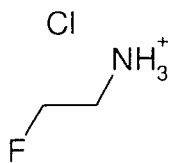
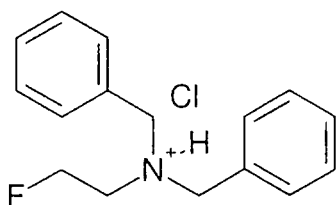


Figure 6.8: Minimum conformations of protonated 2-fluoroethanol

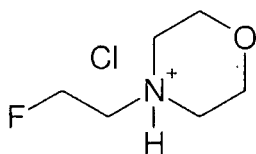
There is little evidence of intramolecular hydrogen bonding—the $\text{H} \cdots \text{F}$ separations are large enough that any interactions will have a small effect (if any) on the conformation adopted. In all cases the $\text{H} \cdots \text{F}$ separation is equal to or greater than the van der Waals contact distance (2.7 angstrom). This is in contrast with the theoretically calculated gas-phase structures, where the $\text{H} \cdots \text{F}$ distance is between 2.2 and 2.6 angstroms. Of course, in the solid state we must also take account of intermolecular interactions. The X-ray crystal structures are shown in Figures 6.11, 6.13, 6.15, 6.17 and 6.19. For all systems considered, the dominant intermolecular interaction is $\text{N-H} \cdots \text{Cl}$ hydrogen bonding. It is not possible, therefore, to attribute the adoption of the *gauche* conformation solely to the molecular *gauche* effect. The *gauche* effect will be a contributing factor, but intermolecular interactions will also have an influence.



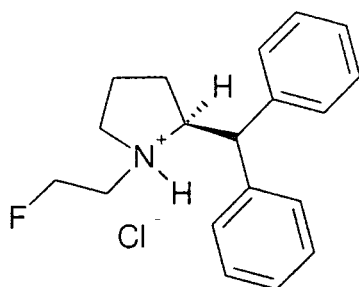
2-fluoroethylammonium chloride



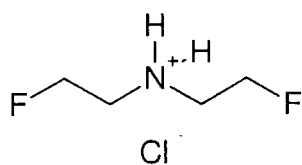
N,N-dibenzyl-2-fluoroethylammonium hydrochloride



4-(2-Fluoroethyl) morpholin-4-ium chloride



N-2-Fluoroethylamine hydrochloride



di(2-fluoroethyl)amine hydrochloride

Figure 6.9: Systems for which solid-state X-ray crystal structures have been determined.

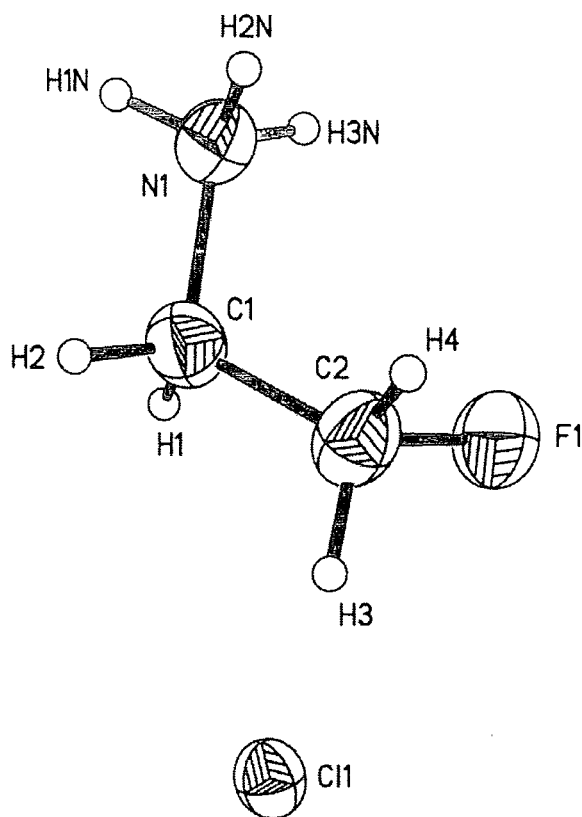


Figure 6.10: Molecular solid-state structure of 2-fluoroethylammonium chloride

6.5 Summary

In summary, we have used the B97-2 functional—which was determined from a fit involving high quality electron densities—to study the *gauche* effect. Extensive *gauche* effects are observed in protonated 2-fluoroethylamine and protonated fluoroethanol. Molecules in the solid state also exhibit the *gauche* preference, although the situation is complicated by the intermolecular N-H \cdots Cl hydrogen bonding.

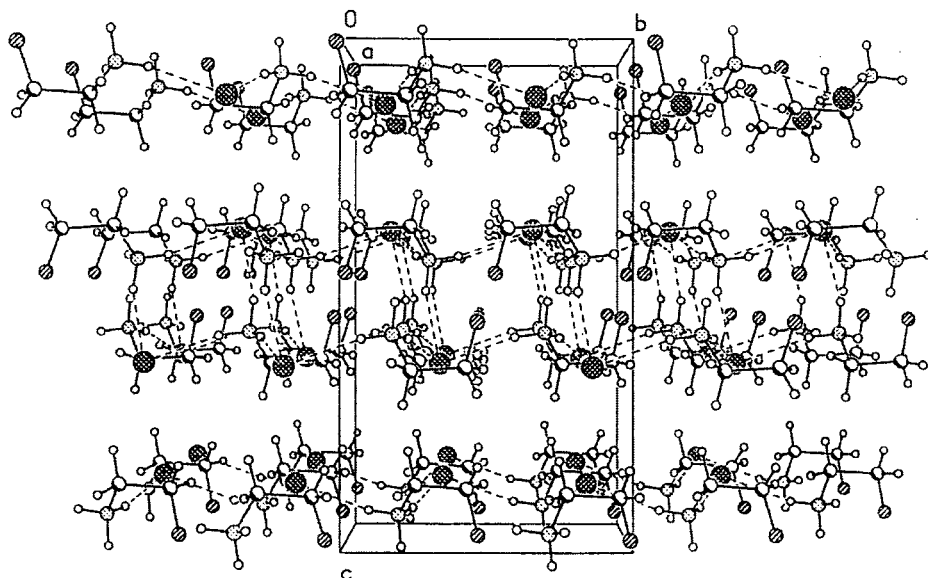


Figure 6.11: X-ray crystal structure of 2-fluoroethylammonium chloride

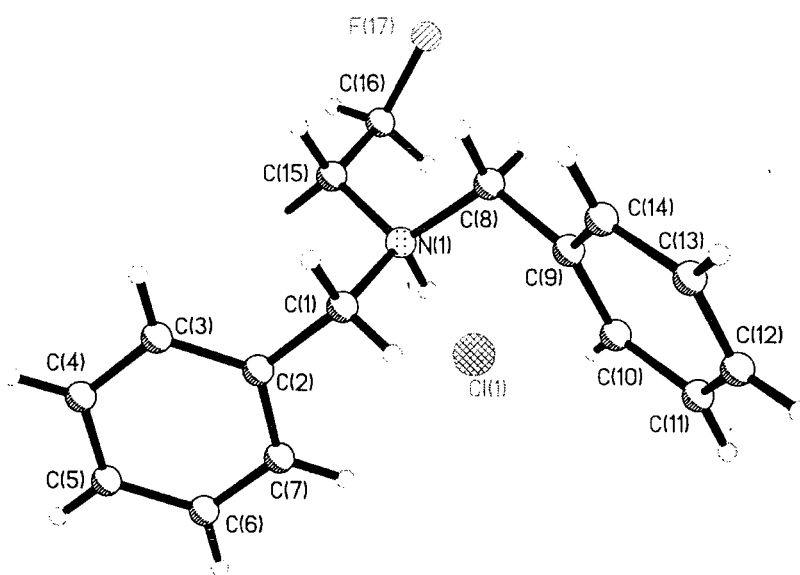


Figure 6.12: Molecular solid-state structure of N,N-dibenzyl-2-fluoroethylammonium hydrochloride

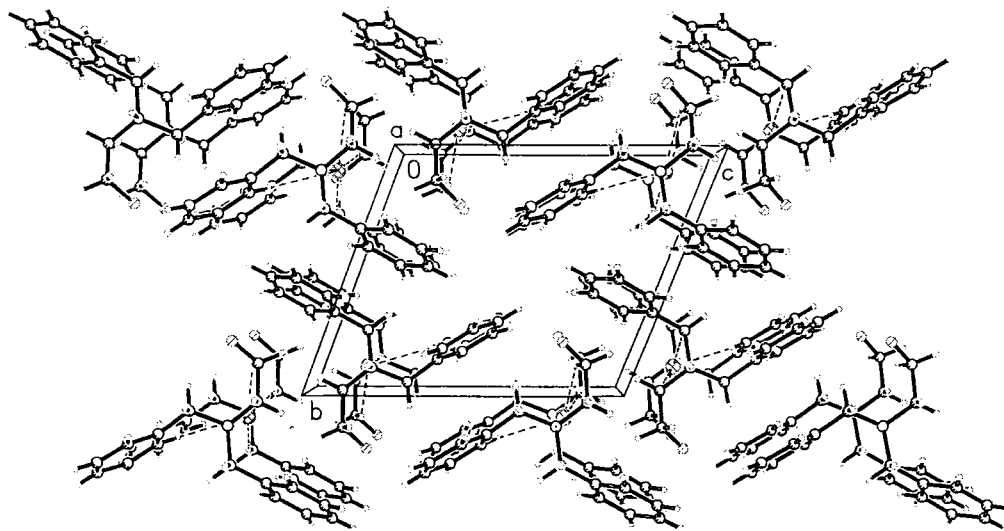


Figure 6.13: X-ray crystal structure of N,N-dibenzyl-2-fluoroethylammonium hydrochloride

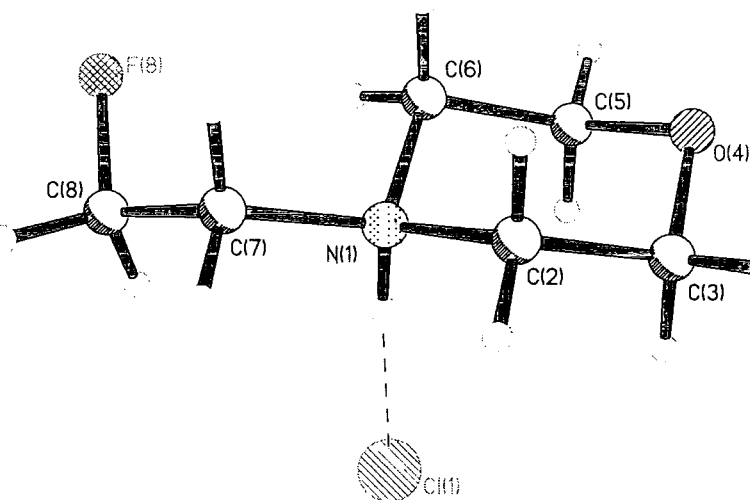


Figure 6.14: Molecular solid-state structure of 4-(2-Fluoroethyl) morpholin-4-ium chloride

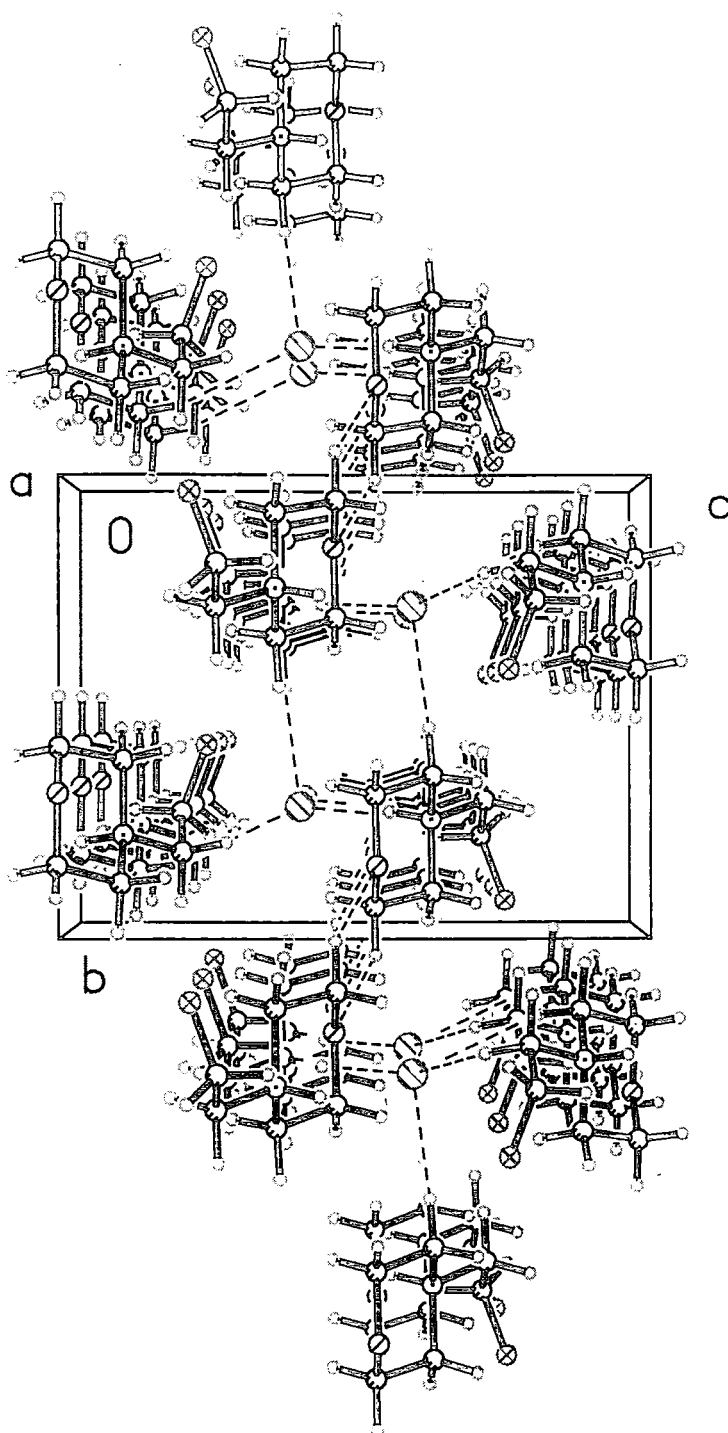


Figure 6.15: X-ray crystal structure of 4-(2-Fluoroethyl) morpholin-4-ium chloride

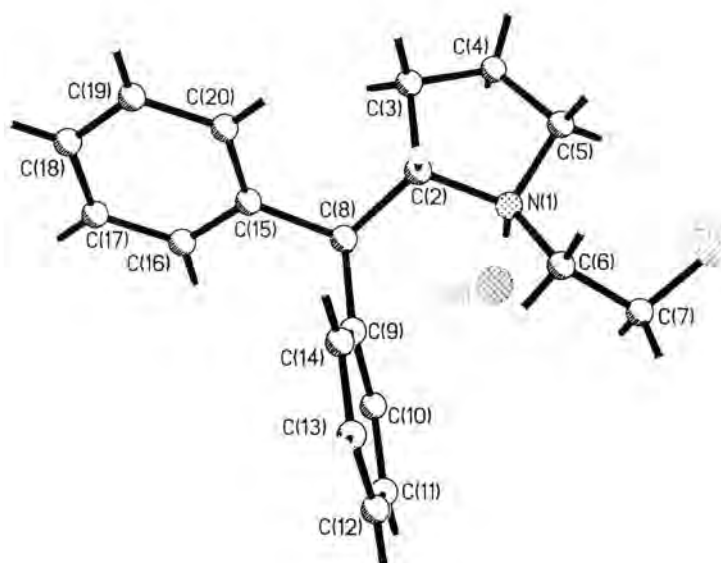


Figure 6.16: Molecular solid-state structure of N-2-Fluoroethylamine hydrochloride

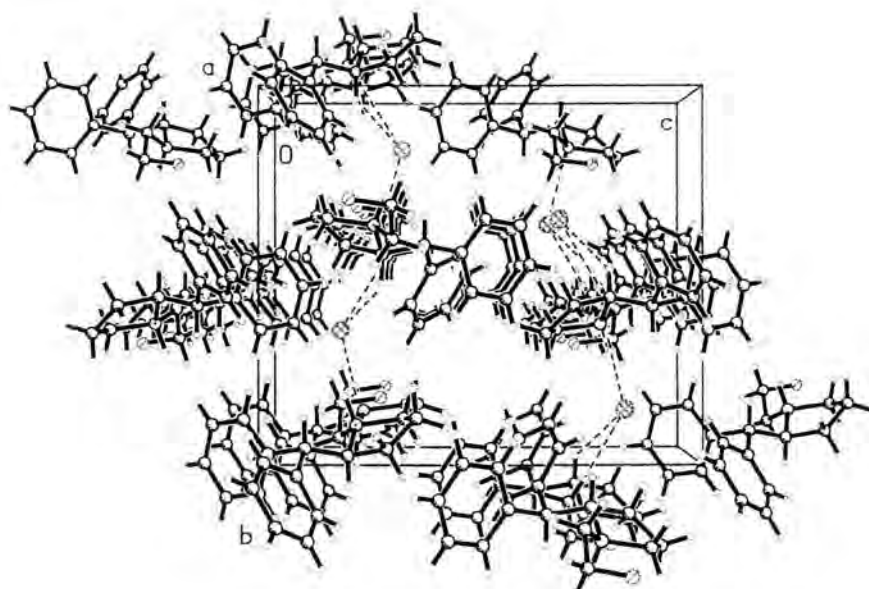


Figure 6.17: X-ray crystal structure of N-2-Fluoroethylamine hydrochloride

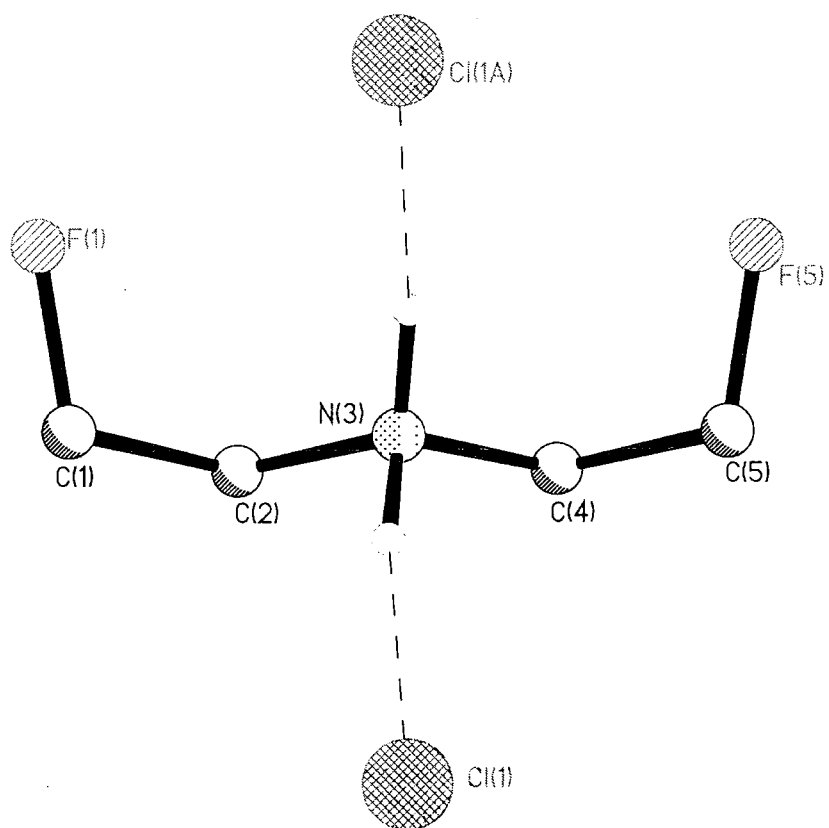


Figure 6.18: Molecular solid-state structure of di(2-fluoroethyl)amine hydrochloride

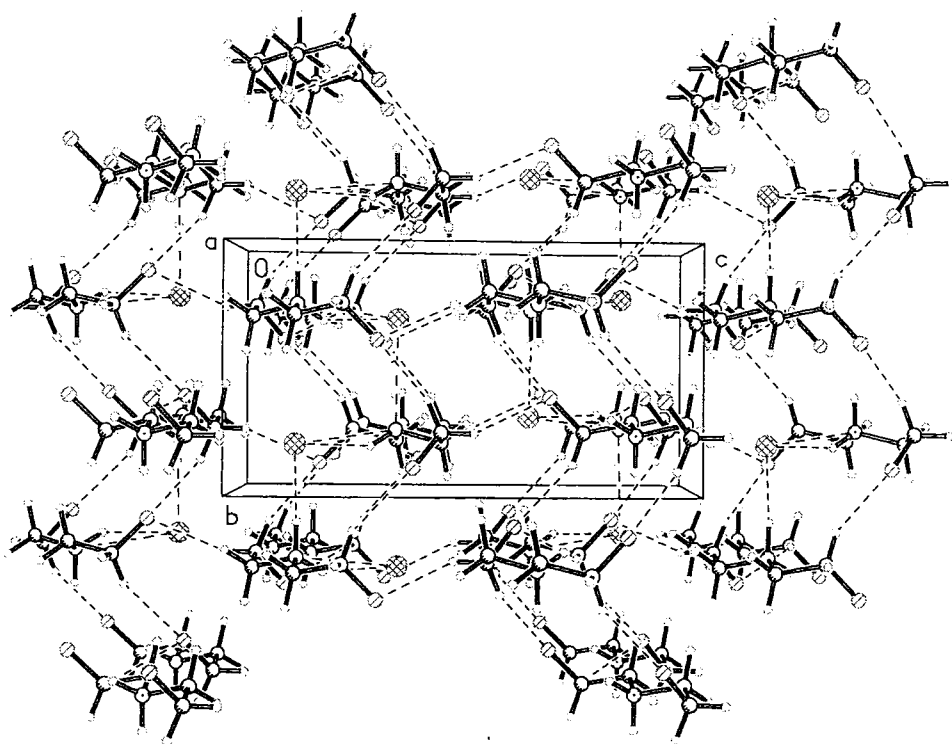


Figure 6.19: X-ray crystal structure of di(2-fluoroethyl)amine hydrochloride

Chapter 7

Concluding remarks

Kohn-Sham density functional theory provides high accuracy calculations of a wide range of molecular properties for a relatively modest computational cost. However, there are some properties for which DFT calculations are of poor quality (such as the determination of shielding constants) and other areas where the applicability of the DFT method is inappropriate (as with long-range dispersion interactions from local functionals). It was the overall aim of this work to use high quality electron densities to improve DFT calculations, either directly, by incorporating them into schemes for practical calculations, or indirectly, by using densities to learn about the Kohn-Sham DFT method.

An investigation of dispersion interactions in the helium dimer highlighted the relation between the density distortion and the dispersion force, and the importance of the correlation potential in the HFKS scheme. The failure of the LYP functional was highlighted; near exact results were obtained using BD(T) densities. The origin of the density distortion was traced to the asymmetric structure of the interaction correlation potential. Similar structure was observed in the correlation potential of the hydrogen molecule. Research into the development of correlation functionals, exchange-correlation functionals or correction schemes for existing functionals that display the correct correlation potential structure, might lead to an improved description of dispersion interactions within Kohn-Sham theory.

Orbitals and eigenvalues from potentials associated with high quality densities were used in Kohn-Sham response property calculations. Dramatic improvements in calculated results previously reported for shielding constants were repeated for chemical shifts. Electric response properties did not show a striking reduction in error with the use of MKS orbitals and eigenvalues. However, it has been shown that DFT polarisability calculations can approach the accuracy of coupled cluster methods if orbitals and eigenvalues are generated from a high quality density and an appropriate F_{xc} is used. Also, the sensitivity of valence excitations to F_{xc} has been demonstrated. Further investigation of magnetic response properties using orbitals and eigenvalues generated using high quality densities is warranted on the basis of these results. The sensitivity of valence excitations to F_{xc} also provides an opportunity for the development of functionals for electric response properties.

The calculation of Kohn-Sham eigenvalues and related properties using the ZMP method revealed the underestimation of HOMO-LUMO eigenvalue differences by conventional functionals. Forcing GGA HOMO-LUMO differences to be equal to ZMP differences showed that this underestimation has a significant impact on NMR shielding constant calculations. Integer discontinuities were also determined and the results were used to explain why GGA HOMO eigenvalues lie well above $-I$. A second approach for correcting the LUMO eigenvalue was also considered. In the development of new functionals, consideration of the requirements for GGA orbitals and eigenvalues (especially the underestimation of eigenvalue differences and the incorrect long-range behaviour of the potential associated with commonly used GGAs) could improve calculated DFT properties.

A functional developed through a fit to high quality electron densities was used to investigate the *gauche* effect in 2-fluoroethylamine, 2-fluoroethanol and their protonated analogues. Large *gauche* preferences were calculated for the protonated systems, which agreed with experimental observations.

Electron densities can offer a great deal of information and insight about

DFT calculations. This information may be of use in the development of new functionals, or in the creation of correction schemes that improve the accuracy of DFT calculations.

Appendix A

Atomic Units

Table A.1: Atomic units

Quantity	Atomic unit	Value in SI units	Symbol (name)
mass	rest mass of electron	$9.1094 \times 10^{-31} \text{kg}$	m_e
charge	elementary charge	$1.6022 \times 10^{-19} \text{C}$	e
action	Planck's constant/ 2π	$1.0546 \times 10^{-34} \text{J s}$	\hbar
length	$4\pi\epsilon_0\hbar/m_e e^2$	$5.2918 \times 10^{-11} \text{m}$	a_0 (bohr)
energy	$\hbar^2/m_e a_0^2$	$4.3597 \times 10^{-18} \text{J}$	E_h (hartree)

To convert between energy units

$$1E_h = 27.2114\text{eV} = 627.51\text{kcal/mol}$$

$$1\text{kcal/mol} = 4.184\text{kJ/mol}$$

To convert bohr to angstrom and vice versa

$$1 \text{ bohr} = 0.52918 \text{ angstrom}$$

$$1 \text{ angstrom} = 1.88972 \text{ bohr}$$

Appendix B

Differentiation of SAPT energy

Korona *et. al.* have proposed an analytical fit to their SAPT potential energy curve for the helium dimer [114]

$$E_{\text{SAPT}} = Ae^{-\alpha R + \beta R^2} - \sum_{n=3}^8 f_{2n}(R, b) \frac{C_{2n}}{R^{2n}} \quad (\text{B.1})$$

where A , α , β and b are adjustable parameters and f_{2n} is the damping function proposed by Tang and Toennies [117]

$$f_{2n}(R) = 1 - \left(\sum_{k=0}^{2n} \frac{(bR)^k}{k!} \right) \exp(-bR) \quad (\text{B.2})$$

In order to obtain an expression for the SAPT force the SAPT energy is differentiated with respect to R . Using the sum rule the energy expression is separated into two sections

$$A \exp(-\alpha R + \beta R^2) \quad (\text{B.3})$$

and

$$\sum_{n=3}^8 f_{2n}(R, b) \frac{C_{2n}}{R^{2n}} = \sum_{n=3}^8 \left[1 - \left(\sum_{k=0}^{2n} \frac{(bR)^k}{k!} \right) \exp(-bR) \right] \frac{C_{2n}}{R^{2n}} \quad (\text{B.4})$$

Taking the second section first, ignoring the summation leaves

$$\left[1 - \left(\sum_{k=0}^{2n} \frac{(bR)^k}{k!} \right) \exp(-bR) \right] \frac{C_{2n}}{R^{2n}} \quad (\text{B.5})$$

which can be rearranged as

$$\frac{C_{2n}}{R^{2n}} - \sum_{k=0}^{2n} \frac{(bR)^k}{k!} \exp(-bR) \frac{C_{2n}}{R^{2n}} \quad (\text{B.6})$$

Using the sum rule again this can be divided into

$$\frac{C_{2n}}{R^{2n}} \quad \text{and} \quad \sum_{k=0}^{2n} \frac{(bR)^k}{k!} \exp(-bR) \frac{C_{2n}}{R^{2n}} \quad (\text{B.7})$$

Once again, taking the second part first and ignoring the summation

$$\frac{(bR)^k}{k!} \exp(-bR) \frac{C_{2n}}{R^{2n}} \quad (\text{B.8})$$

which is rearranged as follows

$$\begin{aligned} \frac{(bR)^k}{k!} \exp(-bR) \frac{C_{2n}}{R^{2n}} &= \frac{C_{2n} b^k R^k}{R^{2n} k!} \exp(-bR) \\ &= \frac{C_{2n} R^{-2n} b^k R^k}{k!} \exp(-bR) \\ &= \frac{C_{2n} R^{-2n+k} b^k}{k!} \exp(-bR) \end{aligned} \quad (\text{B.9})$$

which can be differentiated using the product rule

$$\frac{d}{dR} = u \frac{dv}{dR} + v \frac{du}{dR} \quad (\text{B.10})$$

where

$$u = \frac{C_{2n} b^k R^{-2n+k}}{k!} \quad \text{hence} \quad \frac{du}{dR} = \frac{(-2n+k) C_{2n} b^k R^{-2n+k-1}}{k!} \quad (\text{B.11})$$

and

$$v = \exp(-bR) \quad \text{hence} \quad \frac{dv}{dR} = -b \exp(-bR) \quad (\text{B.12})$$

and hence

$$\begin{aligned} \frac{d}{dR} &\left(\frac{C_{2n} R^{-2n+k} b^k}{k!} \exp(-bR) \right) \\ &= \frac{C_{2n} b^k R^{-2n+k}}{k!} \exp(-bR) (-b) + \exp(-bR) \frac{(-2n+k) C_{2n} b^k R^{-2n+k-1}}{k!} \\ &= \frac{C_{2n} b^k R^{-2n+k}}{k!} \exp(-bR) \left[(-b) + (-2n+k) R^{-1} \right] \\ &= \frac{C_{2n} b^k R^k}{R^{2n} k!} \exp(-bR) \left[(-b) + \frac{(-2n+k)}{R} \right] \end{aligned} \quad (\text{B.13})$$

replacing the summation and rearranging gives

$$\frac{d}{dR}(u + v) = \sum_{k=0}^{2n} \left[(-b) + \frac{(-2n + k)}{R} \right] \frac{C_{2n}}{R^{2n}} \frac{(bR)^k}{k!} \exp(-bR) \quad (\text{B.14})$$

which leaves two other parts to differentiate

$$\begin{aligned} \frac{d}{dR} \frac{C_{2n}}{R^{2n}} &= \frac{d}{dR} C_{2n} R^{-2n} \\ &= -2n C_{2n} R^{-2n-1} \\ &= \frac{-2n C_{2n}}{R^{2n+1}} \end{aligned} \quad (\text{B.15})$$

and

$$\frac{d}{dR} A \exp(-\alpha R + \beta R^2) = (-\alpha + 2\beta R) A \exp(-\alpha R + \beta R^2) \quad (\text{B.16})$$

Combining the three parts and including all summations gives the final expression

$$\begin{aligned} F_{\text{SAPT}} &= (-\alpha + 2\beta R) A \exp(-\alpha R + \beta R^2) \\ &\quad - \sum_{n=3}^8 \left[\frac{-2n C_{2n}}{R^{2n+1}} g \right] \end{aligned} \quad (\text{B.17})$$

where

$$g = \left[\sum_{k=0}^{2n} \left(-b + \frac{(2n + k)}{R} \right) \frac{C_{2n}}{R^{2n}} \frac{(bR)^k}{k!} \exp(-bR) \right] \quad (\text{B.18})$$

Appendix C

Geometries and experimental
data used in calculations

Table C.1: Optimised BP86/TZP molecular geometries, Cartesian co-ordinates, Angstroms

Atom	X	Y	Z	Atom	X	Y	Z	Atom	X	Y	Z
CO				O ₃				CH ₂ CCH ₂			
C	0.000	0.000	0.000	O	0.000	0.000	0.000	C	0.000	0.000	0.000
O	0.000	0.000	1.140	O	1.290	0.000	0.000	C	0.000	1.309	0.000
CO ₂				O	-0.602	1.141	0.000	C	0.000	-1.309	0.000
C	0.000	0.000	0.000	HF				H	0.935	1.875	0.000
O	0.000	0.000	1.174	H	0.000	0.000	0.000	H	0.000	1.875	0.000
O	0.000	0.000	-1.174	F	0.000	0.000	0.935	H	0.000	-1.875	0.935
F ₂				NH ₃				H	0.000	-1.875	-0.935
F	0.000	0.000	-0.712	N	0.000	0.000	0.000	C ₂ H ₂			
F	0.000	0.000	0.712	H	-0.400	0.943	0.000	C	0.000	0.000	0.000
OF ₂				H	-0.400	-0.471	-0.816	C	1.207	0.000	0.000
O	0.000	0.000	0.000	H	-0.400	-0.471	0.816	H	-1.072	0.000	0.000
F	1.433	0.000	0.000	CH ₄				H	2.279	0.000	0.000
F	-0.365	1.385	0.000	C	0.000	0.000	0.000	H ₂ CO			
HOF				H	1.096	0.000	0.000	O	0.000	0.000	0.000
O	0.000	0.000	0.000	H	-0.365	1.034	0.000	C	1.213	0.000	0.000
H	0.984	0.000	0.000	H	-0.365	-0.517	-0.895	H	1.803	0.950	0.000
F	-0.191	1.446	0.000	H	-0.365	-0.517	0.895	H	1.803	-0.950	0.000
NF ₃				C ₂ H ₆				CH ₃ CHO			
N	0.000	0.000	0.000	C	0.000	0.000	0.000	C	0.000	0.000	0.000
F	-0.624	1.262	0.000	C	1.532	0.000	0.000	C	1.218	0.000	0.000
F	-0.624	-0.631	-1.093	H	-0.401	1.024	0.000	C	2.077	1.236	0.000
F	-0.624	-0.631	1.093	H	-0.401	-0.512	-0.887	C	1.780	-0.971	0.000
H ₂ O				H	-0.401	-0.512	0.887	C	2.738	1.222	0.882
O	0.000	0.000	0.000	H	1.933	0.512	0.887	C	2.738	1.222	-0.882
H	0.974	0.000	0.000	H	1.933	-1.024	0.000	C	1.462	2.143	0.000
H	-0.229	0.974	0.000	H	1.933	0.512	-0.887	(CH ₃) ₂ CO			
H ₂ O ₂				C ₂ H ₄				O	0.000	0.000	0.000
O	0.000	0.000	0.000	C	0.000	0.000	0.000	C	1.224	0.000	0.000
O	1.481	0.000	0.000	C	1.334	0.000	0.000	C	2.021	1.295	0.000
H	-0.161	0.967	0.000	H	-0.572	0.930	0.000	C	2.021	-1.295	0.000
H	1.641	-0.315	0.914	H	-0.572	-0.930	0.000	H	2.736	1.310	0.838
HCN				H	1.906	0.930	0.000	H	2.618	1.367	-0.923
H	0.000	0.000	0.141	H	1.906	-0.930	0.000	H	1.343	2.152	0.068
C	0.000	0.000	1.217	C ₅ H ₆				H	2.735	-1.310	-0.838
N	0.000	0.000	2.375	C	0.000	1.399	0.000	H	2.618	-1.367	0.923
N ₂				C	0.000	0.700	-1.212	H	1.343	-2.152	-0.068
N	0.000	0.000	-0.552	C	0.000	-0.700	-1.212	CH ₂ CO			
N	0.000	0.000	0.552	C	0.000	-1.399	0.000	C	0.000	0.000	0.000
N ₂ O				C	0.000	-0.700	1.212	C	0.000	1.315	0.000
N	0.000	0.000	0.019	C	0.000	0.700	1.212	O	0.000	-1.175	0.000
N	0.000	0.000	1.159	H	0.000	2.491	0.000	H	0.947	1.851	0.000
O	0.000	0.000	-1.181	H	0.000	1.245	-2.157	H	-0.947	1.851	0.000
N ₂ O ₃				H	0.000	-1.245	-2.157	CF ₄			
C	0.000	0.000	0.000	H	0.000	-2.491	0.000	C	0.000	0.000	0.000
N	1.151	0.000	0.000	H	0.000	-1.245	2.157	F	1.339	0.000	0.000
N	1.664	1.862	0.000	H	0.000	1.245	2.157	F	-0.446	1.262	0.000
O	0.687	2.591	0.000					F	-0.446	-0.631	-1.093
O	2.853	2.126	0.000					F	-0.446	-0.631	1.093

Table C.1: (continued)

Atom	X	Y	Z	Atom	X	Y	Z	Atom	X	Y	Z
			CH ₂ CHCHO						CH ₃ CN		
O	0.000	0.000	0.000	C	0.000	0.000	0.000	C	0.000	0.000	0.000
C	1.223	0.000	0.000	N	1.473	0.000	0.000	C	1.458	0.000	0.000
C	2.058	1.216	0.000	H	-0.474	0.999	0.000	H	-0.378	1.031	0.000
C	3.397	1.126	0.000	H	-0.359	-0.545	-0.883	H	-0.378	-0.515	-0.893
H	1.800	-0.962	0.000	H	-0.359	-0.545	0.883	H	-0.378	-0.515	0.893
H	1.534	2.175	0.000	H	1.818	0.513	0.815	N	2.621	0.000	0.000
H	3.887	0.148	0.000	H	1.818	0.513	-0.815	CH ₂ NN			
H	4.041	2.006	0.000	C ₅ H ₅ N			C	0.000	0.000	0.000	
			(CH ₂) ₂ O	N	0.000	1.409	0.000	N	0.000	1.300	0.000
O	1.243	0.000	0.000	C	0.000	0.704	-1.145	N	0.000	2.449	0.000
C	0.000	0.737	0.000	C	0.000	0.704	1.145	H	0.000	-0.506	0.960
C	0.000	-0.737	0.000	C	0.000	-0.694	-1.200	H	0.000	-0.506	-0.960
H	-0.218	1.274	-0.928	C	0.000	-0.694	1.200	CH ₃ NO ₂			
H	-0.218	1.274	0.928	C	0.000	-1.409	0.000	C	0.000	0.000	0.000
H	-0.218	-1.274	0.928	H	0.000	1.312	-2.102	N	1.506	0.000	0.000
H	-0.218	-1.274	-0.928	H	0.000	1.312	2.102	H	-0.344	1.036	0.000
			C ₃ O ₂	H	0.000	-1.218	-2.184	H	-0.332	-0.560	-0.879
C	0.000	0.000	0.000	H	0.000	-1.218	2.184	H	-0.313	-0.523	0.911
C	0.000	1.277	0.000	H	0.000	-2.438	0.000	O	2.078	1.062	0.278
C	0.000	-1.277	0.000	C ₅ H ₅ N→O			O	2.062	-1.074	-0.261	
O	0.000	2.453	0.000	N	0.000	1.408	0.000	CH ₃ F			
O	0.000	-2.453	0.000	C	0.000	0.701	-1.185	C	0.000	0.000	0.000
			"carbene"	C	0.000	0.701	1.185	F	1.401	0.000	0.000
C	1.000	1.214	0.000	C	0.000	-0.684	-1.197	H	-0.351	1.040	0.000
C	1.000	-1.002	0.686	C	0.000	-0.684	1.197	H	-0.351	-0.520	-0.901
C	1.000	-1.002	-0.686	C	0.000	-1.408	0.000	H	-0.351	-0.520	0.901
N	1.000	0.348	1.064	H	0.000	1.337	-2.076	CH ₂ F ₂			
N	1.000	0.349	-1.063	H	0.000	1.337	2.076	C	1.000	0.000	0.000
C	1.000	-2.153	1.640	H	0.000	-1.205	-2.188	H	0.401	0.920	0.000
C	1.000	-2.152	-1.649	H	0.000	-1.205	2.188	H	0.401	-0.920	0.000
C	1.000	0.831	2.441	H	0.000	-2.461	0.000	F	1.801	0.000	1.117
C	1.000	0.829	-2.437	O	0.000	2.694	0.000	F	1.801	0.000	-1.117
H	1.000	-0.017	3.134	CH ₃ N(NO)CH ₃			CHF ₃				
H	1.891	1.443	2.625	N	0.000	0.000	0.000	C	0.000	0.000	0.000
H	0.109	1.443	2.625	N	1.353	0.000	0.000	H	1.096	0.000	0.000
H	1.000	-3.100	1.083	O	-0.539	1.116	0.000	F	-0.471	1.269	0.000
H	1.888	-2.155	2.292	C	1.990	-1.303	-0.000	F	-0.471	-0.634	-1.099
H	0.112	-2.155	2.292	C	2.147	1.219	-0.000	F	-0.471	-0.634	1.099
H	1.000	-1.798	-2.687	H	1.197	-2.059	-0.000	COF ₂			
H	1.888	-2.792	-1.525	H	2.619	-1.429	-0.895	O	0.000	0.000	0.000
H	0.112	-2.792	-1.525	H	2.619	-1.429	0.894	C	1.182	0.000	0.000
H	1.000	1.922	-2.390	H	1.444	2.060	0.001	F	1.973	1.077	0.000
H	1.895	0.490	-2.978	H	2.786	1.259	0.895	F	1.973	-1.077	0.000
H	0.105	0.490	-2.978	H	2.784	1.261	-0.896	CF ₃ CN			
			C ₂ F ₄	CH ₃ NC			C	0.000	0.000	0.000	
C	0.000	0.000	0.000	C	0.000	0.000	0.000	C	1.480	0.000	0.000
C	1.329	0.000	0.000	N	1.423	0.000	0.000	F	-0.469	1.266	0.000
F	-0.730	1.113	0.000	H	-0.372	1.032	0.000	F	-0.469	-0.633	-1.096
F	-0.730	-1.113	0.000	H	-0.372	-0.516	-0.894	F	-0.469	-0.633	1.096
F	2.059	1.113	0.000	H	-0.372	-0.516	0.894	N	2.641	0.000	0.000
F	2.059	-1.113	0.000	C	2.602	0.000	0.000				

Table C.2: Geometries of systems and additional basis functions used for vertical excitation energy calculations. All bond lengths in Angstroms.

System	Bond length(s)	Bond angle	Additional diffuse functions
CO	1.128		$2s$, $1p$ and $1d$ diffuse functions at centre of bond functions are average of C and O exponents ¹
N ₂	1.098		N diffuse functions ¹ at centre of bond also additional p function (exponent 0.00543) ²
H ₂ CO	1.203 1.102	121.9	C diffuse functions ¹ on carbon atom only
C ₂ H ₄	1.331 1.081	121.4	C diffuse functions ¹ midway between carbon atoms

¹defined in ref. [201]

²to ensure reasonable description of highest ${}^1\Sigma_u^+$ excitation

Table C.3: Geometries of systems for shielding and polarisability calculations. Bonds lengths in Angstroms, bond angles in degrees.

System	Bond length	Bond angle	System	Bond length	Bond angle
C ₂ H ₂	1.203		H ₂ S	1.336	92.1
	1.063		HCl	1.275	
C ₂ H ₄	1.331	121.4	HCN	1.065	
	1.081			1.153	
CH ₄	1.086	109.5	HF	0.917	
Cl ₂	1.988		N ₂	1.098	
CO	1.128		N ₂ O	NN	1.128
CO ₂	1.160			NO	1.843
F ₂	1.412		NH ₃	1.012	106.7
H ₂ CNN	HC 1.074	HCH 125.2	O ₃	1.272	116.8
	CN 1.297	NCH 117.4	OF ₂	1.405	103.4
	NN 1.139		PH ₃	1.419	93.5
H ₂ CO	1.203	121.9	PN	1.491	
	1.102		SO ₂	1.430	119.3
H ₂ O	0.957	104.5			

Table C.4: Experimental vertical ionisation potentials (I) and electron affinities (A)

System	$I(\text{eV})^1$	$A(\text{eV})^2$	$I + A(\text{eV})$	$I + A(\text{Hartree})$
HF	16.12	-6.0	10.12	0.372
H ₂ O	12.62	-6.4	6.22	0.229
CH ₄	13.6	-7.8	5.80	0.213
CO	14.01	-1.8	12.21	0.449
N ₂	15.58	-2.2	13.38	0.492
H ₂ S	10.5	-2.0	8.50	0.312
NH ₃	10.82	-5.6	5.22	0.192
HCN	13.61	-2.3	11.31	0.416
C ₂ H ₂	11.49	-2.6	8.89	0.327
C ₂ H ₄	10.68	-1.8	8.88	0.326
H ₂ CO	13.77	-1.5	9.40	0.345
CO ₂	13.77	-3.8	9.97	0.366
PH ₃	10.59	-1.9	8.69	0.319

¹ ref. [202]² ref. [203]

Appendix D

Publications and conferences

D.1 Publications

1. “The observation of a large *gauche* preference when 2-fluoroethylamine and 2-fluoroethanol become protonated” Caroline R. S. Briggs, Mark J. Allen, David O’Hagan, David J. Tozer, Alexandra M. Z. Slawin, Andrés E. Goeta and Judith A. K. Howard, *Org. Biol. Mol. Chem.*, **2**, (2004), 732.
2. “Improved NMR chemical shifts in density functional theory” Mark J. Allen, Thomas W. Keal and David J. Tozer, *Chem. Phys. Lett.*, **380**, (2003), 70.
3. “Polarisabilities and excitation energies from the Multiplicative Kohn-Sham (MKS) approach” Mark J. Allen and David J. Tozer, *Mol. Phys.*, **101**, (2003), 421.
4. “Helium dimer dispersion forces and correlation potentials in density functional theory” Mark J. Allen and David J. Tozer, *J. Chem. Phys.*, **117**, (2002), 11113.

5. "Eigenvalues, integer discontinuities and NMR shielding constants in Kohn-Sham theory" Mark J. Allen and David J. Tozer, *Mol. Phys.*, **100**, (2002), 433.
6. "Kohn-Sham calculations using hybrid exchange-correlation functionals with asymptotically corrected potentials" Mark J. Allen and David J. Tozer, *J. Chem. Phys.*, **113**, (2000), 5185.

D.2 Conferences and seminars attended

9th July 2003

13th Annual Northern Universities Meeting on Chemical Physics (ANUMOCP XIII)

Chemical Physics Group

University of Durham

18–23rd August 2002

Molecular Physics and Quantum Chemistry

A Summer School

Jesus College, University of Oxford

31st July–2nd August 2002

Exploring Modern Computational Chemistry, EMC²

University of Nottingham

10–14th September 2001

9th International Conference on the Applications of the Density Functional Theory in Chemistry and Physics

San Lorenzo de El Escorial, Madrid, Spain

14th June 2001

Recent advances in quantum chemistry

A symposium in honour of Nicholas Handy's 60th birthday

Dept. of Chemistry, University of Cambridge

18–20th April 2001

Faraday discussion 118, Cluster Dynamics

Royal Society of Chemistry

Dept. of Chemistry, University of Durham

14th February 2001

Calculating the distribution of bonding energy in polyatomic molecules

Dr Sian T. Howard

Dept. of Chemistry, Cardiff University

24th January 2001

Chemical Interated Circuits: organic synthesis and analysis on a small scale

Dr Andrew deMello

Dept. of Chemistry, Imperial College, London

17th January 2001

Applications of polarised NEXAFS spectroscopy to the structural characterisation of soft molecular interfaces

Professor Kevin Roberts

Dept. of Chemical Engineering, University of Leeds

10th January 2001

Micelles, reversed micelles and shell-crosslinked micelles based on tertiary amine methacrylates

Professor S. P. Armes

School of Chemistry, Physics and Environmental Science,

University of Sussex

6th December 2000

Dual activation approach to electroanalysis; ultrasound, microwaves and laser activation

Professor Richard Compton

University of Oxford

29th November 2000

Life, death and the carotenoids

Professor T. George Truscott

University of Keele

22nd November 2000

Synthesis of novel dendrimers and hyperbranched polymers

Dr Wayne Hayes

University of Reading

8th November 2000

Cosmic: a universal, DNA-based language for communicating with aliens and other intelligent lifeforms

Dr J. P. L. Cox

Bath University

25th October 2000

Science, art and drug discovery. A personal perspective

Dr S. F. Campbell

Former Senior Vice President of Pfizer

23rd June 2000

An Afternoon of Computational Chemistry

Dept. of Chemistry, University of Cambridge

Bibliography

- [1] E. Schrödinger, *Phys. Rev.*, **28**, (1926), 1049.
- [2] L. de Broglie, *Ann. de Physique*, **3**, (1925), 22.
- [3] M. Born, *Z. Physik*, **37**, (1926), 863; *Z. Physik*, **38**, (1926), 803.
- [4] M. Born and J. R. Oppenheimer, *Ann. Physik*, **84**, (1927), 457.
- [5] M. Born and K. Huang, in *Dynamical Theory of Crystal Lattices*, (Oxford University Press, New York, 1954).
- [6] V. Fock, *Z. Physik*, **61**, (1930), 126.
- [7] J. C. Slater, *Phys. Rev.*, **35**, (1930), 210.
- [8] D. R. Hartree, *Proc. Cambridge Phil. Soc.*, **24**, (1928), 89.
- [9] J. A. Pople and R. K. Nesbet, *J. Chem. Phys.*, **22**, (1954), 571.
- [10] C. C. J. Roothaan, *Rev. Mod. Phys.*, **23**, (1951) 69.
- [11] G. G. Hall, *Proc. Roy. Soc.*, **A205**, (1951), 541.
- [12] T. A. Koopmans, *Physica*, **1**, (1934), 104.
- [13] P.-O. Löwdin, *Adv. Chem. Phys.*, **2**, (1959), 207.
- [14] J. Čížek, *J. Chem. Phys.*, **45**, (1966), 4256.
- [15] J. Čížek, *Adv. Chem. Phys.*, **14**, (1969), 35.

- [16] J. Čížek and J. Paldus, *Int. J. Quantum Chem.*, **5**, (1971), 359.
- [17] K. A. Brueckner, *Phys. Rev.*, **96**, (1954), 508.
- [18] R. K. Nesbet, *Phys. Rev.*, **109**, (1958), 1632.
- [19] R. A. Chiles and C. E. Dykstra, *J. Chem. Phys.*, **74**, (1981), 4544.
- [20] N. C. Handy, J. A. Pople, M. Head-Gordon, K. Raghavachari and G. W. Trucks, *Chem. Phys. Lett.*, **164**, (1989), 185.
- [21] R. Kobayashi, N. C. Handy, R. D. Amos, G. W. Trucks, M. J. Frisch and J. A. Pople, *J. Chem. Phys.*, **95**, (1991), 6723.
- [22] R. Kobayashi, R. D. Amos and N. C. Handy, *Chem. Phys. Lett.*, **184**, (1991), 195.
- [23] L. H. Thomas, *Proc. Cambridge Philos. Soc.*, **23**, (1927), 542. Reprint appears in N. H. March, *Self-Consistent Fields in Atoms*, (Pergamon, Oxford, 1975), p. 195.
- [24] E. Fermi, *Z. Physik*, **48**, (1928), 73. Translation from original German appears in N. H. March, *Self-Consistent Fields in Atoms*, (Pergamon, Oxford, 1975), p. 205.
- [25] P. A. M. Dirac, *Proc. Cambridge Phil. Soc.*, **26**, (1930), 376.
- [26] P. Hohenberg and W. Kohn, *Phys. Rev. B*, **136**, (1964), 864.
- [27] W. Kohn and L. J. Sham, *Phys. Rev.*, **140**, (1965), A1133.
- [28] F. Bloch, *Z. Physik*, **57**, (1929), 545.
- [29] D. M. Ceperley and B. J. Alder, *Phys. Rev. Lett.*, **45**, (1980), 566.
- [30] S. J. Vosko, L. Wilk, M. Nusair, *Can. J. Phys.*, **58**, (1980), 1200.
- [31] B. Delley, *J. Chem. Phys.*, **94**, (1991), 7245.

- [32] J. Andzelm and E. Wimmer, *J. Chem. Phys.*, **96**, (1992), 1280.
- [33] B. G. Johnson, P. M. W. Gill and J. A. Pople, *J. Chem. Phys.*, **98**, (1993), 5612.
- [34] A. D. Becke, *Phys. Rev. A*, **33**, (1986), 2786.
- [35] R. O. Jones and O. Gunnarsson, *Phys. Rev. Lett.*, **55**, (1985), 107.
- [36] F. Herman, J. P. Van Dyke and I. B. Ortenburgen, *Phys. Rev. Lett.*, **22**, (1969), 807.
- [37] F. Herman, J. P. Van Dyke and I. B. Ortenburgen, *Int. J. Quantum Chem. Quantum Chem. Symp.*, **3**, (1970), 827.
- [38] A. D. Becke, *J. Chem. Phys.*, **84**, (1986), 4524.
- [39] A. D. Becke, *Phys. Rev. A*, **38**, (1988), 3098.
- [40] C.-O. Almbladh and U. von Barth, *Phys. Rev. B*, **31**, (1985), 3231.
- [41] C. Lee, W. Yang and R. G. Parr, *Phys. Rev B*, **37**, (1988), 785.
- [42] R. Colle and O. Salvetti, *Theor. Chim. Acta.*, **37**, (1975), 329.
- [43] B. Miehlich, A. Savin, H. Stoll and H. Preuss, *Chem. Phys. Lett.*, **157**, (1989), 200.
- [44] F. A. Hamprecht, A. J. Cohen, D. J. Tozer and N. C. Handy, *J. Chem. Phys.*, **109**, (1998), 6264.
- [45] A. D. Becke, *J. Chem. Phys.*, **107**, (1997), 8554.
- [46] D. J. Tozer and N. C. Handy, *J. Chem. Phys.*, **108**, (1998), 2545.
- [47] D. J. Tozer and N. C. Handy, *J. Phys. Chem. A*, **102**, (1998), 3162.
- [48] N. C. Handy and D. J. Tozer, *Mol. Phys.*, **94**, (1998), 707.

- [49] G. Menconi, P. J. Wilson, and D. J. Tozer, *J. Chem. Phys.*, **114**, (2001), 3958.
- [50] J. P. Perdew, K. Burke and M. Ernzerhof, *Phys. Rev. Lett.*, **77**, (1996), 3865.
- [51] T. W. Keal and D. J. Tozer, *J. Chem. Phys.*, **119**, (2003), 3015.
- [52] E. Clementi and S. J. Chakravorty, *J. Chem. Phys.*, **93**, (1990), 2591.
- [53] C. F. Fischer, J. B. Lagowski and S. H. Vosko, *Phys. Rev. Lett.*, **59**, (1987), 2263.
- [54] J. B. Lagowski and S. H. Vosko, *J. Phys. B*, **21**, (1988), 203.
- [55] A. D. Becke, *J. Chem. Phys.*, **98**, (1993), 1372.
- [56] A. D. Becke, *J. Chem. Phys.*, **98**, (1993), 5648.
- [57] J. P. Perdew, J. A. Chevary, S. H. Vosko, K. A. Jackson, M. R. Pederson, D. J. Singh, and C. Fiolhais, *Phys. Rev. B*, **46**, (1992), 6671.
- [58] P. J. Stephens, F. J. Devlin, C. F. Chabalowski and M. J. Frisch, *J. Phys. Chem*, **98**, (1994), 11623.
- [59] P. J. Wilson, T. J. Bradley and D. J. Tozer, *J. Chem. Phys.*, **115**, (2001), 9233.
- [60] M. Ernzerhof and G. E. Scuseria, *J. Chem. Phys.*, **110**, (1999), 5029.
- [61] C. Adamo and V. Barone, *J. Chem. Phys.*, **110**, (1999), 6158.
- [62] J. P. Perdew, M. Ernzerhof and K. Burke, *J. Chem. Phys.*, **105**, (1996), 9982.
- [63] Q. Zhao and R. G. Parr, *Phys. Rev. A*, **46**, (1992), 2337.
- [64] Q. Zhao and R. G. Parr, *J. Chem. Phys.*, **98**, (1993), 543.

- [65] Q. Zhao, R. C. Morrison and R. G. Parr, *Phys. Rev. A*, **50**, (1994), 2138.
- [66] M. Levy and J. P. Perdew, in *Density Functional Methods in Physics*, edited by R. M. Dreizler and J. da Providencia (Plenum, New York, 1985).
- [67] D. J. Tozer, V. E. Ingamells and N. C. Handy, *J. Chem Phys.*, **105**, (1996), 9200.
- [68] D. J. Tozer, K. Somasundram and N. C. Handy, *Chem. Phys. Lett.*, **265**, (1997), 614.
- [69] P. J. Wilson and D. J. Tozer, *Chem. Phys. Lett.*, **337**, (2001), 341.
- [70] R. D. Amos et al., CADPAC6.5. The Cambridge Analytic Derivatives Package, Cambridge UK.
- [71] A. J. Stone, *The Theory of Intermolecular Forces* (Oxford University Press, Oxford, 1997).
- [72] S. F. Boys and F. Bernardi, *Mol. Phys.*, **19**, (1970), 553.
- [73] S. Kristyán and P. Pulay, *Chem. Phys. Lett.*, **229**, (1994), 175.
- [74] J. M. Pérez-Jordá and A. D. Becke, *Chem. Phys. Lett.*, **233**, (1995), 134.
- [75] P. Hobza, J. Šponer, and T. Reschel, *J. Comp. Chem.*, **16**, (1995), 1315.
- [76] D. C. Patton and M. R. Pederson, *Phys. Rev. A.*, **56**, (1997), R2495.
- [77] Y. Zhang, W. Pan, and W. Yang, *J. Chem. Phys.*, **107**, (1997), 7921.
- [78] N. Kurita and H. Sekino, *Chem. Phys. Lett.*, **348**, (2001), 139.
- [79] X. Wu, M. C. Vargas, S. Nayak, V. Lotrich, and G. Scoles, *J. Chem. Phys.*, **115**, (2001), 8748.

- [80] C. Adamo and V. Barone, *J. Chem. Phys.*, **108**, (1998), 664.
- [81] S. Tsuzuki and H. P. Lüthi, *J. Chem. Phys.*, **114**, (2001), 3949.
- [82] J. M. Pérez-Jordá, E. San-Fabián, and A. J. Pérez-Jiménez, *J. Chem. Phys.*, **110**, (1999), 1916.
- [83] E. J. Meijer and M. Sprik, *J. Chem. Phys.*, **105**, (1996), 8684.
- [84] S. Tsuzuki, T. Uchimaru, and K. Tanabe, *Chem. Phys. Lett.*, **287**, (1998), 202.
- [85] A. Milet, T. Korona, R. Moszynski, and E. Kochanski, *J. Chem. Phys.*, **111**, (1999), 7727.
- [86] T. A. Wesolowski, *J. Chem. Phys.*, **113**, (2000), 1666.
- [87] O. Couronne and Y. Ellinger, *Chem. Phys. Lett.*, **306**, (1999), 71.
- [88] T. A. Wesolowski, O. Parisel, Y. Ellinger, and J. Weber, *J. Phys. Chem. A*, **101**, (1997), 7818.
- [89] A. K. Rappé and E. R. Bernstein, *J. Phys. Chem. A*, **104**, (2000), 6117.
- [90] A. D. Becke, *Phys. Rev. A*, **38**, (1988), 3098.
- [91] J. P. Perdew, in *Electronic Structure of Solids '91*, edited by P. Zeishe and H. Eschrig (Akademie Verlag, Berlin, 1991), p.11
- [92] T. van Mourik and R. J. Gdanitz, *J. Chem. Phys.*, **116**, (2002), 9620.
- [93] J. F. Ogilvie and F. Y. H. Wang, *J. Mol. Struct.*, **273**, (1992), 277.
- [94] J. F. Ogilvie and F. Y. H. Wang, *J. Mol. Struct.*, **291**, (1993), 313.
- [95] G. Menconi and D. J. Tozer, *Chem. Phys. Lett.*, **360**, (2002), 38.
- [96] Q. Wu and W. Yang, *J. Chem. Phys.*, **116**, (2002), 515.

- [97] E. Zaremba and W. Kohn, *Phys. Rev. B*, **13**, (1976), 2270.
- [98] K. Rapcewicz and N. W. Ashcroft, *Phys. Rev. B*, **44**, (1991), 4032.
- [99] J. F. Dobson and B. P. Dinte, *Phys. Rev. Lett.*, **76**, (1996), 1780.
- [100] Y. Andersson, D. C. Langreth and B. I. Lundqvist, *Phys. Rev. Lett.*, **76**, (1996), 102.
- [101] E. Hult, Y. Andersson, B. I. Lundqvist and D. C. Langreth, *Phys. Rev. Lett.*, **77**, (1996), 2092.
- [102] E. Hult, H. Rydberg, B. I. Lundqvist and D. C. Langreth, *Phys. Rev. B*, **59**, (1999), 4708.
- [103] S. J. A. van Gisbergen, J. G. Snijders and E. J. Baerends, *J. Chem. Phys.*, **103**, (1995), 9347.
- [104] A. G. Ioannou, S. M. Colwell and R. D. Amos, *Chem. Phys. Lett.*, **278**, (1997), 278.
- [105] W. Kohn, Y. Meir and D. E. Makarov, *Phys. Rev. Lett.*, **80**, (1998), 4153.
- [106] J. F. Dobson and J. Wang, *Phys. Rev. Lett.*, **82**, (1999), 2123.
- [107] M. Lein, J. F. Dobson and E. K. U. Gross, *J. Comp. Chem.*, **20**, (1999), 12.
- [108] M. Fuchs and X. Gonze, *Phys. Rev. B*, **65**, (2002), 235109.
- [109] E. Engel, A. Höck and R. M. Dreizler, *Phys. Rev. A*, **61**, (2000), 032502.
- [110] J. F. Dobson, D. McLennan, A. Rubio, J. Wang, T. Gould, H. M. Le and B. P. Dinte, *Aust. J. Chem.*, **54**, (2001), 513.
- [111] H. L. Williams and C. F. Chabalowski, *J. Phys. Chem. A*, **105**, (2001), 646.

- [112] A. J. Misquitta and K. Szalewicz, *Chem. Phys. Lett.*, **357**, (2002), 301.
- [113] R. P. Feynman, *Phys. Rev.*, **56**, (1939), 340.
- [114] T. Korona, H. L. Williams, R. Bukowski, B. Jeziorski, and K. Szalewicz. *J. Chem. Phys.*, **106**, (1997), 5109.
- [115] G. K.-L. Chan, D. J. Tozer and N. C. Handy, *J. Chem. Phys.*, **107**, (1997), 1536.
- [116] G. Menconi, D. J. Tozer and S. Liu, *Phys. Chem. Chem. Phys.*, **2**, (2000), 3739.
- [117] K. T. Tang and J. P. Toennies, *J. Chem. Phys.*, **80**, (1984), 3726.
- [118] H. Hellmann in *Einführung in die Quantenchemie* (Franz Deuticke, Leipzig, Germany, 1937)
- [119] J. O. Hirschfelder and M. A. Eliason, *J. Chem. Phys.*, **47**, (1967), 1164.
- [120] K. L. C. Hunt, *J. Chem. Phys.*, **92**, (1990), 1180.
- [121] H. Nakatsuji *J. Am. Chem. Soc.*, **96**, (1974), 24.
- [122] R. F. W. Bader and A. K. Chandra, *Can. J. Chemistry*, **46**, (1968), 953.
- [123] R. G. A. Bone and R. F.W. Bader, *J. Phys. Chem.*, **100**, (1996), 10892.
- [124] R. F. W. Bader, *Atoms in Molecules—A Quantum Theory*, (Oxford University Press, Oxford, 1990), p. 325.
- [125] J. Hernández-Trujillo and R. F. W. Bader, *J. Phys. Chem. A*, **104**, (2000), 1779.
- [126] C. J. Umrigar and X. Gonze, *Phys. Rev. A*, **50**, (1994), 3827.
- [127] C. A. Coulson and I. Fischer, *Philos. Mag. ser. 7*, **40**, (1949), 386.

- [128] P. J. Wilson, R. D. Amos and N. C. Handy, *Chem. Phys. Lett.*, **312**, (1999), 475.
- [129] V. G. Malkin, O. L. Malkina, M. E. Casida, and D. R. Salahub, *J. Am. Chem. Soc.*, **116**, (1994), 5898.
- [130] L. Olsson and D. Cremer, *J. Chem. Phys.*, **105**, (1996), 8995.
- [131] S. Patchkovskii, J. Autschbach, and T. Ziegler, *J. Chem. Phys.*, **115**, (2001), 26.
- [132] J. Poater, E. van Lenthe, and E. J. Baerends, *J. Chem. Phys.*, **118**, (2003), 8584.
- [133] E. J. Baerends, D. E. Ellis and R. Pos, *Chem. Phys.*, **2**, (1973), 41.
- [134] L. Versluis and T. Ziegler, *J. Chem. Phys.*, **88**, (1988), 322.
- [135] G. te Velde and E. J. Baerends, *J. Comput. Phys.*, **99**, (1992), 84.
- [136] C. Fonseca, J. G. Snijders, G. te Velde and E. J. Baerends, *Theor. Chem. Acc.*, **99**, (1998), 391.
- [137] S. Huzinaga, *Approximate Atomic Functions*, (University of Alberta, Edmonton, 1971).
- [138] W. Kutzelnigg, U. Fleischer and M. Schlindler, *NMR-Basic Principles and Progress*, vol. 23, (Springer, Heidelberg, 1990).
- [139] A. E. Hansen and T. D. Bouman, *J. Chem. Phys.* **82**, (1985), 5035.
- [140] P. J. Wilson and D. J. Tozer, *J. Chem. Phys.*, **116**, (2002), 10139.
- [141] M. Bühl, "NMR Chemical Shift Computation: Structural Applications", in *Encyclopedia of Computational Chemistry*, P. v. R. Schleyer (Editor in Chief), (Wiley, Chichester, 1998).
- [142] D. J. Tozer, *J. Chem Phys.* **112**, (2000), 3507.

- [143] D. J. Tozer and N. C. Handy, *J. Chem. Phys.*, **109**, (1998), 10180.
- [144] M. E. Casida, K. C. Casida and D. R. Salahub, *Intl. J. Quantum Chem.*, **70**, (1998), 933.
- [145] M. Gruning, O. V. Gritsenko, S. J. A. van Gisbergen and E. J. Baerends, *J. Chem. Phys.*, **114**, (2001), 652.
- [146] S. J. A. van Gisbergen, F. Kootstra, P. R. T. Schipper, O. V. Gritsenko, J. G. Snijders and E. J. Baerends, *Phys. Rev. A*, **57**, (1998), 2556.
- [147] E. K. U. Gross and W. Kohn, *Adv. Quantum Chem.*, **21**, (1990), 255.
- [148] E. K. U. Gross, C. A. Ullrich and U. J. Gossmann, in *Density Functional Theory*, edited by E. K. U. Gross and R. M. Dreizler, NATO ASI Series (Plenum, New York, 1994), p. 149.
- [149] M. E. Casida, in *Recent Advances in Density Functional Methods*, Part I, edited by D. P. Chong (Singapore, World Scientific, 1995), p. 155.
- [150] E. K. U. Gross, J. F. Dobson and M. Petersilka, in *Density Functional Theory II*, edited by R. F. Nalewajski, *Vol 181 of Topics in Current Chemistry* (Springer, Berlin, 1996), p. 81.
- [151] S. M. Colwell, N. C. Handy and A. M. Lee, *Phys. Rev. A*, **53**, (1996), 1316.
- [152] A. J. Sadlej, *Coll. Czech. Chem. Comm.*, **53**, (1988), 1995.
- [153] A. J. Sadlej, *Theor. Chim. Acta.*, **79**, (1991), 123.
- [154] C. Van Caillie and R. D. Amos, *Chem. Phys. Lett.*, **291**, (1998), 71.
- [155] A. J. Russell and M. A. Spackman, *Mol. Phys.*, **84**, (1995), 1239.
- [156] A. J. Russell and M. A. Spackman, *Mol. Phys.*, **90**, (1997), 251.

- [157] M. A. Spackman, *J. Chem. Phys.*, **94**, (1991), 1288.
- [158] A. J. Cohen and Y. Tantirungrotechai, *Chem. Phys. Lett.*, **299**, (1998), 465.
- [159] E. S. Nielsen, P. Jørgensen, and J. Oddershede, *J. Chem. Phys.*, **73**, (1980), 6238; K. P. Huber and G. Herzberg, in *Constants of Diatomic Molecules*, (Van Nostrand Reinhold, 1979).
- [160] S. B. Ben-Shlomo and U. Kaldor, *J. Chem. Phys.*, **92**, (1990), 3680.
- [161] D. J. Clouthier and D. A. Ramsay, *Ann. Rev. Phys. Chem.*, **34**, (1983), 31; S. Taylor, D. G. Wilden, and J. Comer, *Chem. Phys.*, **70**, (1982), 291.
- [162] L. Serrano-Andrés, M. Merchán, I. Nebot-Gil, R. Lindh, and B. O. Roos, *J. Chem. Phys.*, **98**, (1993), 3151.
- [163] J. Garza, R. Vargas, J. A. Nichols and D. A. Dixon, *J. Chem. Phys.*, **114**, (2001), 639.
- [164] F. R. Manby and P. J. Knowles, *J. Chem. Phys.*, **112**, (2000), 7002.
- [165] A. A. Jarecki and E. R. Davidson, *Chem. Phys. Lett.*, **300**, (1999), 44.
- [166] P. Politzer and F. Abu-Awwad, *Theor. Chem. Acc.*, **99**, (1998), 83.
- [167] X. L. Hua, X. J. Chen and W. A. Goddard, *Phys. Rev. B*, **55**, (1997), 16103.
- [168] R. Stowasser and R. Hoffmann, *J. Am. Chem. Soc.*, **121**, (1999), 3414.
- [169] A. Savin, C. J. Umrigar and X. Gonze, *Chem. Phys. Lett.*, **288**, (1998), 391.
- [170] J. P. Perdew and M. Levy, *Phys. Rev. B*, **56**, (1997), 16021.
- [171] J. P. Perdew, R. G. Parr, M. Levy and J. L. Balduz, *Phys. Rev. Lett.*, **49**, (1982), 1691.

- [172] J. P. Perdew and M. Levy, *Phys. Rev. Lett.*, **51**, (1983), 1884.
- [173] G. K.-L. Chan, *J. Chem. Phys.*, **110**, (1999), 4710.
- [174] J. P. Perdew, in *Density functional methods in Physics*, Vol B123 of NATO ASI Series, edited by R. M. Dreizler and J. da Providencia (Plenum Press, New York, 1985) p. 265.
- [175] R. A. Kendall, T. H. Dunning Jr. and R. J. Harrison, *J. Chem. Phys.*, **96**, (1992), 6796.
- [176] P. J. Wilson, R. D. Amos and N. C. Handy, *Chem. Phys. Lett.*, **312**, (1999), 475.
- [177] J. Gauss and J. F. Stanton, *J. Chem. Phys.*, **104**, (1996), 2574.
- [178] T. D. Bouman and A. E. Hansen, *Chem. Phys. Lett.*, **175**, (1990), 292.
- [179] K. Rund, T. Helgaker, R. Kobayashi, P. Jorgensen, K. L. Bak and H. J. A. Jensen, *J. Chem. Phys.*, **100**, (1994), 8178.
- [180] W. Kutzelnigg, U. Fleischer and M. Schindler, in *NMR-Basic Principles and Progress*, (Springer, Heidelberg, Vol. 23, 1990).
- [181] J. R. Cheeseman, G. W. Trucks, T. A. Keith and M. J. Frisch, *J. Chem. Phys.*, **104**, (1996), 5497.
- [182] J. Gauss and J. F. Stanton, *J. Chem. Phys.*, **102**, (1995), 251.
- [183] J. Gauss, *Chem. Phys. Lett.*, **191**, (1992), 614.
- [184] H. Fukui, T. Baba, J. Narumi, H. Inomata, K. Miura and H. Matsuda, *J. Chem. Phys.*, **105**, (1996), 4692.
- [185] J. P. Perdew and M. Levy, *Phys. Rev. Lett.*, **51**, (1983), 1884.
- [186] D. J. Tozer, *Phys. Rev. A*, **56**, (1997), 2726.
- [187] S. Wolf, *Acc. Chem. Res.*, **5**, (1972), 102.

- [188] D. O'Hagan, C. Bilton, J. A. K. Howard, L. Knight and D. J. Tozer, *J. Chem. Soc., Perkin Trans. 2*, (2000), 605.
- [189] C. R. S. Briggs, D. O'Hagan, J. A. K. Howard and D. S. Yufit, *J. Fluorine. Chem.*, **119**, (2003), 9.
- [190] R. J. Abraham and J. R. Monasterios, *Org. Mag. Reson.*, **5**, (1973), 305.
- [191] C. R. S. Briggs, D. O'Hagan, H. S. Rzepa and A. M. Z. Slawin, *J. Fluorine. Chem.*, **125**, (2004), 19.
- [192] N. C. Craig, A. Chen, K. H. Suh, S. Klee, G. C. Mellau, B. P. Winniewisser and M. Winniewisser, *J. Am. Chem. Soc.*, **119**, (1997), 4789.
- [193] R. D. Amos, N. C. Handy, P. G. Jones, A. J. Kirby, J. K. Parker, J. M. Percy and M. D. Su, *J. Chem. Soc., Perkin Trans. 2*, (1992), 549.
- [194] K. B. Wiberg, *Acc. Chem. Res.*, **29**, (1996), 229.
- [195] D. Parker, K. Senanayake, J. Vepsäläinen, S. Williams, A. S. Batsanov and J. A. K. Howard, *J. Chem. Soc., Perkin Trans. 2*, (1997), 1445.
- [196] T. K. Brunck and F. Weinhold, *J. Am. Chem. Soc.*, **101**, (1979), 1700.
- [197] P. Dionne and M. St-Jacques, *J. Am. Chem. Soc.*, **109**, (1987), 2616.
- [198] N. D. Epiotis, R. L. Yates, J. R. Larson, C. R. Kirmaier and F. Bernardi, *J. Am. Chem. Soc.*, **99**, (1977), 8379.
- [199] D. A. Dixon and B. E. Smart, *J. Phys. Chem.*, **95**, (1991), 1609.
- [200] C. R. S. Briggs, M. J. Allen, D. O'Hagan, D. J. Tozer, A. M. Z. Slawin, A. E. Goetha and J. A. K. Howard, *Org. Biomol. Chem.*, **2**, (2004), 732.
- [201] M. E. Casida, C. Jamorski, K. C. Casida and D. R. Salahub, *J. Chem. Phys.*, **108**, (1998), 4439.

- [202] HF: M. S. Banna, D. A. Shirley, *J. Chem. Phys.*, **63**, (1975), 4759; H₂O: K. Kimura, S. Katsumata, Y. Achiba, T. Yamazaki and S. Iwata, *Handbook of HeI Photoelectron Spectra of Fundamental Organic Compounds*, (Japan Scientific Soc. Press, Tokyo, 1981); CH₄, C₂H₂ and C₂H₄: G. Bieri and L. Asbrink, *J. Electron Spectrosc. Relat. Phenom.*, **20**, (1980), 149; CO and N₂: A. W. Potts and T. A. Williams, *J. Electron Spectrosc. Relat. Phenom.*, **3** (1974), 3; H₂S: G. Bieri, L. Asbrink and W. Von Niessen, *J. Electron Spectrosc. Relat. Phenom.*, **27** (1982), 129; NH₃: H. Baumgartel, H. -W. Jochims, E. Ruhl, H. Bock, R. Dammel, J. Minkwitz and R. Nass, *Inorg. Chem.*, **28**, (1989), 943; HCN: J. Kreile, A. Schweig and W. Thiel, *Chem. Phys. Lett.*, **87**, (1982), 473; H₂CO: "Ionization Potentials, Appearance Potentials and Heats of Formation of Gaseous Positive Ions", NSRDS-NBS 26, 1969; PH₃: A. H. Cowley, R. A. Kemp, M. Lattman and M. L. McKee, *Inorg. Chem.*, **21**, (1982), 85; CO₂: J. H. D. Eland and J. Berkowitz, *J. Chem. Phys.*, **67**, (1977), 5034.
- [203] R. G. Pearson, *Inorg. Chem.*, **27**, (1988), 734.

